



Virginia Commonwealth University  
**VCU Scholars Compass**

---

Theses and Dissertations

Graduate School


---

2023

## Molecular Mechanisms of Prdm16 as a Tumor Suppressor in Pancreatic Ductal Adenocarcinoma

Eric Hurwitz  
*Virginia Commonwealth University*

Follow this and additional works at: <https://scholarscompass.vcu.edu/etd>

 Part of the [Medical Cell Biology Commons](#), [Medical Genetics Commons](#), [Medical Molecular Biology Commons](#), [Medical Pathology Commons](#), and the [Oncology Commons](#)

© The Author

---

Downloaded from

<https://scholarscompass.vcu.edu/etd/7208>

This Dissertation is brought to you for free and open access by the Graduate School at VCU Scholars Compass. It has been accepted for inclusion in Theses and Dissertations by an authorized administrator of VCU Scholars Compass. For more information, please contact [libcompass@vcu.edu](mailto:libcompass@vcu.edu).

# **Molecular Mechanisms of Prdm16 as a Tumor Suppressor in Pancreatic Ductal Adenocarcinoma**

Virginia Commonwealth University

Richmond, Virginia

March 17<sup>th</sup>, 2023

A dissertation submitted in partial fulfillment of the requirements for  
the degree of Doctor of Philosophy at  
Virginia Commonwealth University

By

**ERIC HURWITZ**

Bachelor of Science, University of Mary Washington, 2018

**ADVISOR: AZEDDINE ATFI, Ph.D**

Leader, Cancer Biology Program

Marry Anderson Harrison Professor in Cancer Research

Massey Cancer Center

Department of Biochemistry and Molecular Biology

Virginia Commonwealth University

## **ACKNOWLEDGEMENTS**

First and foremost, I would like to thank my advisor Dr. Azeddine Atfi. His continued mentorship and guidance throughout the course of my training has allowed me grow as a scientist and person. I admire his incredible work ethic, scientific expertise, and greatly appreciate the opportunity to conduct my PhD training in his lab. I would like to thank my committee members: Dr. Paula Bos, Dr. Paul Dent, Dr. Khalid Matin, and Dr. Iain Morgan. Their highly impactful feedback and input throughout the duration of my research has been pivotal. Together, they helped elevate my training experience and challenge me to think in unconventional ways. To the Clinical and Translational Research (CCTR) program, I am deeply appreciative for the incredibly supportive, welcoming, and kind department that was provided during my training and feel incredibly grateful for all the scientific and career advice. I would like to thank the present (Dr. Parash Parajuli, Creighton Friend, Ting-Xuan Lu, Deanna Campbell, Dr. Qasim Khan) and past (Allyn Bryan, Thomas Foy, Sumit Saha, Dr. Sarah Thomas) members of the Atfi lab for creating an enjoyable and exciting lab environment. To my friends, thank you for standing by me through all the ups and downs; I will never forget it. Lastly, I would like to thank my family. I can't thank them enough for providing me with unwavering support and I truly would not be the person I am today without them.

## LIST OF FIGURES

<b>Figure 1:</b> Low <i>Prdm16</i> expression is significantly associated with low PDAC patient survival .....	56
<b>Figure 2:</b> <i>Prdm16</i> is transiently expressed during human PDAC progression .....	57
<b>Figure 3:</b> <i>Prdm16</i> is transiently expressed during PDAC progression in vivo .....	58
<b>Figure 4:</b> <i>KSC</i> mice display prolonged survival relative to <i>KIC</i> and <i>KPC</i> mice .....	59
<b>Figure 5:</b> <i>Prdm16</i> is transiently expressed during PDAC progression in <i>KIC</i> and <i>KPC</i> mice .....	60
<b>Figure 6:</b> <i>Prdm16</i> expression remains elevated during IPMN-to-PDAC progression in <i>KSC</i> mice .....	61
<b>Figure 7:</b> <i>Prdm16</i> expression is elevated in E-cadherin positive cells .....	62
<b>Figure 8:</b> Patients with low <i>Prdm16</i> expression exhibit decreased survival if they carry <i>SMAD4</i> mutations .....	63
<b>Figure 9:</b> <i>Prdm16</i> was successfully deleted in <i>Prdm16</i> <sup>KO</sup> mice .....	64
<b>Figure 10:</b> Ablation of <i>Prdm16</i> does not impact pancreatic histology .....	65
<b>Figure 11:</b> Ablation of <i>Prdm16</i> does not impact normal pancreatic function .....	66
<b>Figure 12:</b> <i>Prdm16</i> ablation does not perturb normal pancreatic function .....	67
<b>Figure 13:</b> Ablation of <i>Prdm16</i> does not impact blood glucose levels .....	67
<b>Figure 14:</b> Ablation of <i>Prdm16</i> in <i>KC</i> mice results in reduced survival .....	69
<b>Figure 15:</b> Inactivation of <i>Prdm16</i> accelerates- <i>Kras</i> <sup>G12D</sup> driven PDAC .....	70
<b>Figure 16:</b> <i>Prdm16</i> ablation expedites- <i>Kras</i> <sup>G12D</sup> driven PDAC .....	71
<b>Figure 17:</b> Ablation of <i>Prdm16</i> in <i>KSC</i> mice results in reduced survival .....	72
<b>Figure 18:</b> Inactivation of <i>Prdm16</i> dramatically accelerates PDAC progression in <i>KSC</i> mice .....	73
<b>Figure 19:</b> <i>Prdm16</i> is required for the IPMN-to-PDAC progression .....	74
<b>Figure 20:</b> <i>KSPrC</i> tumors present elevated metastatic potential .....	75
<b>Figure 21:</b> Human PDAC cell lines with functional and inactivated <i>PRDM16</i> injected into NSG mice did not exhibit different tumor growth or metastasis .....	76
<b>Figure 22:</b> <i>KSPrC</i> tumors metastasize to the lung .....	77
<b>Figure 23:</b> <i>KSC</i> mice have augmented <i>Prdm16</i> expression .....	78
<b>Figure 24:</b> Treatment of TGF- $\beta$ in mouse and human PDAC cell lines induces <i>Prdm16</i> expression .....	79
<b>Figure 25:</b> <i>SMAD4</i> inactivation mimics TGF- $\beta$ stimulation .....	80



<b>Figure 26:</b> Smad4 binds to the promoter of <i>PRDM16</i> irrespective of TGF- $\beta$ signaling .....	81
<b>Figure 27:</b> Smad3 and Smad2 bind to the <i>PRDM16</i> promoter upon TGF- $\beta$ stimulation .....	82
<b>Figure 28:</b> Prdm16 binds to its own promoter in the absence of TGF- $\beta$ signaling .	83
<b>Figure 29:</b> Prdm16 interacts with Smad4 on the <i>PRDM16</i> promoter when TGF- $\beta$ signaling is not present.....	84
<b>Figure 30:</b> Prdm16 represses its own transcription via Smad4.....	85
<b>Figure 31:</b> <i>KT<math>\beta</math>C</i> and <i>KSPrC</i> mice exhibit similar survival rates .....	86
<b>Figure 32:</b> <i>KSPrC</i> and <i>KT<math>\beta</math>C</i> mice exhibit a PDAC phenotype that mimic each other .....	88
<b>Figure 33:</b> <i>KSPrC</i> and <i>KT<math>\beta</math>C</i> mice display a matching PanIN-to-PDAC progression .....	89
<b>Figure 34:</b> Model for the functional interaction between Smad4 and Prdm16 during PDAC formation and progression.....	92

## LIST OF ABBREVIATIONS

AML	Acute myeloid leukemia
ATCC	American Type Culture Collection
BMPs	bone morphogenetic proteins
BrdU	5'-Bromo-2'-Deoxyuridine
CAFs	cancer-associated fibroblasts
ChIP	Chromatin immunoprecipitation
CK19	cytokeratin 19
CTGF	connective tissue growth factor
DMEM	Dulbecco's modified Eagle's medium
ECL	Enhanced chemiluminescence
ECM	extracellular matrix
EGF	epidermal growth factor
EGFR	epidermal growth factor receptor
EMT	Epithelial-to-mesenchymal transition
FBS	fetal bovine serum
FOLFIRINOX	Folinic acid, Fluorouracil, Irinotecan, and Oxaliplatin
G12	glycine-12
GAPs	GTPase activated proteins
GEFs	guanine nucleotide exchange factors
GEMMs	genetically engineered mouse models
GSEA	gene set enrichment analysis
H&E	hematoxylin and eosin
H3K4	histone-3 Lysine-4
IACUC	Institutional Animal Care and Use Committee
IF	immunofluorescence
IHC	immunohistochemistry
iMEFs	Immortalized mouse embryonic fibroblasts
IP	immunoprecipitation
IPMN	intraductal papillary mucinous neoplasia
JNK	JUN N-terminal kinase
<i>KC/Kras<sup>G12D</sup></i>	<i>LSL-Kras<sup>G12D</sup>;Pdx1-Cre</i>
<i>KIC</i>	<i>LSL-Kras<sup>G12D</sup>;p16<sup>Luc+/+</sup>;Pdx1-Cre</i>
<i>KPC</i>	<i>LSL-Kras<sup>G12D</sup>;LSL-Trp53<sup>fl/fl</sup>;Pdx1-Cre</i>
<i>KPrC</i>	<i>LSL-Kras<sup>G12D</sup>;Prdm16<sup>fl/fl</sup>;Pdx1-Cre</i>
<i>KSC</i>	<i>LSL-Kras<sup>G12D</sup>;Smad4<sup>fl/fl</sup>;Pdx1-Cre</i>
<i>KSPrC</i>	<i>LSL-Kras<sup>G12D</sup>;Smad4<sup>fl/fl</sup>;Prdm16<sup>fl/fl</sup>;Pdx1-Cre</i>
<i>KTβC</i>	<i>LSL-Kras<sup>G12D</sup>;TβR2<sup>fl/fl</sup>;Pdx1-Cre</i>
L1CAM	L1 cell adhesion molecule
LOH	loss of heterozygosity
LoxP	X-over P1
<i>LSL-Kras<sup>G12D</sup></i>	<i>Loxp-Stop-Loxp-Kras<sup>G12D</sup></i>

MAPK	mitogen activated protein kinase
MCN	mucinous cystic neoplasia
Mdm2	mouse double minute 2 homolog
MDSCs	myeloid-derived suppressor cells
MMPs	matrix metalloproteinases
mTOR	mechanistic target of rapamycin
NF- $\kappa$ B	nuclear factor- $\kappa$ B
NK	natural killer
Nox4	NADPH oxidase 4
NSG	NOD <i>scid</i> gamma
p14	p14Arf/p19Arf
p16	p16Ink4a
<i>p16<sup>Luc</sup></i>	<i>p16Ink4A-Luciferase</i>
PanIN	pancreatic intraepithelial neoplasia
PDAC	pancreatic ductal adenocarcinoma
PDGFR $\beta$	platelet-derived growth factor receptor $\beta$
PI3K	phosphoinositide 3-kinase
PNEC	pancreatic neuroendocrine carcinoma
Prdm16	PR domain containing 16
<i>Prdm16<sup>fl/fl</sup></i>	<i>Prdm16<sup>fl/fl</sup>;Pdx1-Cre</i>
PSCs	pancreatic stem cells
RNAi	RNA interference
ROCK	Rho-associated protein kinase
ROS	reactive oxygen species
SBE	Smad conserved binding elements
scRNA-seq	Single-cell RNA sequencing
SEM	Standard error of the mean
<i>SMAD4.Mut</i>	<i>Mutant Smad4</i>
<i>SMAD4.WT</i>	<i>Wildtype SMAD4</i>
TCGA	The Cancer Genome Atlas
TGF- $\beta$	transforming growth factor-beta
TMA	tissue microarrays
T $\beta$ RI	TGF-beta type I receptor
T $\beta$ RII	TGF-beta type II receptor
Ucp1	uncoupling protein 1
UMMC	University of Mississippi Medical Center
VCU	Virginia Commonwealth University
WB	immunoblotting
$\alpha$ -SMA	alpha-smooth muscle actin

# TABLE OF CONTENTS

<b>1</b>	<b>INTRODUCTION .....</b>	<b>10</b>
1.1	Anatomy and physiology of the pancreas .....	10
1.2	Pancreatic Ductal Adenocarcinoma - PDAC.....	12
1.2.1	Subtypes and statistics .....	12
1.2.2	Precursor lesions.....	12
1.3	Standard of care treatments for PDAC.....	13
1.4	Genetic alterations and mouse models in PDAC.....	14
1.4.1	<i>KRAS</i> .....	15
1.4.2	<i>CDKN2A</i> .....	18
1.4.3	<i>TP53</i> .....	20
1.4.4	<i>SMAD4</i> .....	22
1.4.5	<i>TβRII</i> .....	24
1.5	TGF-β signaling in PDAC.....	25
1.5.1	TGF-β as a tumor suppressor.....	26
1.5.2	TGF-β as a tumor promoter .....	27
1.5.3	TGF-β signaling.....	28
1.6	Prdm16.....	28
1.6.1	Adipose tissue and metabolism .....	29
1.6.2	Heterochromatin formation, cancer, and TGF-β signaling.....	30
<b>2</b>	<b>ANTAGONISM BETWEEN PRDM16 AND SMAD4 SPECIFIES THE TRAJECTORY AND PROGRESSION OF PANCREATIC CANCER .....</b>	<b>34</b>
2.1	Abstract .....	34
2.2	Introduction.....	36
2.3	Materials and Methods.....	40
2.3.1	Plasmids .....	40
2.3.2	Antibodies.....	41
2.3.3	Cell Lines and Culture.....	42
2.3.4	In vitro and in vivo cell proliferation assays .....	43
2.3.5	Mice .....	44
2.3.6	Clinical Samples.....	45

2.3.7	Kaplan-Meier survival analysis in patients with wild-type or mutant <i>SMAD4</i> .....	45
2.3.8	<i>PRDM16</i> expression in patients with or without <i>SMAD4</i> mutations... ..	46
2.3.9	qRT-PCR .....	46
2.3.10	Chromatin Immunoprecipitation Assay.....	48
2.3.11	Luciferase Reporter Assay.....	49
2.3.12	Co-immunoprecipitation .....	50
2.3.13	Immunoblotting.....	50
2.3.14	Histology, Immunohistochemistry and Immunofluorescence .....	51
2.3.15	Statistical Analysis.....	54
2.4	Results.....	56
2.4.1	Transient expression of Prdm16 during PDAC progression.....	56
2.4.2	Prdm16 accelerates Kras <sup>G12D</sup> -driven PDAC.....	63
2.4.3	Requirement of Prdm16 for IPMN-to-PDAC progression .....	71
2.4.4	Repression of Prdm16 expression by Smad4.....	77
2.4.5	Concomitant inactivation of Prdm16 and Smad4 recapitulates the global inactivation of TGF- $\beta$ signaling .....	85
2.5	Discussion .....	89
<b>3</b>	<b>SUMMARY AND FUTURE DIRECTIONS.....</b>	<b>122</b>

## ABSTRACT

The transcription factor Prdm16 functions as a potent suppressor of transforming growth factor-beta (TGF- $\beta$ ) signaling, whose inactivation is deemed essential to the progression of pancreatic ductal adenocarcinoma (PDAC). Using the Kras<sup>G12D</sup>-based mouse model of human PDAC, we surprisingly found that ablating *Prdm16* did not block but instead accelerated PDAC formation and progression, suggesting that Prdm16 might function as a tumor suppressor in this malignancy. Subsequent genetic experiments showed that ablating *Prdm16* along with *Smad4* resulted in a shift from a well-differentiated and confined neoplasm to a highly aggressive and metastatic disease, which was associated with a striking deviation in the trajectory of the premalignant lesions. Mechanistically, we found that Smad4 interacted with and recruited Prdm16 to repress its own expression, therefore pinpointing a model in which Prdm16 functions downstream of Smad4 to constrain the PDAC malignant phenotype. Collectively, these findings unveil an unprecedented antagonistic interaction between the tumor suppressors Smad4 and Prdm16 that functions to restrict PDAC progression and metastasis.

# 1 INTRODUCTION

## 1.1 Anatomy and physiology of the pancreas

The pancreas is a gland behind the stomach comprised of anatomically distinct head, body, and tail segments. It is approximately seven and a half centimeters in length, three ounces in weight, and has a pear-shaped form with the head situated on the right side of the abdomen and the tail extending towards the left ([Innes and Carey, 1994](#); [Kreel et al., 1977](#)). The pancreas carries out both endocrine and exocrine functions, with the release of hormones into the bloodstream, and secretion digestive enzymes into the small intestine through a network of ducts, respectively. Endocrine hormones, such as insulin and glucagon, assist in the regulation of blood sugar levels by either facilitating the uptake and storage of glucose in cells or promoting the breakdown of glycogen and fats to generate energy. Amylase, lipase and trypsin, which are a part of the exocrine tissue, aid in the breakdown of carbohydrates, fats, and proteins in the diet into smaller molecules that can be absorbed and used by the body ([Roder et al., 2016](#)).

The pancreas is composed of various types of cells, consisting of acinar, islet, ductal, stellate, and stem cells ([Apte et al., 2012](#); [Bonner-Weir and Sharma, 2002](#); [Slack, 1995](#)). Acinar cells make up the majority of the exocrine tissue in the pancreas and are responsible for synthesizing and secreting digestive enzymes into the small intestine ([Williams, 2010](#)). The Islets of Langerhans (also referred to as islets) are clusters of cells found within the pancreas that produce hormones which play a critical role in regulating glucose metabolism. Islets are composed of several different types

of cells, including  $\alpha$ ,  $\beta$ ,  $\delta$ , and PP cells which produce glucagon, insulin, somatostatin, and pancreatic polypeptide, respectively ([Brereton et al., 2015](#)). Pancreatic ductal cells are primarily responsible for synthesizing a bicarbonate rich fluid that works to neutralize the acidity of the stomach chyme which is required for the proper digestion of food as well as protecting the pancreas and the other organs of the gastrointestinal tract from the corrosive effects of stomach ([Grapin-Botton, 2005](#)). Furthermore, ductal cells also express various transcription factors, such as Hnf6, Pdx-1, and HNF1b, which each play a key role in pancreatic development ([Reichert and Rustgi, 2011](#)). Pancreatic stellate cells are located in the periacinar and perivascular regions of the pancreas where their function is to facilitate in creating the extracellular matrix (ECM). Under physiological conditions, pancreatic stellate exist in a quiescent state, however, when the pancreas experiences damage, these cells become activated, proliferate, and migrate to the site of injury promoting tissue repair and remodeling of the ECM ([Jin et al., 2020](#)). Upon activation, pancreatic stellate cells differentiate into myofibroblasts, which can be distinguished by their contractile actin stress fibers and expression of alpha-smooth muscle actin ( $\alpha$ -SMA), providing them with the capability to exert tension and influence the mechanical properties of the surrounding tissue ([Ferdek and Jakubowska, 2017](#); [Hinz and Gabbiani, 2003](#)). Lastly, pancreatic stem cells (PSCs) are a subpopulation of cells within the pancreas that can differentiate into all cell types within the organ and play an important role in preventing of damage, fibrosis, and inflammation of the pancreas ([Chela et al., 2020](#)). The accumulation dysfunctional pancreatic processes can ultimately result in the development of severe diseases, such as pancreatitis, diabetes, or pancreatic cancer.



## **1.2 Pancreatic Ductal Adenocarcinoma - PDAC**

### **1.2.1 Subtypes and statistics**

Pancreatic cancer can be defined by two histologically distinct subtypes of pancreatic ductal adenocarcinoma (PDAC) or pancreatic neuroendocrine carcinoma (PNEC), where PDAC represents the majority of exocrine tumors. Pancreatic cancer is one of the most lethal solid malignancies, evidenced by its ranking as the fourth leading cause of cancer-related deaths ([Cancer.net, 2022](#)). Despite a low incidence rate of 3%, PDAC is highly lethal due to the fact that patients are often not diagnosed until they present both advanced local progression and metastatic disease. Consequently, the 5-year survival rate of pancreatic cancer only remains at 12% with a highly unfavorable prognosis ([Society, 2023](#)).

### **1.2.2 Precursor lesions**

PDAC tumors most commonly develop from precursor lesions called pancreatic intraepithelial neoplasia (PanIN), which progress through stages 1, 2, and 3 before reaching full-blown PDAC ([Mizrahi et al., 2020](#)). Alternatively, PDAC can arise from intraductal papillary mucinous neoplasia (IPMN), defined by lesions greater than 1 cm in size with low, intermediate, and high grade classifications ([F. T. Bosman, 2010](#)). Finally, a third type of premalignant lesion termed mucinous cystic neoplasia (MCN) that commonly occurs in the tail and body of the pancreas can also develop into PDAC ([Mizrahi et al., 2020](#)). Notably, MCN is far less common than IPMN and can

be histologically distinguished by the presence of ovarian-like stroma ([F. T. Bosman, 2010](#)).

### **1.3 Standard of care treatments for PDAC**

Individualized treatment plans for PDAC are developed based on a variety of factors, such as tumor stage, location, general patient health, and patient preferences ([Seghers et al., 2022](#)). Surgery is typically the first-line treatment for localized PDAC, where the most common surgical procedure is commonly called a Whipple procedure which entails removing the head of the pancreas, gallbladder, bile duct, and a portion of the stomach and small intestine. Other surgical options consist of a distal pancreatectomy (removal of the body and tail of the pancreas in addition to usually the spleen) or less commonly a total pancreatectomy (the removal of the entire pancreas) ([Institute, 2020](#)). Given that PDAC is typically diagnosed in late and advanced stages, only about 10% of patients are candidates for surgery ([Mohammad, 2018](#)). Therefore, another common modality of treatment for PDAC is radiation therapy, which utilizes high-energy X-rays or other forms of radiation to terminate cancer cells ([Institute, 2020](#)). Radiation therapy can also be utilized in conjunction with chemotherapy to reduce the size of tumors prior to surgery or to alleviate symptoms in patients who are unable to undergo surgery. For chemotherapy, the two regimens most frequently employed to treat PDAC are FOLFIRINOX (consisting of Folinic acid, Fluorouracil, Irinotecan, and Oxaliplatin) and gemcitabine nab-paclitaxel (Gemcitabine conjugated with nanoparticle albumin-bound paclitaxel). ([Grossberg et al., 2020](#)). Overall, the best approach for an

individual patient is often a combination of treatments tailored to the patient's specific needs and circumstances. It's important to note that despite the advances in cancer therapeutics, PDAC remains one of the most challenging cancer types to treat and often has a poor prognosis ([Wu et al., 2019](#)).

## **1.4 Genetic alterations and mouse models in PDAC**

Landmark advancements in research tools have led to the creation of genetically engineered mouse models (GEMMs) for investigating the progression of human PDAC. For instance, several mouse models for PDAC use the Cre-Lox system as a genetic manipulation technique to enable the conditional activation or suppression of particular genes in a target tissue like the pancreas ([Kim et al., 2018](#)). This system involves the utilization of Cre recombinase, an enzyme that facilitates recombination, to bind specific DNA sequences called locus of X-over P1 (LoxP) sites that are located on the genome of the mouse. The LoxP sites are palindromic DNA sequences that are inverted relative to each other. When the Cre recombinase enzyme binds to both LoxP sites, it induces a recombination event that can yield a deletion, insertion, or inversion of DNA sequences located between the two LoxP sites ([Nagy, 2000](#)). In the context of PDAC, researchers can use the Cre-Lox system to conditionally express or knockout specific genes. For instance, the Cre-Lox system can be used to either express an oncogene or inactivate a tumor suppressor gene, resulting in tumor formation ([Magnuson and Osipovich, 2013](#)). These genetically engineered models can facilitate the understanding of cellular and molecular processes that drive PDAC progression to develop new treatments for the disease.

A majority of mice used to generate models with pancreas-specific genetic alterations are crossed with *Pdx1-Cre* mice, which express Cre recombinase in all pancreatic progenitor cells that differentiate into acinar, ductal, and islets tissue during the earliest stages of development at E8.5 (Gu et al., 2003). For example, a mouse model of the oncogene *Kras* can be developed by crossing a *Pdx1-Cre* mouse with a *Lox-Stop-Lox (LSL)-Kras<sup>G12D</sup>* mouse, resulting in the offspring containing pancreas-specific expression of oncogenic *Kras*, designated as *LSL-Kras<sup>G12D</sup>;Pdx1-Cre* (Tuveson et al., 2004). Mouse models have also been developed in order to investigate the role of transgenes in different compartments of the pancreas (i.e., acinar, duct, and islet). For instance, mouse models utilizing the Ptf1a-p48 (p48) transcription factor result in transgene gain or loss-of-function specific to acinar cells of the pancreas, where p48 is expressed slightly later than *Pdx1* during development at E9.5 (Hingorani et al., 2003). Similarly, the *Ins2* and *Sox9* transcription factors lead to genetic alterations in  $\beta$  (in the islet of Langerhans) and ductal cells, respectively (Magnuson and Osipovich, 2013).

#### 1.4.1 KRAS

The *LSL-Kras<sup>G12D</sup>;Pdx1-Cre* mouse model (referred to as *Kras<sup>G12D</sup>* mouse model) was the first of its kind to accurately simulate the natural progression of human PDAC in mice (Hingorani et al., 2003). In this model, researchers utilized the Cre-Lox system to induce the expression of oncogenic *Kras* specifically in the pancreas, leading to the formation of PDAC after roughly 20 weeks of age. (Tuveson et al., 2004). The

*Kras*<sup>G12D</sup> mouse model can be further modified to more accurately reflect the complexity of human PDAC by introducing additional transgenes.

Kras is a GTPase which operates as a molecular switch that becomes active when it binds to GTP and inactive when bound to GDP (Bos et al., 2007). Kras, like other members of the Ras family of proteins, is comprised of two domains: a membrane-targeting domain and a G domain (Buscail et al., 2020). Under physiological conditions, Kras remains inactivated as it is bound to GDP. However, when an extracellular ligand interacts with its receptor (such as epidermal growth factor (EGF) interacting with epidermal growth factor receptor (EGFR)), Kras associates with GTP and becomes activated, thereby triggering a range of intracellular processes (Waters and Der, 2018). The cycling of Kras between its GTP and GDP forms is controlled by guanine nucleotide exchange factors (GEFs), which promote the exchange of nucleotides, and GTPase activated proteins (GAPs), inducing the hydrolysis of GTP bound to Kras (Buscail et al., 2020).

In PDAC, *KRAS* is frequently mutated at glycine-12 (G12), which impairs its normal GTPase function and prevents GAPs from converting GTP to GDP (Waters and Der, 2018). Specifically, the mutation at glycine-12 in *KRAS* accounts for 98% of all mutations in the gene, with *KRAS*<sup>G12D</sup> being the most common form of this mutation (Bryant et al., 2014). Other less common point mutations that occur in the *KRAS* gene are at codons 11, 13, 61, or 146 (Bijlsma et al., 2017; Bournet et al., 2016; Delpu et al., 2011; Haigis, 2017). Mutations in *KRAS* are considered an initiation mutation, as it is observed in 90% of low grade PanIN lesions resulting in the inability for GAPs to hydrolyze GTP bound to Kras, leading in the constitutive

activation of downstream signaling pathways that promote cell survival and proliferation ([di Magliano and Logsdon, 2013](#); [Hezel et al., 2006](#)).

Kras interacts with more than 80 different proteins, activating a number of growth-promoting pathways, including the nuclear factor- $\kappa$ B (NF- $\kappa$ B), mitogen activated protein kinase (MAPK), phosphoinositide 3-kinase (PI3K)/Akt, mechanistic target of rapamycin (mTOR), and JUN N-terminal kinase (JNK). Kras activation also stimulates the expression of c-Jun, c-Myc, and Elk transcription factors, leading to an increase in cell proliferation, survival, differentiation, and transformation ([Jonckheere et al., 2017](#)). The current model of PDAC posits an initiating mutation in the *KRAS* oncogene followed by subsequent inactivating mutations in the tumor suppressor genes *CDKN2A*, *SMAD4*, and *TP53* lead to disease progression and metastasis ([Hayashi et al., 2021](#); [Iacobuzio-Donahue, 2012](#)).

The prevalence of oncogenic *KRAS* mutations in nearly 90% of human PDAC cases highlights its critical role in initiation of the disease ([Hayashi et al., 2021](#)). However, while it is widely recognized that a mutation in *KRAS* is necessary for the start of PDAC, there was previously still some debate about whether this mutation is necessary to sustain PDAC. To address whether mutant *KRAS* is necessary for PDAC maintenance, Ying et al. developed a mouse model encompassing the ability to switch oncogenic *Kras* (*Kras*<sup>G12D</sup>) on and off. Interestingly, their results revealed that oncogenic *Kras* is pivotal for the persistent growth of PDAC lesions ([Ying et al., 2012](#)). Other studies have shown that mutations in *Kras* can modify tumor metabolism and upregulate glycolysis, which is the primary source of energy for many tumor cells ([Chiaradonna et al., 2005](#); [Chiaradonna et al., 2006](#); [Vander Heiden et al., 2009](#);

[Vizan et al., 2005](#)). *Kras* has been shown to promote glycolysis by stimulating the expression of the glucose transporter GLUT1, which mediates increased glucose uptake and elevated levels of glycolysis. This mechanism allows for continued cell survival in glucose-deprived conditions and increased production of lactate ([Gaglio et al., 2011](#); [Yun et al., 2009](#)). Other than perturbations in glycolysis, *Kras* mutations have been also shown to stimulate LC3 expression, indicating increased levels of autophagy. Studies have shown that both genetic depletion of autophagy (*Atg5* ablation) and pharmacological inhibition (chloroquine treatment) yielded decreased PDAC cell growth both in vitro and in vivo, suggesting that autophagy is essential for sustaining PDAC cells with *Kras* mutations. Mechanistically, inhibition of autophagy resulted in increased reactive oxygen species (ROS), decreased mitochondrial oxidative phosphorylation, and elevated DNA damage ([Yang et al., 2011](#)). Apart from its effect on tumor cell metabolism, considered one of the hallmarks of cancer, *Kras* mutations have been shown to promote tumor growth through other mechanisms, including chemotherapy resistance and evasion of immune cell detection ([Hanahan, 2022](#); [Tao et al., 2014](#)).

#### 1.4.2 CDKN2A

Following a mutation in *KRAS*, studies have discovered that inactivation of the tumor suppressor gene *CDKN2A* occurs in about 98% of PDAC cases, where the *CDKN2A* gene encodes for the two proteins p16Ink4a (p16) and p14Arf (p14) ([Saiki et al., 2021](#)). The p16 protein serves as a Cdk4/Cdk6 inhibitor preventing their association with D-type cyclins and functions to arrest the G1-S phase transition of the cell cycle

(Zhao et al., 2016). The p14 protein is expressed through an alternative open reading frame on the *CDKN2A* gene and stimulates p53-dependent cell cycle arrest via repression of mouse double minute 2 homolog (Mdm2), thereby preventing p53 degradation. Inactivation of *CDKN2A* can occur by multiple mechanisms, such as homozygous deletion, hypermethylation, or the concomitant loss of a wild-type allele paired with a mutation (Lin et al., 2020).

In order to study the function of *CDKN2A* in PDAC, GEMMs have been developed ablating *CDKN2A* with the Cre-Lox system. Inactivation of *p16Ink4a* alone was insufficient to result in PDAC malignancy (Sharpless et al., 2001). Therefore, mouse models were created with both the activation of oncogenic Kras ( $Kras^{G12D}$ ) expression and deletion of the tumor suppressor gene *p16Ink4a* exclusive to the pancreas. Using this model, Bardeesy et al. demonstrated that concomitant inactivation of *p16Ink4a* with expression of  $Kras^{G12D}$  in mice (referred to as *KIC* mice) results in a more rapid progression from the PanIN to PDAC phenotype relative to mice with  $Kras^{G12D}$  expression alone. Histological analysis revealed that *KIC* mice develop the ductal adenocarcinoma phenotype as indicated by H&E and immunohistochemical staining against the ductal marker CK19 (Bardeesy et al., 2006a).

In PDAC, *CDKN2A* inactivation occurs predominantly during PanIN stage 2 (Wilentz et al., 1998). Notably, inactivation of *CDKN2A* is crucial for PDAC disease progression, as the p16 protein expressed from the *CDKN2A* gene is responsible for inducing senescence after a mutation in *KRAS* (Maitra et al., 2003). Additional studies have also shown that *KIC* tumors exhibit augmented expression of NADPH oxidase



4 (Nox4), an enzyme that oxidizes NADPH, elevating glycolysis level and shedding light on one of the mechanisms by which *p16INK4A* inactivation promotes PDAC progression (Ju et al., 2017). It is interesting to note that *p14ARF* is only inactivated in cases where *CDKN2A* is deleted, which accounts for only 40% of *CDKN2A* inactivation mechanisms (Rozenblum et al., 1997; Schutte et al., 1997). Additionally, epigenetic modifications that inhibit *p16Ink4a* transcription do not impact p14, hinting that p14 inactivation is a downstream effect of disabling p16 and is considered to be less critical than that of p16. Despite these results, p14 has still been shown to impede key proliferative pathways, such as NF- $\kappa$ B, c-Myc, and ribosomal RNA processing in a p53-independent manner (Qi et al., 2004; Rocha et al., 2003; Sugimoto et al., 2003). Together, these data suggest that p14 still maintains a crucial role as a tumor suppressor gene, but not to the same extent as p16.

#### 1.4.3 TP53

Under basal conditions, p53 acts as a cell cycle inhibitor to facilitate DNA repair or apoptosis. If a cell experiences significant damage, p53 acts to promote apoptosis and prevents the transmission of damaged DNA to future cell divisions in order to maintain genomic integrity (Ozaki and Nakagawara, 2011). However, *TP53* mutations, which are considered the most prevalent across all types of cancer, often result in its inactivation (Baugh et al., 2018). In PDAC, 50-75% of human cases exhibit *TP53* mutations which commonly occur during later stages of the disease, such as PanIN stage 3 (Morton et al., 2010). *TP53* mutations can transpire in the form of a missense mutation or loss of heterozygosity (LOH), arising either in residues involved

in DNA-interaction or within its own structure that prevent its ability to appropriately bind DNA (Barton et al., 1991; Joerger and Fersht, 2007; Rozenblum et al., 1997). As a result, p53 is unable to properly function as a transcription factor promoting the expression of cell cycle arrest and pro-apoptotic factors, including p21, Bax, Noxa, and Puma in response to DNA damage or cellular stress (Khoo et al., 2014).

Given that *TP53* mutations occur in the later stages of PDAC, mouse models that study its function are often generated in combination with *Kras*<sup>G12D</sup> expression to better mimic human disease. The customarily used mouse model involves concomitant *Kras*<sup>G12D</sup> expression with *Trp53*<sup>R172H</sup> and *Pdx1* using the Cre-Lox system (referred to as *KP*<sup>R172H</sup>*C* mice). *KP*<sup>R172H</sup>*C* mice consistently display a rapid progression from PanIN to PDAC by 10 weeks of age with lesions that recapitulate human PDAC. Furthermore, the onset of PDAC in *KP*<sup>R172H</sup>*C* mice takes place at a rate significantly quicker than that of mice with *Kras*<sup>G12D</sup> expression alone (Hingorani et al., 2005). Interestingly, landmark studies revealed that either loss or mutation of the *Trp53* gene drives the survival and accumulation of cells that express the oncogenic *Kras*<sup>G12D</sup>, causing a quick premalignant-to-full-blown PDAC progression. Mutant *Trp53* also drives PDAC advancement and metastasis through its ability to escape *Kras*<sup>G12D</sup>-induced growth arrest. In contrast to p53 deficient tumors, which do not exhibit any metastases, tumors with mutant p53 have been shown to function metastatically (Morton et al., 2010). Other important studies have shown that mutant p53 encourages the expression of platelet-derived growth factor receptor  $\beta$  (PDGFR $\beta$ ) by interacting with p73, thereby promoting a metastatic phenotype in PDAC through a feedforward loop that increases cell motility and invasiveness. The

validity of these findings was confirmed through experiments utilizing small molecules and RNA interference (RNAi) to inhibit PDGFR $\beta$ , which resulted in the prevention of cell invasion in vitro and metastasis in vivo ([Weissmueller et al., 2014](#)). Additionally, tumors with mutant p53 display increased fibrosis and reduced infiltration of cytotoxic CD8+ T cells, providing one potential mechanism by which these cells can evade the immune system, as it decreases response to cancer therapeutics. Moreover, it provides insight into why the PDAC microenvironment is often characterized by a lack of immune cell infiltration, also known as an "immunologically cold" environment. Finally, mutant p53 can induce chemoresistance in tumors through multiple mechanisms, including the stimulation of target genes involved in cell cycle progression, such as *Cdk1* and *CCNB1*, as well as mediating the downregulation of miR-223 ([Fiorini et al., 2015](#); [Masciarelli et al., 2014](#)). The aforementioned data collectively demonstrates the significant effect of TP53 in disrupting cell proliferation pathways and the tumor microenvironment, both of which are critical in the development of PDAC and determining patient prognosis ([Maddalena et al., 2021](#)).

#### 1.4.4 SMAD4

Another gene frequently disrupted in PDAC is *SMAD4*, with mutations present in about 55% of all PDAC cases ([Hahn et al., 1996](#)). *SMAD4* is situated on chromosome 18q, where its associated protein consists of two domains: MH1 and MH2 domains connected by a linker. While the MH1 domain functions to interact with the Smad conserved binding elements (SBE) on DNA, the MH2 domain is responsible for its transcriptional activity ([Furukawa et al., 2006](#); [Zhao et al., 2018](#)). *SMAD4* inactivation

in PDAC can result from either mutations or homozygous deletion of both copies of the gene. (Hahn et al., 1996). According to Xia et al., approximately 30% of PDAC cases exhibit homozygous deletion of the *SMAD4* gene, 20% show inactivation of the gene, and 90% display a loss of one of the two copies of *SMAD4* on chromosome 18q (Xia et al., 2015). Mouse models involving *Smad4* to study PDAC have been generated predominantly in the context of *Kras*<sup>G12D</sup>, as ablation of *Smad4* alone resulted in no changes in pancreatic development or physiology (referred to as *KSC* mice). However, the onset of PDAC formation in *KSC* mice occurs significantly quicker compared to those with *Kras*<sup>G12D</sup> expression alone. Interestingly, *KSC* mice are known to develop premalignant lesions that resemble IPMN in humans compared to their *Kras*<sup>G12D</sup> counterparts, which develop PanIN prior to progressing to full-blown PDAC. Additionally, tumors with inactivated *Smad4* are resistant to metastasis, as indicated by elevated levels of epithelial markers, such as E-cadherin (Bardeesy et al., 2006b). Key studies by Whittle et al. confirmed the same observation, where mice deleted of *Smad4* also did not display any metastasis. Whittle et al. also identified that Runx3, a member of the runt-related transcription factors, acts as a molecular switch to promote metastasis in tumors with sufficient *Smad4* by remodeling the ECM (Whittle et al., 2015).

*Smad4* also functions to suppress tumor growth through several mechanisms. For example, the inactivation of *SMAD4* in PDAC has been shown to result in increased expression of CD133, a stem cell marker known to be required for PDAC maintenance (Chen et al., 2014). Additionally, *SMAD4* inactivation in the context of oncogenic *Kras*<sup>G12D</sup> expression stimulates the transcription and activation of EGFR

and erbB2 in vivo, as evidenced by increased levels of phosphorylated Erk1/2 and Akt, which are downstream targets of erbB receptors (Zhao et al., 2010). Finally, it has been demonstrated that PDAC cells with a mutation in *SMAD4* can generate an immunosuppressive tumor microenvironment through the recruitment of myeloid-derived suppressor cells (MDSCs) accomplished by reducing calcium flux and increasing glycolytic activity (Basso et al., 2017).

#### 1.4.5 *TβRII*

Mutations or deletions of the *TGF-beta type II receptor (TβRII)* gene have been identified in approximately 4% of all PDAC cases (Iacobuzio-Donahue, 2012; Ijichi et al., 2006). Deletion of *TβRII* in combination with *Kras*<sup>G12D</sup> expression (referred to as *KTβC* mice) has been shown to result in highly aggressive PDAC with a short latency period. In these mice, the majority of animals develop PDAC between 7-10 weeks of age in addition to metastasis. Moreover, *KTβC* mice follow the PanIN-to-PDAC sequence as opposed to the IPMN-to-PDAC progression trajectory seen in mice with *Smad4* inactivation. Mice with heterozygous loss of *TβRII* in combination with *Kras*<sup>G12D</sup> expression also develop tumors with a similar histological appearance to *KTβC* tumors, but with a longer latency period compared to mice with homozygous loss of *TβRII*. Overall, these data suggest that inactivation of *TβRII* likely cooperates with *Kras* signaling activity in order to promote the development of PDAC (Ijichi et al., 2006). Intriguingly, studies have demonstrated that tumors with both *Kras*<sup>G12D</sup> expression and *TβRII* ablation maintain functional expression of the *Smad4* at the protein level, as well as normal expression of the p53 protein (demonstrated by

gamma irradiation). Conversely, these tumors showed variable levels of p16ink4a protein and an absence of p19Arf (p14Arf) protein, despite the fact that p19Arf is expressed from an alternative open reading frame of the *CDKN2A* gene. It was further demonstrated that *p19ARF* mRNA was detected in tumors with concomitant Kras<sup>G12D</sup> expression and *TβRII* inactivation, leaving future work to investigate the distinct observation at the level of the mRNA and protein. Additional observations suggest that the inactivation of *TβRII* does not affect the induction of the PI3K/Akt pathway, despite previous studies suggesting that TGF-β and Kras may synergistically activate this pathway (Ijichi et al., 2006; Janda et al., 2002). Studies investigating the mechanism underlying the aggressive PDAC phenotype in *KTβC* mice revealed elevated levels of connective tissue growth factor (CTGF) in the stroma of these mice, particularly in close proximity to the tumor. In contrast, CTGF was not detected in the stroma of mice with Kras<sup>G12D</sup> expression alone, indicating that the concomitant effects of oncogenic Kras with *TβRII* inactivation contribute to the more aggressive PDAC phenotype (Ijichi et al., 2006). Stromal expression of CTGF has been shown to stimulate tumor cell production of CXC chemokines, promoting PDAC progression and was validated by the fact that treatment with Cxcr2 inhibitors decreased stromal CTGF expression, reduced tumor progression, and prolonged survival (Ijichi et al., 2011).

## 1.5 TGF-β signaling in PDAC

The transforming growth factor beta (TGF-β) signaling pathway is a critical cellular cascade responsible for regulating various biological processes, including cell

growth, differentiation, and apoptosis (David and Massague, 2018). The TGF- $\beta$  signaling pathway normally helps to regulate cell proliferation and maintain homeostasis, but in cancer cells, this same pathway becomes manipulated to support cell survival, proliferation, and immune evasion (Massague, 2008). In the later stages of PDAC, TGF- $\beta$  signaling is frequently hyperactivated and promotes the formation of desmoplastic stroma (Friess et al., 1993). Additionally, several components of the TGF- $\beta$  signaling pathway are altered throughout PDAC, including mutations in *TGF- $\beta$  receptors (type I and type II)*, overexpression of TGF- $\beta$ 1 ligand, and loss of TGF- $\beta$  inhibitory proteins such as Smad4 (Dardare et al., 2020; Goggins et al., 1998; Park et al., 2020). Intriguingly, the TGF- $\beta$  signaling pathway possesses a dual role as both a tumor promoter and suppressor depending on the context and stage of signaling, where these alterations lead to aberrant TGF- $\beta$  signaling activity, which facilitate tumor cell growth (Massague, 2008).

#### 1.5.1 TGF- $\beta$ as a tumor suppressor

TGF- $\beta$  functions as a tumor suppressor primarily in normal and premalignant cells (Dardare et al., 2020). For example, TGF- $\beta$  can diminish cell cycle progression by inhibiting *p15<sup>INK4B</sup>* expression and p21<sup>Cip1</sup>, which prevents the association between cyclin D-Cdk4/6 and cyclin E/A-CDK2 complexes, respectively (Dardare et al., 2020; Gomis et al., 2006; Seoane et al., 2004). The TGF- $\beta$  signaling pathway also functions as a tumor suppressor by inducing apoptosis via epithelial-to-mesenchymal transition, where Smad4 interacts with Smad2/3 to promote Snail and Sox4 expression, which in turn represses Klf5 expression (David et al., 2016). Lastly, TGF-

$\beta$  can also suppress PDAC cell growth in a p53-independent manner ([Singh et al., 2007](#)).

#### 1.5.2 TGF- $\beta$ as a tumor promoter

As a tumor promoter, TGF- $\beta$  functions during the later stages of PDAC malignancy. For example, TGF- $\beta$  activity upregulates the transcription factors Snail, Slug, Twist1, or Zeb1 to drive EMT and vascular endothelial growth to support angiogenesis ([Ferrari et al., 2009](#); [Hanahan, 2022](#)). Furthermore, TGF- $\beta$  signaling stimulates the differentiation of fibroblasts and endothelial cells into myofibroblasts (also known as cancer-associated fibroblasts (CAFs)) in the PDAC microenvironment, which promote tumor cell invasion through the secretion of cytokines, like TNF- $\alpha$ , and/or matrix metalloproteinases (MMPs) ([Calon et al., 2014](#); [Zeisberg et al., 2007](#)). The TGF- $\beta$  signaling pathway also possesses immunosuppressive effects that are responsible for diminishing the activity of macrophages, natural killer (NK) cells, T cells, and dendritic cells ([Dardare et al., 2020](#)). Finally, TGF- $\beta$  secreted by pancreatic stellate cells can decrease the expression of L1 cell adhesion molecule (L1CAM), which leads to increased cell stemness and promotes the progression of PDAC tumors ([Cave et al., 2020](#)). Utilizing the aforementioned pathways, tumors can evade the inhibitory effects of the TGF- $\beta$  signaling pathway during the early stages of PDAC and instead take advantage of its other downstream effects to promote tumor growth.



### 1.5.3 TGF- $\beta$ signaling

The TGF- $\beta$  signaling pathway is a complex cascade of molecular events that begins with the binding of the TGF- $\beta$  molecule to the TGF- $\beta$  type II receptor (T $\beta$ RII) belonging to the superfamily of serine/threonine kinase receptors. Upon ligand binding, T $\beta$ RII forms a heterodimer with the TGF- $\beta$  type I receptor (T $\beta$ RI), where activated T $\beta$ RII phosphorylates and stimulates T $\beta$ RI kinase activity. This leads to the downstream phosphorylation of receptor-associated Smad proteins (Smad2 and Smad3), which can both complex with the co-Smad protein, Smad4, and translocate to the nucleus to regulate target gene transcription. TGF- $\beta$  signaling also activates non-Smad signaling pathways such as MAPK, PI3K and Rho-associated protein kinase (ROCK) pathways ([David and Massague, 2018](#); [Feng and Derynck, 2005](#); [Massague et al., 2005](#)).

## 1.6 Prdm16

The PR domain containing 16 (*PRDM16*) gene is situated on the long arm of chromosome 1 at position 36 (1p36) in humans. There are multiple isoforms of Prdm16, however, the two predominant isoforms are the full-length protein and its short form, which lacks PR domain located at the N-terminus and is expressed via an internal promoter ([Nishikata et al., 2003](#)). Previous research surrounding Prdm16 has been in the context of adipose tissue, metabolism, heterochromatin formation, cancer, and TGF- $\beta$  signaling ([Chi and Cohen, 2016](#)).

### 1.6.1 Adipose tissue and metabolism

Adipose tissue is made up of two types of adipocytes: white adipocytes and brown adipocytes. White adipocytes store energy in the form of triglycerides, while brown adipocytes are responsible for energy expenditure in the form of heat through a process called thermogenesis (Ohno et al., 2012). The high energy expenditure of brown adipose tissue is associated with an anti-obesity phenotype, which is characterized by the presence of uncoupling protein 1 (Ucp1) that functions to convert chemical energy into heat contributing to the thermogenic properties of brown adipose tissue (Seale et al., 2011; Seale et al., 2007). In addition to white and brown adipose tissue, there is also "beige" fat, which originates from white adipocytes but shares many metabolic characteristics with brown adipose tissue. Interestingly, it has been discovered that *Prdm16* serves as a master regulator in the process of differentiating white-to-beige adipocytes (Seale et al., 2007). Studies have demonstrated that transgenic mice with *Prdm16* overexpression display beige fat that exhibits a metabolic phenotype similar to that of brown fat, where mice display increased levels of energy expenditure and insulin sensitivity, even when fed a high-fat diet (Seale et al., 2011; Seale et al., 2007). Similarly, ablation of *Prdm16* in fat cells, using the *adiponectin-Cre* mouse model, leads to a loss of beige fat function and insulin resistance. Additional in vivo studies revealed that deleting *Prdm16* in myoblast progenitor cells using the *Myf5-Cre* mouse model led to compensation by *Prdm3* and that ablation of both *Prdm3* and *Prdm16* during brown fat development resulted in mice unable to effectively form brown fat. Together, these data suggest that *Prdm16* functions in myoblast precursor cells to function as a molecular switch

for stimulating brown fat development through interacting with PPAR- $\gamma$ , C/EBP $\beta$ , C-terminal binding proteins, and PGC-1 $\alpha\beta$  (Harms et al., 2014; Kajimura et al., 2009; Kajimura et al., 2008; Seale et al., 2008; Seale et al., 2007). Studies have demonstrated that *Prdm16* is also necessary for promoting cell survival, and that its deletion can result in perturbations in the composition of intestinal cell types. Particularly, *Prdm16* has been found to regulate fatty acid oxidation in the crypts of the small intestine by binding to several genes involved in this process, including *Slc27a*, *Cpt2*, *Acaa2*, *Acs1*, *Decr1*, *Hadh*, and *Eci2*. The binding of *Prdm16* to the promoter of these genes was demonstrated by a decreased amount of H3K27Ac in cells with mutant *Prdm16* compared to control, indicating that *Prdm16* is required for proper gene expression and regulation of fatty acid oxidation in the small intestine. Overall, these data suggest that *Prdm16* plays a crucial role in maintaining homeostasis in the intestinal epithelium (Stine et al., 2019).

#### 1.6.2 Heterochromatin formation, cancer, and TGF- $\beta$ signaling

In addition to its role in adipose tissue, *Prdm16* has been shown to play a crucial function in heterochromatin formation, as it is responsible for methylating H3K9. Similar to *Prdm16*, experiments demonstrated that *Prdm3* also functions as a methyltransferase to convert H3K9 to H3K9me1. Further investigation revealed that downregulation of either *Prdm3* or *Prdm16* alone did not affect the formation of heterochromatin, but the simultaneous knockdown of both *Prdm3* and *Prdm16* led to a considerable decrease in the accumulation of H3K9me3 in the pericentric area. Double knockdown of *Prdm3* and *Prdm16* also reduced other epigenetic

modifications, such as H3K27me1 and H4K20me3 (histone modifications), 5-methylcytosine (DNA methylation), and HP1 $\alpha$  (chromatin-associated factor). Additionally, viability was significantly decreased in cells with knockdown of both *Prdm3* and *Prdm16* and further exacerbated when *Suv39h* is deleted. These cells also exhibited elevated levels of  $\beta$ -galactosidase and decreased 5'-Bromo-2'-Deoxyuridine (BrdU) as markers of senescence and cell cycle progression, respectively. Furthermore, double knockdown of *Prdm3* and *Prdm16* in cells resulted in un-structuring the nuclear lamina, as the collection of these data together demonstrate the pivotal role of *Prdm16* in heterochromatin formation and maintaining genomic integrity (Pinheiro et al., 2012).

Studies have also explored the role of *Prdm16* in cancer, where it acts as a methyltransferase on H3K4 on chromatin, inhibiting the formation of the MLL-AF9 fusion protein in leukemia. Specifically, the PR domain of *Prdm16* was found to inhibit the formation of MLL fusion genes which promote leukemogenesis in vitro. In vivo experiments using mice injected with *MLL-AF9* fusion gene in combination with *vector control*, *wildtype Prdm16*, or *mutant Prdm16* demonstrated that *Prdm16* functions to inhibit the progression of acute myeloid leukemia (AML). Similarly, cells with *Prdm16* deletion that were transduced with *MLL-AF9* experienced a more rapid progression of leukemogenesis both in vitro and in vivo. Differential expression gene analysis and gene set enrichment analysis (GSEA) comparing *MLL-AF9* with *wildtype* and *mutant Prdm16* revealed that *Prdm16* suppresses MLL-AF9 fusion protein formation by indirectly repressing of the *HoxA* gene cluster through GF11B (Zhou et al., 2016).

Another well-established role of Prdm16 is its function as a tumor suppressor in lung cancer. TCGA analysis indicated that Prdm16 mRNA and protein are reduced in tumor tissue relative to normal. *PRDM16* also had prognostic significance in lung adenocarcinoma, where patients with low *PRDM16* expression had worse survival compared to those with high *PRDM16* expression. Consistent with these findings, low expression of *PRDM16* was also correlated with a higher TNM stage and lymph node status. Subsequent in vitro experiments revealed that knockdown of *PRDM16* prompted cell migration, invasion, and an upregulation of mesenchymal markers of EMT. In vivo data recapitulated similar results, where cells overexpressing *PRDM16* had elevated epithelial levels of EMT markers, such as high E-cadherin, low Snail, and low Slug expression. Mechanistically, it was found that Prdm16 acts to suppress tumor metastasis in by inhibiting *MUC4* expression, which is key protein during EMT (Fei et al., 2019; Ponnusamy et al., 2013).

Prdm16 has also been found to play a role in gastric cancer and function as an inhibitor of TGF-beta signaling. Interestingly, both *PRDM16* and *SKI* are located near one another on chromosome 1 (1p36.32), where the expression of both genes was found to be co-amplified. Likewise, both Ski and Prdm16 were highly expressed in human gastric cancer tissue relative to normal tissue. In vitro experiments using cells with knockdown of either *SKI*, *PRDM16*, or both *SKI* and *PRDM16* revealed that individual knockdown did not affect the activation of TGF- $\beta$  signaling, evidenced by phosphorylation and nuclear localization of Smad2/3. However, knockdown of both *SKI* and *PRDM16* led to enhanced *PAI-1* expression, hinting that Prdm16 may function as an inhibitor of TGF- $\beta$  signaling. ChIP experiments revealed that Prdm16

binds to Smad2, Smad3, and HDAC1, where the interaction between Smad3 and HDAC1 was strengthened in the presence of Prdm16. Moreover, Prdm16 also interacts with Ski and strengthens the interaction between Ski-Smad3 in addition to Smad3-bound Ski to DNA. Interestingly, knockdown of both *SKI* and *PRDM16* reduced the interactions of both Smad2/3 and HDAC1 to the SBE of *p21* and *SMAD7*. Collectively, the evidence indicates that Prdm16 collaborates with Ski to enhance the durability of the Smad3-HDAC1 complex binding to the TGF- $\beta$  target gene promoter, ultimately leading to suppression of TGF- $\beta$  signaling activity. Other studies have confirmed this observation, where siRNA used to knockdown *PRDM16* led to elevated TGF- $\beta$  signaling activity ([Warner et al., 2007](#)). All together, these data show that Prdm16 plays a substantial role in a number of cellular processes as a regulator of the browning of fat, heterochromatin formation, tumor suppression, and TGF- $\beta$  signaling impediment.

## 2 ANTAGONISM BETWEEN PRDM16 AND SMAD4 SPECIFIES THE TRAJECTORY AND PROGRESSION OF PANCREATIC CANCER

Eric Hurwitz, Parash Parajuli, Seval Ozkan, Celine Prunier, Thien Ly Nguyen, Deanna Campbell, Creighton Friend, Allyn Austin Bryan, Ting-Xuan Lu, Steven Christopher Smith, Mohammed Shawkat Razzaque, Keli Xu, and Azeddine Atfi

### 2.1 Abstract

The transcription factor *Prdm16* functions as a potent suppressor of transforming growth factor-beta (TGF- $\beta$ ) signaling, whose inactivation is deemed essential to the progression of pancreatic ductal adenocarcinoma (PDAC). Using the *Kras*<sup>G12D</sup>-based mouse model of human PDAC, we surprisingly found that ablating *Prdm16* did not block but instead accelerated PDAC formation and progression, suggesting that *Prdm16* might function as a tumor suppressor in this malignancy. Subsequent genetic experiments showed that ablating *Prdm16* along with *Smad4* resulted in a shift from a well-differentiated and confined neoplasm to a highly aggressive and metastatic disease, which was associated with a striking deviation in the trajectory of the premalignant lesions. Mechanistically, we found that *Smad4* interacted with and recruited *Prdm16* to repress its own expression, therefore pinpointing a model in which *Prdm16* functions downstream of *Smad4* to constrain the PDAC malignant

phenotype. Collectively, these findings unveil an unprecedented antagonistic interaction between the tumor suppressors Smad4 and Prdm16 that functions to restrict PDAC progression and metastasis.



## 2.2 Introduction

Pancreatic ductal adenocarcinoma (PDAC) is the most aggressive type of pancreatic cancer, currently ranked as the fourth leading cause of cancer-related deaths in the United States ([Connor and Gallinger, 2022](#); [Hidalgo, 2010](#)). Most of PDAC patients present with both locally invasive tumors and widespread metastasis, thus rendering ineffective the resection of the primary tumor as well as the applicability of the dismal therapeutic options available ([Hidalgo, 2010](#); [Stathis and Moore, 2010](#)). Consequently, the outcome of PDAC patients remains extremely poor, with an overall 5-year survival rate of less than 11%.

PDAC tumors emerge through three types of distinct precursor lesions called pancreatic intraepithelial neoplasia (PanIN), intraductal papillary mucinous neoplasia (IPMN) and mucinous cystic neoplasia (MCN), respectively ([Connor and Gallinger, 2022](#); [Yonezawa et al., 2008](#)). These early-stage lesions harbor various genetic alterations, the earliest and most pervasive of which are activating mutations in *KRAS*, occurring in ~90% of PDAC tumors ([Hayashi et al., 2021](#)). The current model posits that mutational activation of *KRAS* represents an essential initiating event, whereas subsequent accumulation of inactivating mutations in the tumor suppressor genes *p16INK4a*, *SMAD4* and *TP53* are necessary for PDAC to progress and metastasize ([Hayashi et al., 2021](#); [Iacobuzio-Donahue, 2012](#)). Significant efforts have been made over the past two decades to create genetically engineered mouse models (GEMMs) that faithfully recapitulate the prominent features of human PDAC. For instance, pancreas-specific expression of *Kras*<sup>G12D</sup> in mice is sufficient to initiate PanINs, which occasionally progress into invasive PDAC following a long latency

period, supporting the general notion that oncogenic activation of *KRAS* represents the main initiating genetic event in PDAC (Buscail et al., 2020; Hingorani et al., 2005; Tuveson et al., 2004; Westphalen and Olive, 2012). Concomitant expression of *Kras*<sup>G12D</sup> and deletion of any of the three cardinal tumor suppressors, e.g., *Trp53*, *p16Ink4a*, *Smad4*, accelerate PDAC progression, though the nature and final outcome of the tumors might differ. Indeed, while mice with the combined expression of *Kras*<sup>G12D</sup> and deletion of *Trp53* (*KPC*) or *p16Ink4a* (*KIC*) develop PanINs that progress very rapidly to highly aggressive and metastatic PDAC, mice with the combined expression of *Kras*<sup>G12D</sup> and deletion of *Smad4* (*KSC*) develop mostly IPMNs, which also progress to invasive PDAC, but the terminal disease develops with a much slower onset and manifests an attenuated metastatic phenotype (Bardeesy et al., 2006a; Bardeesy et al., 2006b; Hingorani et al., 2005; Izeradjene et al., 2007). Other examples of PDAC GEMMs include *KT $\beta$ C* mice, which harbor *Kras*<sup>G12D</sup> and deletion of *the transforming growth factor-beta (TGF- $\beta$ ) type II receptor (T $\beta$ RII) gene*, the latter being inactivated by mutations or deletions in 4% of PDAC (Iacobuzio-Donahue, 2012; Ijichi et al., 2006).

TGF- $\beta$  signaling regulates a wide array of biological processes vital for normal cell growth, function and homeostasis (David and Massague, 2018; Massague, 2008). TGF- $\beta$  initiates signaling by inducing the assembly of a receptor complex composed of two types of transmembrane serine/threonine kinases called T $\beta$ RI and T $\beta$ RII. In that complex, the constitutive kinase of T $\beta$ RII phosphorylates and activates the kinase activity of T $\beta$ RI, which then propagates the signal to the nucleus through phosphorylation of Smad2 and Smad3 (David and Massague, 2018; Feng and

Derynck, 2005; Massague et al., 2005). Once phosphorylated, Smad2 or Smad3 associates with Smad4, and the two complexes accumulate in the nucleus to regulate expression of TGF- $\beta$  target genes through cooperative interactions with transcriptional cofactors or corepressors (David and Massague, 2018; Feng and Derynck, 2005; Massague, 2008; Massague et al., 2005).

Because of the widespread roles of TGF- $\beta$  signaling in cellular functions, there must be multiple levels of positive and negative regulations to fine-tune initiation, magnitude or termination of the response depending on the cell type or physiological context. One example of the mechanisms that limits TGF- $\beta$  signaling involves the transcription factor PR domain containing 16 (Prdm16). Upon accumulation in the nucleus, the Smad3/Smad4 complex associates with the general transcriptional co-activators CBP and p300 to activate transcription of TGF- $\beta$  target genes (David and Massague, 2018; Feng and Derynck, 2005; Massague, 2008; Massague et al., 2005). Conversely, the Smad complex can also associate with Prdm16 and its partner c-Ski, which leads to the recruitment of general transcriptional corepressor complexes containing histone deacetylases and concomitant displacement of CBP and p300, thereby resulting in transcriptional repression (Takahata et al., 2009).

Besides its function as a suppressor of TGF- $\beta$  signaling, Prdm16 has been shown to play key roles in a number of biological processes, including differentiation of brown fat and specification of hematopoietic and neuronal stem cell fate (Chi and Cohen, 2016; Seale et al., 2007; Shimada et al., 2017). Prdm16 possesses a methyltransferase activity that catalyzes the methylation of Lysine-9 on histone-3 (H3K9), a mark associated with heterochromatin formation and gene expression

(Jambhekar et al., 2019; Pinheiro et al., 2012). Recently, Prdm16 loss-of-function has been shown to play an instrumental role in leukemia driven by the MLL fusion oncoprotein (Zhou et al., 2016). Because the *MLL* gene encodes a histone-3 Lysine-4 (H3K4) methyltransferase that is critical in promoting gene expression during hematopoiesis (Xue et al., 2019), it has been postulated that Prdm16 might suppress leukemia pathogenesis owing to its ability to drive heterochromatin formation (Pinheiro et al., 2012; Zhou et al., 2016). At present, whether Prdm16 has any role in cancer pathogenesis and progression that is linked to its function in TGF- $\beta$  signaling is still unknown. Here, we combined several orthogonal approaches and GEMMs to demonstrate that Prdm16 functions downstream of Smad4 to suppress PDAC progression and metastasis. As such, our findings unveil a previously uncharacterized mechanism that orchestrates Prdm16 tumor-suppressive function, and further shed new insights into the molecular etiology of PDAC, a fatal disease for which no effective therapeutics are currently available.

## 2.3 Materials and Methods

### 2.3.1 Plasmids

The CAGA<sub>9</sub>-Lux gene reporter construct was previously described ([Seo et al., 2006](#)). The expression vector pcDNA3.1-Prdm16 was a gift from Dr. Bruce Spiegelman (Addgene #15503). The expression vector pCMV5-HA-Smad4 was a gift from Dr. Joan Massague. To generate the Prdm16-Lux reporter, genomic fragments (1,391 bp) upstream of the transcription initiation site (SST) of the *PRDM16* gene (based on gene association NM\_022114 and Eukaryotic Promoter Database, [epd.epfl.ch](http://epd.epfl.ch)) was amplified by the Genomic-GC PCR amplification kit (BD Biosciences) using human genomic DNA obtained from PANC-1 cells. Unique KpnI and XhoI sites were incorporated at the 5' and 3' ends of the sequence, respectively, to simplify directional cloning into KpnI and XhoI sites in the reporter plasmid, pGL3-basic (Promega). Introduction of inactivating mutation into the SBE sequence (-41 bp from SST) was generated by PCR using the QuickChange Site-Directed Mutagenesis kit according to the manufacturer's instructions (Stratagene). The lentiCRISPRV2 expression vectors encoding *SMAD4* and *PRDM16* gRNAs were purchased from GenScript. The lentiCRISPRV2 expression vectors encoding *SMAD2* and *SMAD3* gRNAs were generated using lentiCRISPRV2 hygro (Addgene #98291) and primers with sequences generated using the Synthego Design tool. All cloned cDNAs and their corresponding mutants were checked by sequencing.

Sequences of gRNAs:

#### *SMAD4*

5'-TTCTTCCTAAGGTTGCACAT-3'

5'-AATACACTTACCAGGATGAT-3'.

#### PRDM16

5'- CTCGTACGGCGAGCCCTCCT-3'

5'- AGGGGTCTTACCGTCCAGGC-3'.

#### SMAD2

5'-TGGCGGCGTGAATGGCAAGA-3

5'-TTCACAACTGGCGGCGTGAA-3'

#### SMAD3

5'-CACCTGCAACCGGCCATCCA-3'

5'-ACACCTGCAACCGGCCATCC-3'

### 2.3.2 Antibodies

Chromatin immunoprecipitation (ChIP), immunoblotting, immunofluorescence or immunohistochemistry were performed using the following antibodies: anti- $\alpha$ -SMA (Cell Signaling, #19245T); anti- $\beta$ -Actin (Bio-Rad, #64225332), anti-amylase (Abcam, #ab21156), anti-chromogranin-A (Abcam, #ab45179), anti-cytokeratin 19 (Abcam, #ab52625), anti-E-cadherin (Cell Signaling, #3195S), anti-glucagon (Cell Signaling, #2760), anti-insulin (Cell Signaling, #4590), anti-JunB (Cell Signaling, #3753), anti-Muc5AC (Abcam, #ab3649), anti-Prdm16 (Abcam, #ab202344 and #ab106410), anti-Smad2 (Cell Signaling, #5339), anti-Smad3, (Cell Signaling, #9523), anti-Smad4, (Cell Signaling, #46535), anti-Smad4 (Santa Cruz, #sc-7966), anti-Smad2/3 (Cell signaling, #8685) and anti-vimentin (Cell signaling, #5741S).

### 2.3.3 Cell Lines and Culture

HEK293T, MIA-PaCa-2, BxPC-3 and PANC-1 cell lines were obtained from the American Type Culture Collection (ATCC). They were cultured in Dulbecco's modified Eagle's medium (DMEM) supplemented with 10% fetal bovine serum (FBS, Atlanta Biologicals, #S11150), antibiotics (Gibco, #P4458) and L-glutamine (Corning, #17921004). The murine pancreatic cancer cell line KPC1 was originally described in our recent publication ([Parajuli et al., 2018](#)). The cell line was established from a *KP53* mouse, which harbored *Kras*<sup>G12D</sup> and one conditional allele of *Trp53* (*LSL-Kras*<sup>G12D</sup>; *LSL-Trp53*<sup>fl/+</sup>; *Pdx1-Cre*). Freshly isolated specimen from the *KP53* mouse with terminal PDAC was gently dissected, minced with scissors, and digested with Dispase II at 2.4 U/ml (Sigma-Aldrich, #4942078001) and Collagenase D at 0.5 mg/ml (Sigma-Aldrich, #11088858001) for 1 hr at 37 °C in an atmosphere of 5% CO<sub>2</sub>. Then, cells were washed three times with PBS, suspended in RPMI 1540 containing 20% FCS, and seeded on fibronectin-coated plates. Cell colonies were subsequently passaged by trypsinization, pooled, and propagated in DMEM supplemented with 10% FBS, antibiotics and L-glutamine. To generate the *PANC-1-SMAD4*<sup>KO</sup> and *PANC-1-SMAD2/3*<sup>KO</sup> cell lines, cells were transduced with the corresponding lentiCRISPRV2-gRNA lentiviruses, selected with puromycin (for *SMAD4*) or hygromycin (For *SMAD2/3*), and all resistant clones were pooled and expanded as a single population. Lentiviruses were produced by transfecting HEK293T cells with lentiviral constructs and the One-Step Lentivirus Packaging System as described by the manufacturer (Takara, #631275). Lentiviral particles in the conditioned media

were harvested after a period of 48 to 72 hr. The conditioned media were then cleaned of cell debris by centrifugation at 5,000xg for 15 min, filtered through a 0.45µm filter, and used immediately for cell transduction.

#### 2.3.4 In vitro and in vivo cell proliferation assays

For the soft agar assay, cell culture dishes (p60) were first prepared using complete DMEM media containing 0.6% agarose (ThermoFisher Scientific, #16500500) and allowed to solidify at room temperature for two hours. Then, cells suspended in complete DMEM media containing 0.3% agarose were added to the dishes preloaded with the 0.6% agarose layer. PANC-1 and BxPC-3 stably expressing control or *PRDM16* gRNA were plated at a density of 1,000 cells per dish and grown for approximately 2 months. Within this time frame, PANC-1 isogenic cell lines developed small but similar colonies in size, whereas neither of the BxPC-3 isogenic cell lines developed colonies. Colonies were visualized and counted using an Olympus CKX53 microscope with the UPlanFL N 4x/0.13 iPC objective.

For the cell proliferation assay, isogenic PANC-1 (50,000 cells/well) and BxPC-3 (100,000 cells/well) cell lines stably expressing control or *PRDM16* gRNA were inoculated into 6-well plates. Three (for PANC-1) and six (for BxPC-3) days after inoculation, cells were trypsinized and mixed with equal volumes of trypan blue (Invitrogen, #T10282) before being counted using an automatic cell counter (Invitrogen Countess 3 FL, #AMQAF2000). Each well was counted twice and averaged to ensure accurate cell counts were obtained.



For the in vivo growth assay, NOD *scid* gamma (NSG) mice were injected subcutaneously with isogenic PANC-1 and BxPC-3 cell lines stably expressing control or *PRDM16* gRNA ( $10^6$  cells) under septic conditions. During the observation period of approximately 2 months, mice were maintained in sterile conditions and sacrificed if they displayed any symptoms of illness. At the end of the observation period, tumors were dissected, weighted and imaged using a 12-megapixel f/1.8 aperture camera.

### 2.3.5 Mice

NOD *scid* gamma (NSG), *Prdm16*<sup>fl/fl</sup>, *Smad4*<sup>fl/fl</sup>, *TβR2*<sup>fl/fl</sup> and *Trp53*<sup>fl/fl</sup> mice were obtained from Jackson Laboratories. *Loxp-Stop-Loxp-Kras*<sup>G12D</sup> (*LSL-Kras*<sup>G12D</sup>) and *Pdx1-Cre* mice were obtained from the NCI Mouse Repository. *p16<sup>lnk4A</sup>-Luciferase* (*p16<sup>Luc</sup>*) was kindly provided by Dr. Sharpless ([Burd et al., 2013](#)). All PDAC mouse models were generated through successive crossbreeding of *Prdm16*<sup>fl/fl</sup>, *Smad4*<sup>fl/fl</sup>, *TβR2*<sup>fl/fl</sup>, *p16<sup>Luc</sup>*, *Trp53*<sup>fl/fl</sup>, *LSL-Kras*<sup>G12D</sup> and *Pdx1-Cre* mice as appropriate. Full descriptions of the genotypes of mice used throughout the study are:

-KC: *LSL-Kras*<sup>G12D</sup>;*Pdx1-Cre*

-*Prdm16*<sup>KO</sup>: *Prdm16*<sup>fl/fl</sup>;*Pdx1-Cre*

-KPrC: *LSL-Kras*<sup>G12D</sup>;*Prdm16*<sup>fl/fl</sup>;*Pdx1-Cre*

-KSC: *LSL-Kras*<sup>G12D</sup>;*Smad4*<sup>fl/fl</sup>;*Pdx1-Cre*

-KSPrC: *LSL-Kras*<sup>G12D</sup>;*Smad4*<sup>fl/fl</sup>;*Prdm16*<sup>fl/fl</sup>;*Pdx1-Cre*

-KPC: *LSL-Kras*<sup>G12D</sup>;*LSL-Trp53*<sup>fl/fl</sup>;*Pdx1-Cre*

-KIC: *LSL-Kras*<sup>G12D</sup>;*p16<sup>Luc</sup>*<sup>+/+</sup>;*Pdx1-Cre*

*-KT $\beta$ C: LSL-Kras<sup>G12D</sup>;T $\beta$ R2<sup>fl/fl</sup>;Pdx1-Cre*

The Institutional Animal Care and Use Committee (IACUC) of the University of Mississippi Medical Center (UMMC) or Virginia Commonwealth University (VCU) approved all animal experiments. All experiments with transgenic mouse models (including *KSP $\alpha$ C* mice) were initiated at UMMC and continued at VCU. We did not see any significant difference in the onset of tumor formation or survival in mice generated or maintained in both sites.

All mice were maintained on a mixed C57BL/6 and FVB/N genetic background. Mice were maintained in twelve-hour light:dark cycles (6:00 AM to 6:00 PM) at 22 °C and fed a standard rodent chow diet. Formation of PDAC in all mice enrolled in the study was confirmed using pancreatic tissue sections stained with hematoxylin and eosin (H&E) or immunostained with an anti-cytokeratin 19 antibody. Blood glucose levels were measured with blood collected from the tail vein using the *ReliON Prime* blood glucose strips. The average of one measurement from 2 to 3 different blood ReliON meters was used for each mouse.

### 2.3.6 Clinical Samples

Human tissue micro arrays for pancreatic tissues (#PA242b, n= 24; #PA483c, n= 48; #PA805c, n= 80) were purchased from US Biomax Inc.

### 2.3.7 Kaplan-Meier survival analysis in patients with wild-type or mutant *SMAD4*

In order to compare the survival of patients with high versus low expression of *PRDM16* in the context of wild-type or mutated *SMAD4*, *PRDM16* expression data

(mRNA expression z-scores relative to all samples (log RNA Seq V2 RSEM) were first downloaded from the TCGA PanCancer Atlas in cBioPortal. Then, patients of the TCGA-PAAD cohort with wild-type (n= 140) or mutated (n= 26) *SMAD4* were identified using the COSMIC database. Next, patients were classified as having high or low *PRDM16* expression based on whether they were above or below the top and bottom quartile of *PRDM16* expression of the TCGA-PAAD cohort, respectively. Lastly, each patient was matched with the corresponding expression of *PRDM16* and *SMAD4* mutational status as well as the time to death or to last follow up (depending on their vital status) to create a Kaplan-Meier survival curve.

#### 2.3.8 *PRDM16* expression in patients with or without *SMAD4* mutations

To assess the expression of *PRDM16* in patients in the context of wild-type or mutated *SMAD4*, *PRDM16* expression data (mRNA expression z-scores relative to all samples, log RNA Seq V2 RSEM) were first downloaded from the TCGA PanCancer Atlas in cBioPortal. Then, patients of the TCGA-PAAD cohort with different types of *SMAD4* mutations were identified using the cBioPortal interface. Patients were then filtered based on those with no alteration or with truncating mutations in *SMAD4* in order to create a violin plot comparing the normalized *PRDM16* expression between these two groups.

#### 2.3.9 qRT-PCR

Total RNA was extracted from frozen mouse tissue samples using TRIzol (Ambion, #15596018) and purified with chloroform (Fisher Scientific, #066903) and ethanol

(Fisher Scientific, #BP2818). The RNA was then reverse-transcribed using a High-Capacity cDNA Reverse Transcription kit (Applied Biosystems, #4368814). The cDNA product was analyzed by qRT-PCR. Briefly, 25ng cDNA and 150nmol of each primer were mixed together with the SsoFast EvaGreen Supermix (BioRad, #1725200). PCR reactions were conducted using a CFX96 Real-Time System (BioRad) in a 96-well plate. The relative mRNA levels were calculated with the comparative CT method and normalized to *GAPDH* mRNA.

Primers used for human samples:

*PRDM16*-For 5'-CTTTGACCACACCCGAAGGT-3'

*PRDM16*-Rev 5'-TGTGGAGAGGAGTGTCTTCG-3'

*JUNB*-For 5'-CCTGGACGATCTGCACAAGA-3'

*JUNB*-Rev 5'-GGTTGGTGTAACGGGAGGT-3'

*GAPDH*-For 5'-CCATGGGGAAGGTGAAGGTC-3'

*GAPDH*-Rev 5'-AGTGATGGCATGGACTGTGG-3'

Primers used for mouse samples:

*Prdm16*-For 5'-TCCCACCAGACTTCGAGCTA-3'

*Prdm16*-Rev 5'-AAAGTCGGCCTCCTTCAGTG-3'

*Gapdh*-For 5'-CACCATCTTCCAGGAGCGAG-3''

*Gapdh*-Rev 5'-CACCATCTTCCAGGAGCGAG-3'

### 2.3.10 Chromatin Immunoprecipitation Assay

Chromatin Immunoprecipitation Assay (ChIP) assays were performed using a kit following the manufacturer's instructions (Millipore, #17-295). Accordingly, cells were first treated with 1% formaldehyde and incubated at 37 °C for 10 min. Next, cells were washed twice with ice-cold PBS containing protease inhibitors. Cells were then scraped and pelleted by centrifugation at 2,000 RPM for 4 min at 4 °C. Then, cells were resuspended in SDS Lysis Buffer (Millipore, #20-163) and incubated for 10 min on ice. After samples were centrifuged for 10 min at 13,000 RPM at 4 °C, the supernatants were diluted ten times by adding ChIP Dilution Buffer (Millipore, #20-153) containing protease inhibitors. The diluted supernatants were then treated with 75 µl of a 50% slurry of Protein-A Agarose/Salmon Sperm DNA (Millipore, #16-157C) at 4 °C for 30 min with agitation. After centrifugation, supernatants were immunoprecipitated with antibodies against Smad4, Smad2, Smad3, Prdm16, GAPDH or isotype-matched control IgG and 60 µl of a 50% slurry of Protein-A Agarose/Salmon Sperm DNA at 4 °C for 1 hr with rotation. Agarose was pelleted using centrifugation at 1,000 RPM for 1 min at 4 °C. The pellets were washed for 5 min in Low Salt Immune Complex Wash Buffer (Millipore, #20-154) once, High Salt Immune Complex Wash Buffer (Millipore, #20-155) once, LiCl Immune Complex Wash Buffer (Millipore, #20-156) once and TE Buffer (Millipore, #20-157) twice. To amplify DNA bound to the immunoprecipitates, elution buffer (1% SDS, 0.1M NaHCO<sub>3</sub>) was added to each sample followed by agitation and incubation for 15 min with rotation at room temperature. Eluates were then mixed with NaCl (final concentration of 0.2 M) and incubated for 4 hr at 65 °C followed by adding EDTA

(0.01 M), Tris-HCl, pH 6.5 (0.04 M), and Proteinase K (0.04 mg/ml). Samples were then incubated for 1 hr at 45 °C and DNA was recovered using phenol/chloroform extraction coupled with ethanol precipitation. Pellets were washed with 70% ethanol and air-dried. Lastly, pellets were resuspended in an appropriate buffer for PCR, and PCR products were analyzed on a 2% agarose gel. The immunoprecipitated DNA was also analyzed by qPCR using locus specific primers and normalized to input DNA. Relative fold enrichment in each locus was quantified relative to the control as described above (qRT-PCR) as well as in our published studies ([Parajuli et al., 2018](#); [Zhang et al., 2015](#)). The following primers were used:

*PRDM16*-For 5'-CATCTCCCCAGCATTGTCAGT-3'

*PRDM16*-Rev 5'-GGAGCGCCGAACACGGAATG-3'

*JUNB*-For 5'-GGCAAAGCCCAGGGTCAATA-3'

*JUNB*-Rev 5'-AAAGCTAGTAAGCGGCCTGG-3'

*GAPDH*-For 5'-CGGGATTGTCTGCCCTAATTAT-3'

*GAPDH*-Rev 5'-GCACGGAAGGTCACGATGT-3'

### 2.3.11 Luciferase Reporter Assay

PANC-1 cells were plated in 6-well plates and transfected with the CAGA<sub>9</sub>-Lux or Prdm16-Lux reporter in the presence of pcDNA3.1-Prdm16, pCMV5-HA-Smad4 or empty vector (pcDNA3.1 or pCMV5-HA as appropriate) using X-tremeGENE9 (Sigma Aldrich, #0635779001). The pRL-SV40 plasmid (Promega, #AF025845) was cotransfected to normalize for transfection efficiency. For CAGA<sub>9</sub>-Lux assays, cells were incubated for 24 hr with the transfection mixtures and then treated with 5ng/ml TGF- $\beta$ 1 (R&D Systems, #7754-BH) for 24 hr before measuring luciferase activity

using the Dual-Luciferase Reporter Assay System (Promega, #E1910). For Prdm16-Lux assays, cells were incubated for 48 hr with the transfection mixtures and then processed for luciferase activity as described for CAGA<sub>9</sub>-Lux. Firefly Luciferase activity was normalized based on Renilla luciferase expressed from pRL-SV40 plasmid.

#### 2.3.12 Co-immunoprecipitation

Cell lysates were prepared in lysis buffer (25 mM Tris-HCl, pH 7.2, 150 mM NaCl, 5 mM MgCl<sub>2</sub>, 5% glycerol and 1% NP40) supplemented with phosphatase inhibitors (Sigma Aldrich, #P5726) and EDTA-free protease inhibitors (Sigma Aldrich, #P8340). Cells were lysed with 1ml of lysis buffer for 10 min on ice and protein concentrations were determined using the BCA reagent (Thermo Scientific, #23227). Then, 90% of the pre-cleared lysates were added to anti-Smad4 antibody for 1 hr at 4°C under constant rocking and then protein A magnetic beads (Promega, #G8781) was added for an additional 1 hr at 4°C. The beads were subsequently pelleted and washed 5 times with lysis buffer and eluted for immunoblotting using 1X SDS-PAGE sample buffer (ThermoFisher Scientific, #NP0007). The other remaining 10% of lysate was used to determine total protein levels by direct immunoblotting.

#### 2.3.13 Immunoblotting

Cell extracts were prepared in lysis buffer containing 20mM Tris HCl (pH 7.5), 150mM NaCl, 1mM EDTA, 1mM EGTA, 1% Triton, 2.5% sodium pyrophosphate, 1mM  $\beta$ -glycerophosphate, 1mM Na<sub>3</sub>VO<sub>4</sub>, 1 $\mu$ g/uL leupeptin, protease inhibitors (Sigma

Aldrich, #P8340) and phosphatase inhibitors (Sigma Aldrich, #P5726). Protein concentrations were determined using the BCA reagent as described earlier, and samples were denatured using SDS sample buffer (BioRad, #1610747). Samples were loaded into a Criterion Tris-Glycine Extended Gel (BioRad, #5671124) and separated by electrophoreses at 60 mA. The gels were then transferred onto a nitrocellulose membrane (BioRad, #1620115) by a wet transfer system (BioRad) at 100V for 1 hr at room temperature. All membranes were then blocked by incubation with 5% dry milk in TBST (TBS with 0.1% Tween20) for 1 hr at room temperature. Membranes were probed with the primary antibody overnight at 4°C in the blocking buffer, washed with TBST and incubated with the peroxidase-conjugated secondary antibody. Enhanced chemiluminescence (ECL) Western blotting substrates (BioRad, #170-5061) were used for the visualization of the results. The acquisition of images was performed using the ChemiDoc MP Imaging System (BioRad).

#### 2.3.14 Histology, Immunohistochemistry and Immunofluorescence

Tissue samples were fixed in 10% formalin and embedded in paraffin. For pancreatic tissue histology, paraffin sections were stained with hematoxylin and eosin (H&E) using standard techniques. Briefly, sections were deparaffinized with xylene and rehydrated in a graded series of ethanol. They were then successively immersed in a hematoxylin solution (Sigma-Aldrich, HHS128-4L) for 2 min, a clarifier solution (Epredia, 7402L) for 15 seconds, and blueing reagent solution (Epredia, 7301L) for 1 min. Between each of the three steps, sections were immersed in water for 1 min. Next, slides were immersed in an eosin solution (Sigma-Aldrich, HT110280-2.5L) for



3 min before being dehydrated 3 times for 3 min in 100% ethanol (VWR, 89370-088) followed by xylene (Koptec, V1001). For immunofluorescence and immunohistochemistry, tissue sections were deparaffinised with xylene and rehydrated in a graded series of ethanol. Antigen-retrieval was performed for 30 min at high temperature in citrate buffer. Then, slides were blocked and incubated overnight with anti-insulin, anti-glucagon, anti-Prdm16, anti-Muc5AC, anti-chromogranin-A, anti- $\alpha$ SMA, anti-E-cadherin, anti-vimentin or IgG-matched isotype control antibody (negative control) at 4°C. For immunofluorescence, slides were incubated with the secondary antibodies conjugated to Alexa-Fluor®568 (Invitrogen, #A11011) or Alex-Fluor®488 (Invitrogen, #A11088), co-stained with DAPI (Vector Laboratories, #H1800), and viewed on a Nikon Ti-E fluorescence microscope. Immunohistochemistry was done with the VECTASTAIN Elite ABC HRP kit (Vector Laboratories; rabbit, #PK6101 or mouse, #PK-6102) as per manufacturer's instructions. Tissue sections were incubated for 30 min in the secondary antibody followed by the VECTASTAIN ABC reagent. Color development was done with the DAB Peroxidase Substrate kit (Vector Laboratories, #SK-4100) with or without Nickel added enhancement as appropriate.

To quantify Prdm16 expression in human samples, the TMA was scanned using the PlanApo 40x 0.95/0.25-0.17mm objective on the Keyence BZ-X810 automated microscope and characterized using the BZ-X800 Analyzer software from Keyence. The expression intensity of 6 images of normal areas and PanIN stages 1, 2, 3 and PDAC lesions were chosen in a random manner. The intensity of Prdm16 expression was obtained automatically using the BZ-X800 Analyzer software from

Keyence and the means of each stage (normal, PanIN stage 1, 2, 3, PDAC) were calculated. Each area/lesion was individually quantified using the area directly around the lesion.

To quantify Prdm16 expression in mouse tissues, slides chosen in a random manner from all mice under study were scanned using the PlanApo 10x 0.45/4.00mm objective on the Keyence BZ-X810 automated microscope and characterized using the BZ-X800 Analyzer software from Keyence. Random images of PanIN and PDAC lesions were taken and quantified only using the area directly around the lesions. Each lesion was individually quantified and the mean  $\pm$  SEM of 6 independent lesions was presented in figures.

The quantifications of Alcian blue staining or CK19, Muc5AC and  $\alpha$ -SMA immunostaining were conducted by first taking images of 6 normal areas or PanIN/PDAC lesions from all mice under study in a random manner using the PlanApo 40x 0.95/0.25-0.17mm objective on the Keyence BZ-X800 microscope. We then individually quantified each image using the Keyence BZ-X800 analyzer software from Keyence. Lastly, the mean  $\pm$  SEM was calculated for each genotype.

To quantify the distribution of PDAC lesions, mouse tissue slides were scanned using the PlanApo 10x 0.45/4.00mm objective on the Keyence BZ-X810 automated microscope and characterized using the BZ-X800 Analyzer software from Keyence. PanIN and IPMN lesions were counted and characterized as either PanIN or IPMN. The surface area for each lesion was obtained from the Keyence software and the mean sum of the surface area for all PanIN or IPMN lesions were calculated for each genotype, including all mice recruited. The percentage of stroma was

identified using the BZ-X800 Analyzer software from Keyence. The distribution of PDAC lesions was then calculated by multiplying the percentage of PanIN surface area divided by the total non-PDAC surface area of the tissue. The same process was repeated for IPMN lesions.

All images were taken using the Zeiss Axio Lab.A1 upright (Zeiss EC Plan-NEOFLUAR 40x/0.9 Pol and Zeiss A-Plan 10x/0.25 objectives), Zeiss Observer.A1 inverted (Zeiss LDA-Plan 40x/0.55 Ph1 objective), or Leica DM1000LED upright microscopes (Leica HI PLAN 40x/0.65 objective). The numerical aperture of the objective lenses are 0.9 and 0.25, 0.55, and 0.65, respectively with a temperature was 1 (10 Kelvin) with an imaging medium of air. The fluorochromes used were Alexa-Fluor®568, Alex-Fluor®488 and DAPI. The cameras used were the Axiocam ICc5, Axiocam503mono, and LeicaDM2900 with the acquisition software was ZEN 2 lite for both Zeiss microscopes and LAS X for the Leica microscope. Subsequent software used for incorporating images into figures were Adobe Photoshop followed Microsoft PowerPoint.

### 2.3.15 Statistical Analysis

The values are expressed as mean  $\pm$  SEM. The error bars (SEM) shown for all results were derived from biological replicates, not technical replicates. Significant differences between two groups were evaluated using either a two-tailed, unpaired Mann-Whitney test or two-tailed, unpaired t-test, which was found to be appropriate for the statistics, as the sample groups displayed a normal distribution and

comparable variance. Statistical significance of survival differences was determined by log-rank test.

## 2.4 Results

### 2.4.1 Transient expression of Prdm16 during PDAC progression

To explore a possible involvement of Prdm16 in PDAC, we conducted Kaplan-Meier analysis using The Cancer Genome Atlas (TCGA) dataset. As shown in [Fig. 1](#), low *PRDM16* expression is associated with poor survival, providing an initial hint that Prdm16 might function as a tumor suppressor in PDAC.

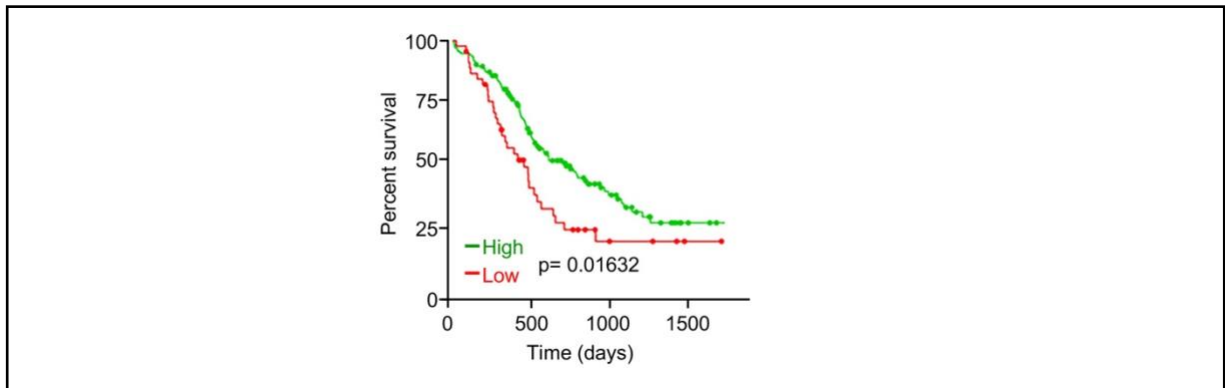
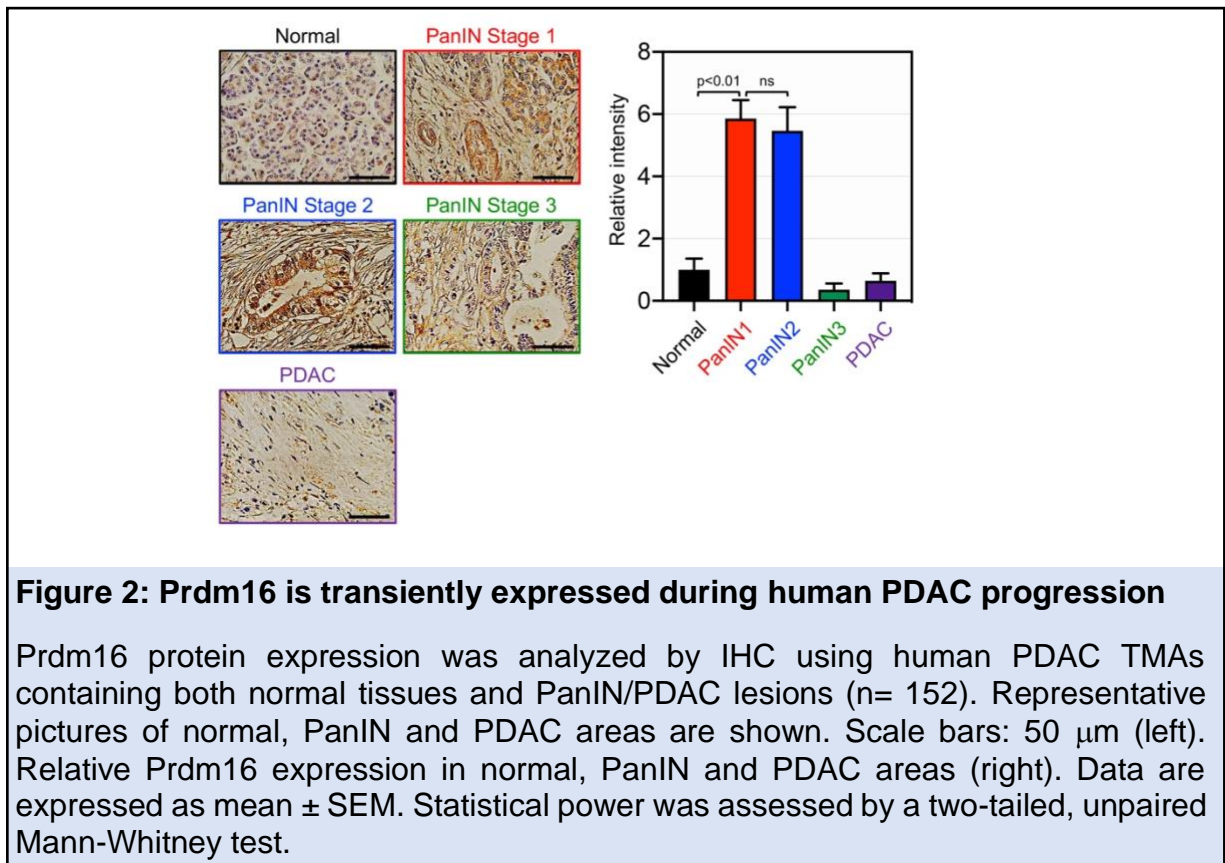


**Figure 1: Low Prdm16 expression is significantly associated with low PDAC patient survival**

Kaplan-Meier survival of PDAC patients based on high versus low Prdm16 expression was conducted using the TCGA dataset. Statistical power was assessed by log-rank test for significance.

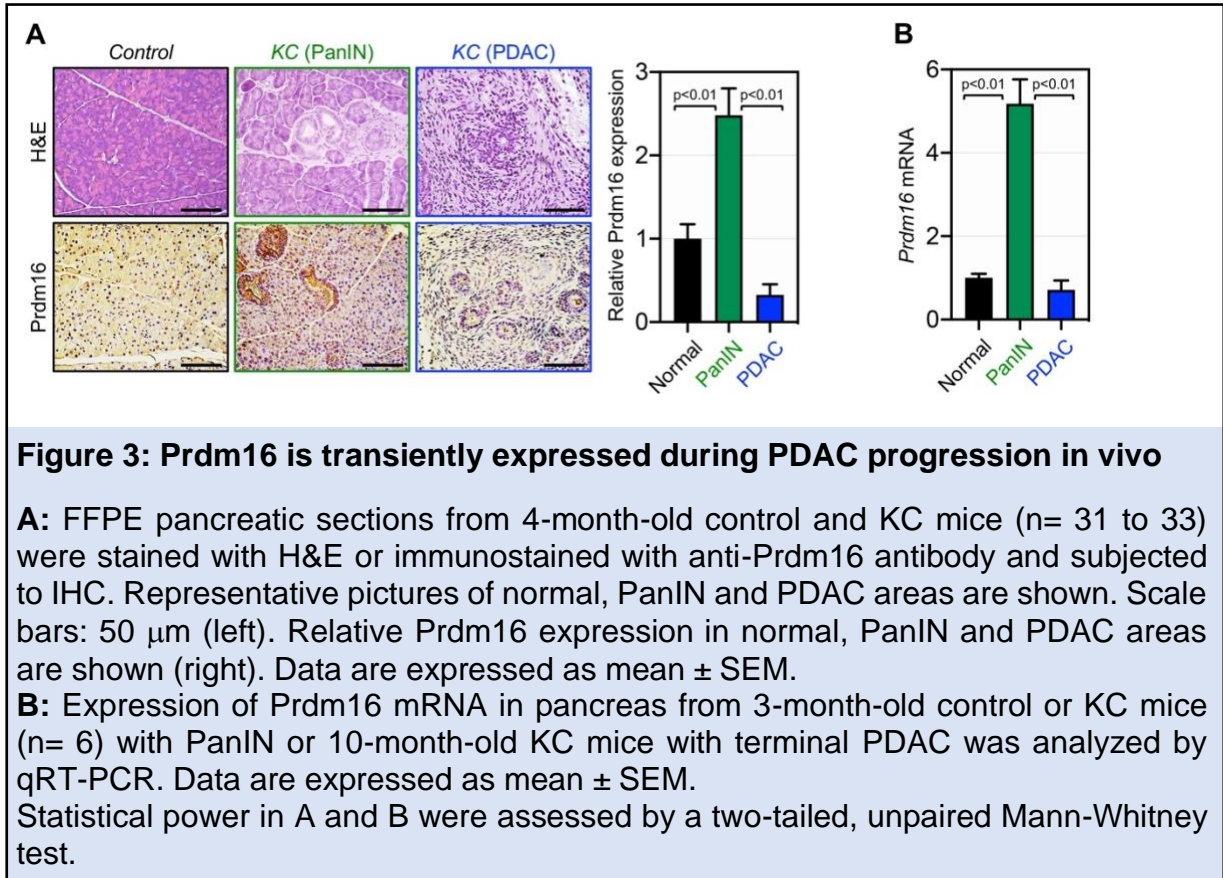
To substantiate this finding, we analyzed Prdm16 expression by immunohistochemistry (IHC) using large human tissue microarrays (TMAs) comprising samples with tumor lesions at various stages (e.g., PanIN1, PanIN2, PanIN3, PDAC) and normal tissues. Using a highly specific antibody to Prdm16 ([see Fig. 9 B](#)), we detected Prdm16 expression in both cancerous lesions and stromal areas ([Fig. 2](#)). Interestingly, Prdm16 expression appeared to fluctuate significantly during PDAC progression, commencing with a relatively low level in normal tissue,

then rising in early PanINs, and finally declining to the background level in invasive PDAC (Fig. 2).



Although this finding fits well with the notion that Prdm16 expression might be downregulated because of the accumulation of late genetic or epigenetic alterations, it did not shed light on the mechanisms leading to its transient expression during PDAC progression. To address this issue rigorously, we sought to utilize GEMMs that faithfully recapitulate the human PDAC in a uniform genetic background (Bardeesy et al., 2006a; Bardeesy et al., 2006b; Hingorani et al., 2005; Izeradjene et al., 2007). We initially utilized mice with pancreas-specific expression of Kras<sup>G12D</sup> alone (KC) and detected transient expression of the Prdm16 protein during PDAC progression, similar to what was observed in human PDAC, being relatively high in PanINs and

very modest to low in normal tissue and invasive PDAC (Fig. 3 A). Confirmation of this result was obtained by comparative qRT-PCR experiments using cohorts of *KC* mice at the age of 3 months when they experience mostly PanINs and 10 months when they display visible signs of terminal PDAC (Fig. 3 B) (Parajuli et al., 2020; Parajuli et al., 2019).



To understand this phenomenon more deeply, we generated mice with *Kras*<sup>G12D</sup> together with deletion of *Trp53* (*KPC*), *p16Ink4a* (*KIC*) or *Smad4* (*KSC*). Noteworthy, we found that *KSC* mice had a longer survival rate than *KIC* and *KPC* mice, while the two latter had almost similar survival (Fig. 4).

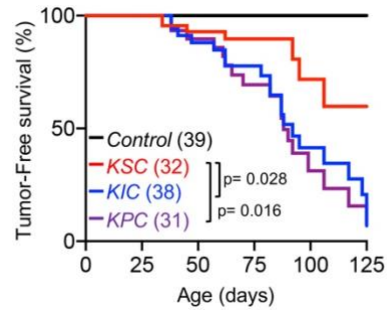


**Figure 4: KSC mice display prolonged survival relative to KIC and KPC mice**

Kaplan-Meier survival analysis of *control*, *KSC*, *KIC* and *KPC* mice (n= 31 to 39). Statistical power was assessed by a log-rank test for significance.

With regards to *Prdm16* expression, we found that *KIC* and *KPC* mice behaved similarly as *KC* mice (Figs. 5 A and B), suggesting that transient expression of *Prdm16* might take place even under the presence of the most common and aggressive genetic alterations that facilitate PDAC progression (Hayashi et al., 2021; Iacobuzio-Donahue, 2012).



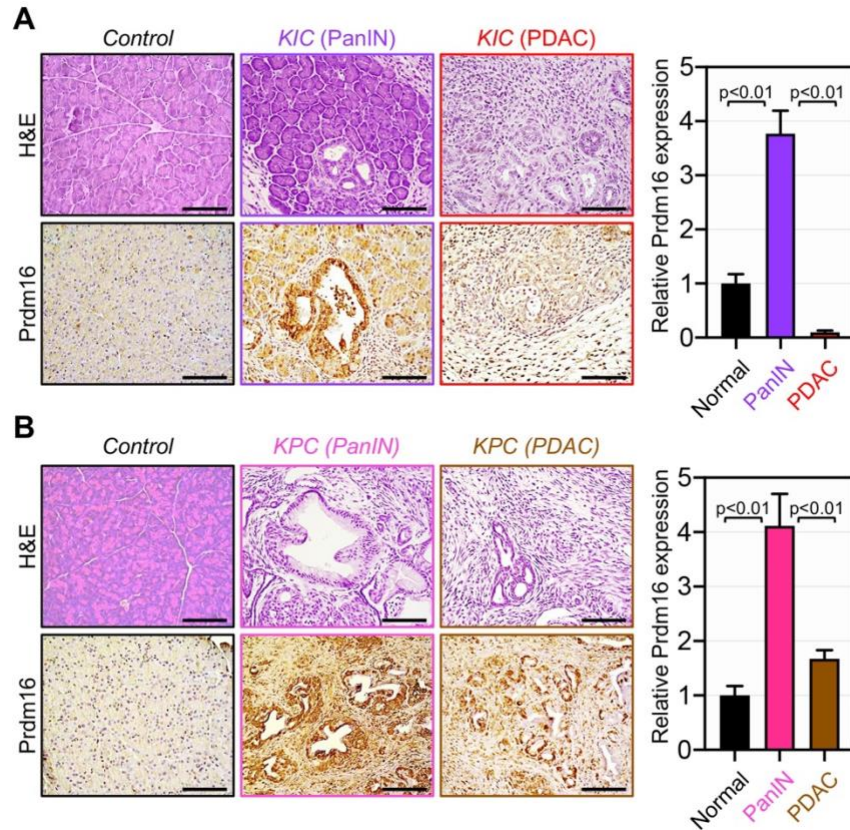


**Figure 5: Prdm16 is transiently expressed during PDAC progression in *KIC* and *KPC* mice**

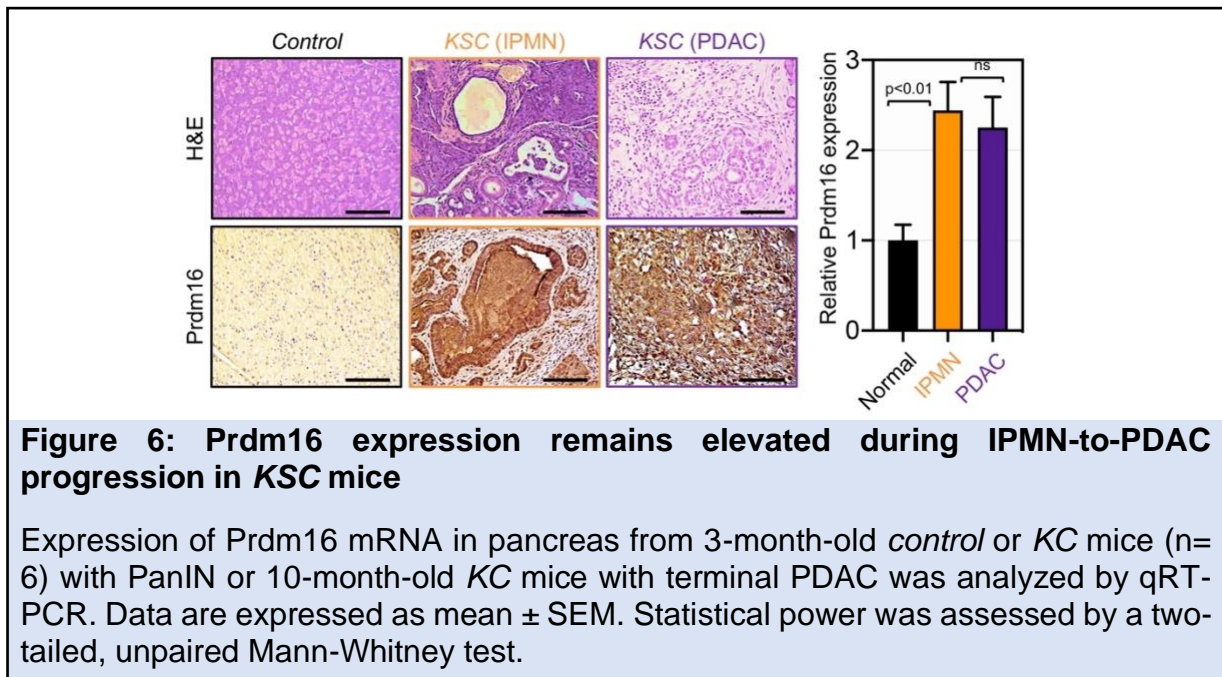
**A:** FFPE pancreatic sections from 4-month-old *control* and *KIC* mice (n= 38 to 39) were stained with H&E or immunostained with anti-Prdm16 antibody and subjected to IHC. Representative pictures of normal, PanIN and PDAC areas are shown. Scale bars: 50  $\mu$ m (left). Relative Prdm16 expression in normal tissue and PanIN or PDAC lesions are shown (right). Data are expressed as mean  $\pm$  SEM.

**B:** FFPE pancreatic sections from 3-month-old *control* and *KPC* mice (n= 31 to 39) were stained with H&E or immunostained with anti-Prdm16 antibody and subjected to IHC. Representative pictures of normal, PanIN and PDAC areas are shown. Scale bars: 50  $\mu$ m (left). Relative Prdm16 expression in normal tissue and PanIN or PDAC lesions are shown (right). Data are expressed as mean  $\pm$  SEM.

Statistical power in A and B were assessed by a two-tailed, unpaired Mann-Whitney test.

But most appealing was the fact that Prdm16 expression in *KSC* mice did not follow this transient pattern of Prdm16 expression, increasing markedly in IPMN lesions but thereafter remaining constant in PDAC lesions (Fig. 6), suggesting that Smad4

might influence Prdm16 expression during the progression from IPMN to full-blown PDAC.



Co-immunofluorescence assays using anti-Prdm16 antibody together with antibodies to E-cadherin (epithelial marker) or vimentin (mesenchymal marker) showed that Prdm16 expression remained very high in E-cadherin<sup>+</sup> cells as compared to vimentin<sup>+</sup> cells (Fig. 7).

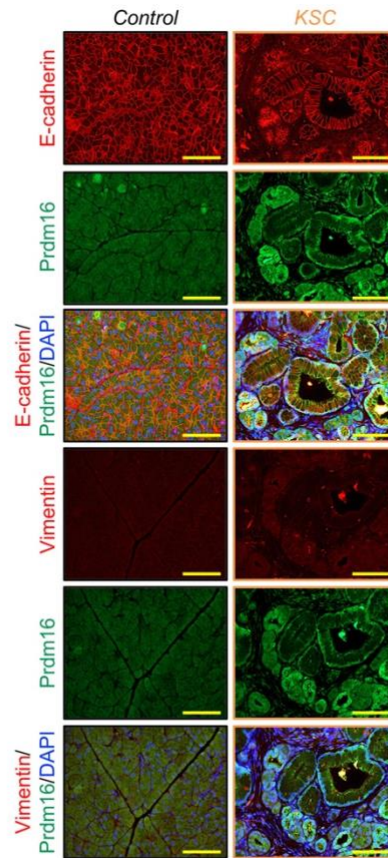


**Figure 7: Prdm16 expression is elevated in E-cadherin positive cells**

FFPE pancreatic sections from *control* and *KSC* mice (n= 31 to 45) were subjected to co-IF using antibodies to Prdm16 and E-cadherin or vimentin. Representative pictures of normal tissue and IPMN or PDAC areas are shown. Scale bars: 50  $\mu$ m.

Consistent with these findings, we found that patients with low expression of Prdm16 had the worst survival if they carry *SMAD4* mutations (Fig. 8 A). Moreover, interrogating the TCGA dataset revealed that samples with deleterious genetic alterations in *SMAD4* display higher expression of *PRDM16* as compared to samples with wild-type *SMAD4* (Fig. 8 B).

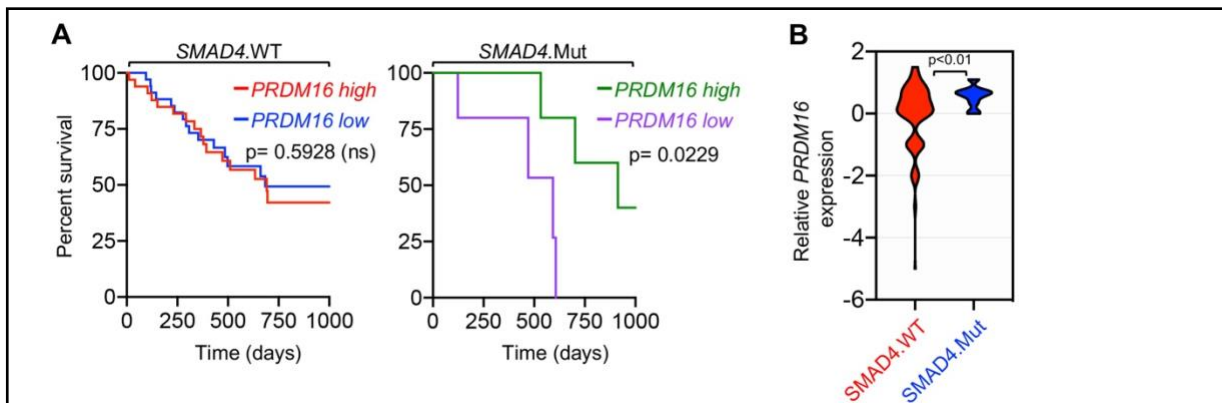


**Figure 8: Patients with low *Prdm16* expression exhibit decreased survival if they carry *SMAD4* mutations**

**A:** Kaplan-Meier survival analysis of patients with wild-type or mutated *SMAD4* based on high versus low *Prdm16* expression was conducted using the TCGA dataset. Statistical power was assessed by log-rank test for significance.

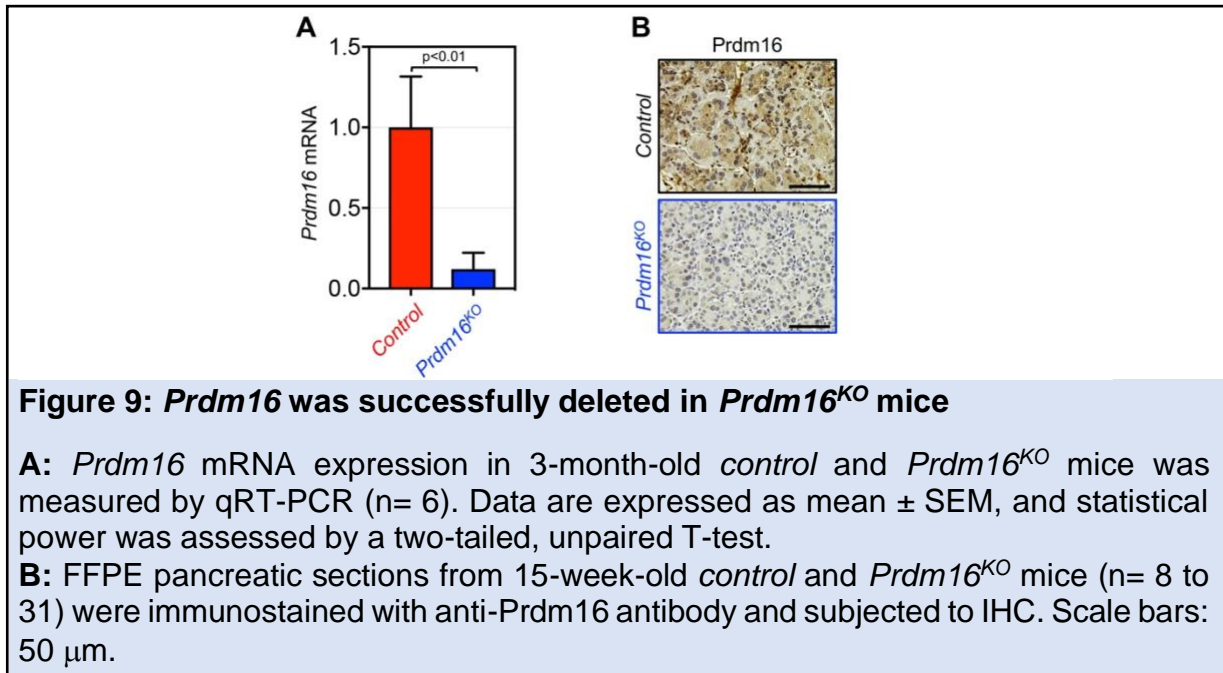
**B:** Relative expression of *Prdm16* in human samples with wild-type or mutated *SMAD4* was conducted using the TCGA dataset. Data are presented as a violin plot. Statistical power was assessed by a two-tailed, unpaired Mann-Whitney test.

As such, these data hint at the existence of an antagonistic association between *Smad4* and *Prdm16* during PDAC progression; we will return to this notion later.

#### 2.4.2 *Prdm16* accelerates *Kras*<sup>G12D</sup>-driven PDAC

The aforementioned data prompted us to investigate whether *Prdm16* could contribute to PDAC initiation, progression or both. To do so, we generated mice with pancreas-specific deletion of *Prdm16* (*Prdm16*<sup>KO</sup>) by crossing mice bearing a floxed allele of *Prdm16* with *Pdx1-Cre* mice, which express Cre recombinase in all pancreatic progenitor cells that give rise to ductal, acinar and islets compartments very early (E8.5) during development (Gu et al., 2003). *Prdm16*<sup>KO</sup> mice were born with the normal Mendelian frequency, develop normally without any signs of anatomic

abnormalities, and were fertile. Effective deletion of *Prdm16* in the pancreatic epithelium was confirmed by RT-PCR and IHC (Figs. 9 A and B).



To investigate whether *Prdm16* deficiency could affect pancreas histology or function, we conducted a comprehensive analysis of pancreatic sections either by hematoxylin and eosin (H&E) staining, IHC or immunofluorescence (IF) encompassing all major tissue compartments, including duct (cytokeratin 19, CK19), acini (amylase), stroma ( $\alpha$ -SMA), and islet (insulin, glucagon, chromogranin-A). We were not able to detect any noticeable changes in all three compartments irrespective of the age of mice analyzed (Figs. 10 - 12).



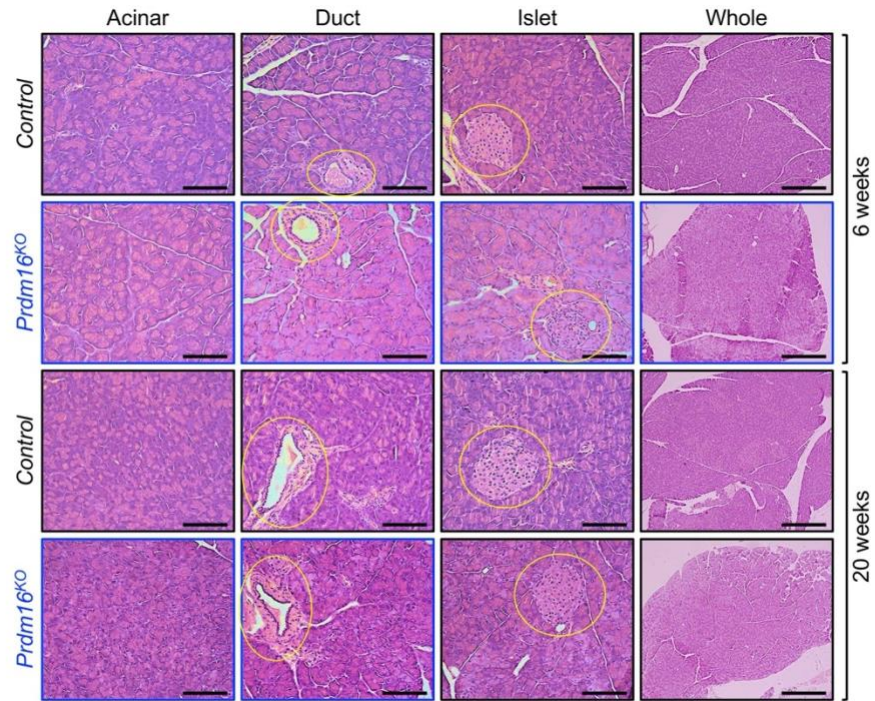


**Figure 10: Ablation of *Prdm16* does not impact pancreatic histology**

FFPE pancreatic sections from *control* and *Prdm16*<sup>KO</sup> mice (n= 8) at 6 or 20 weeks old were stained with H&E. Scale bars: 200 μm for “whole” pictures and 50 μm for all other pictures.

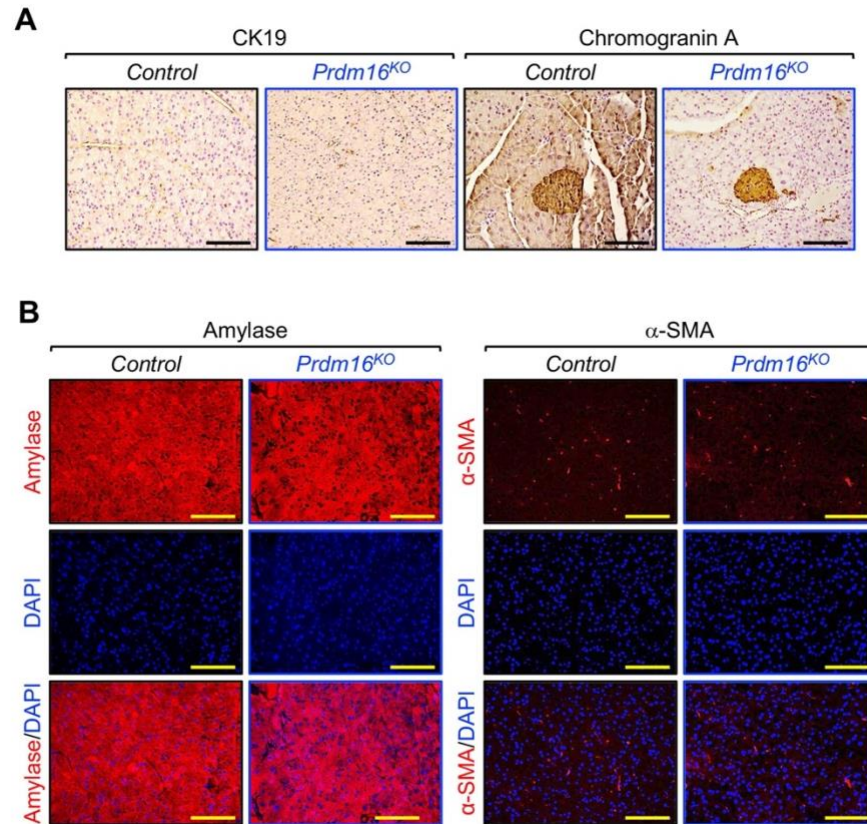


**Figure 11: Ablation of *Prdm16* does not impact normal pancreatic function**

**A:** FFPE pancreatic sections from 15-week-old *control* and *Prdm16*<sup>KO</sup> mice (n= 8 to 31) were immunostained with anti-CK19 or anti-Chromogranin A antibody and subjected to IHC. Scale bars: 50 μm.

**B:** FFPE pancreatic sections from 15-week-old *control* and *Prdm16*<sup>KO</sup> mice (n= 8) were immunoreacted with antibodies to amylase or α-SMA before being subjected to immunofluorescence. Scale bars: 50 μm.

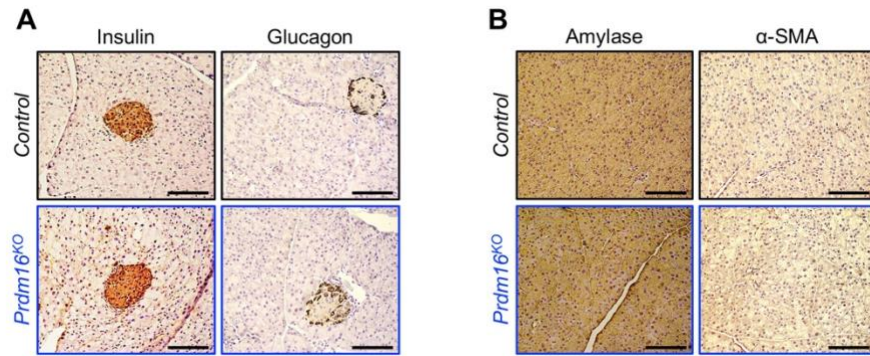


**Figure 12: *Prdm16* ablation does not perturb normal pancreatic function**

**A:** FFPE pancreatic sections from 15-week-old *control* and *Prdm16*<sup>KO</sup> mice (n= 8 to 31) were immunoreacted with antibodies to insulin or glucagon and subjected to IHC. Scale bars: 50 μm.

**B:** FFPE pancreatic sections from 15-week-old *control* and *Prdm16*<sup>KO</sup> mice were subjected to IHC using antibodies to amylase or α-SMA. Scale bars: 50 μm.

Congruently, there was also no difference in fasting blood glucose between wild-type and *Prdm16*<sup>KO</sup> mice (Fig. 13). Thus, inactivation of *Prdm16* throughout embryonic development and postnatal life was insufficient to perturb pancreas homeostasis or drive sporadic pancreatic cancers.

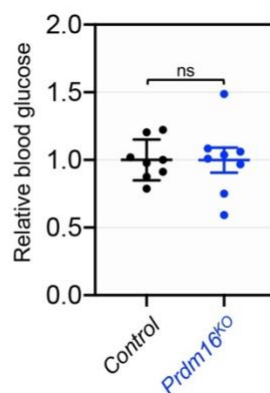


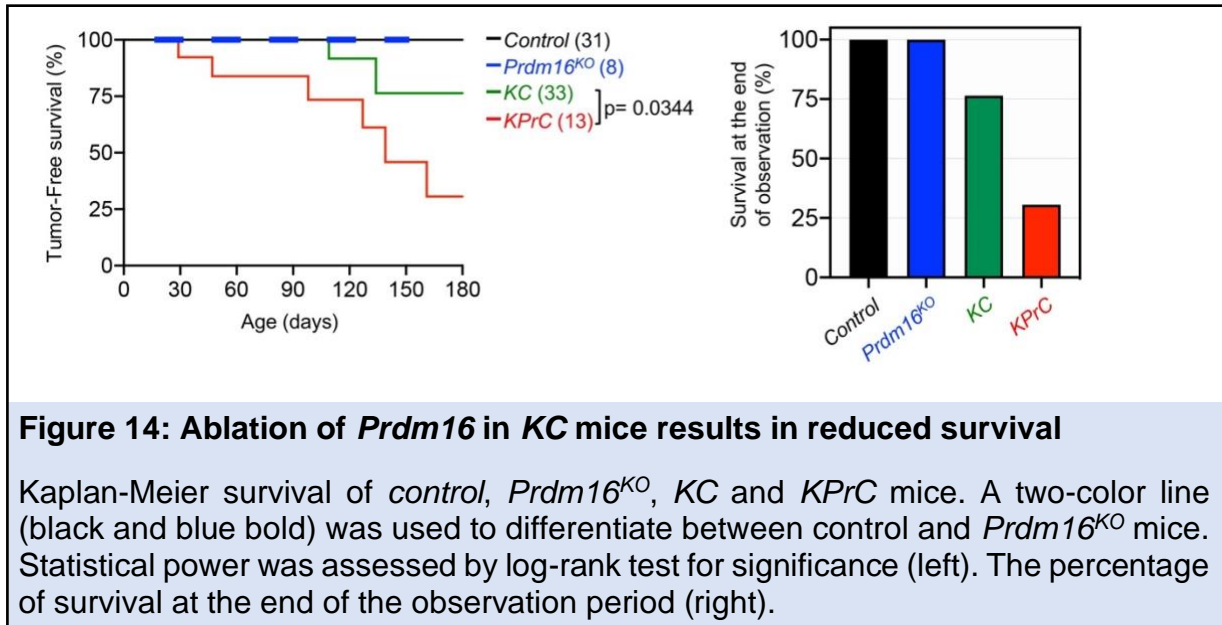
**Figure 13: Ablation of *Prdm16* does not impact blood glucose levels**

Blood glucose of 15-week-old *control* or *Prdm16*<sup>KO</sup> mice (n= 8). Statistical power was assessed by a two-tailed, unpaired Mann-Whitney test.



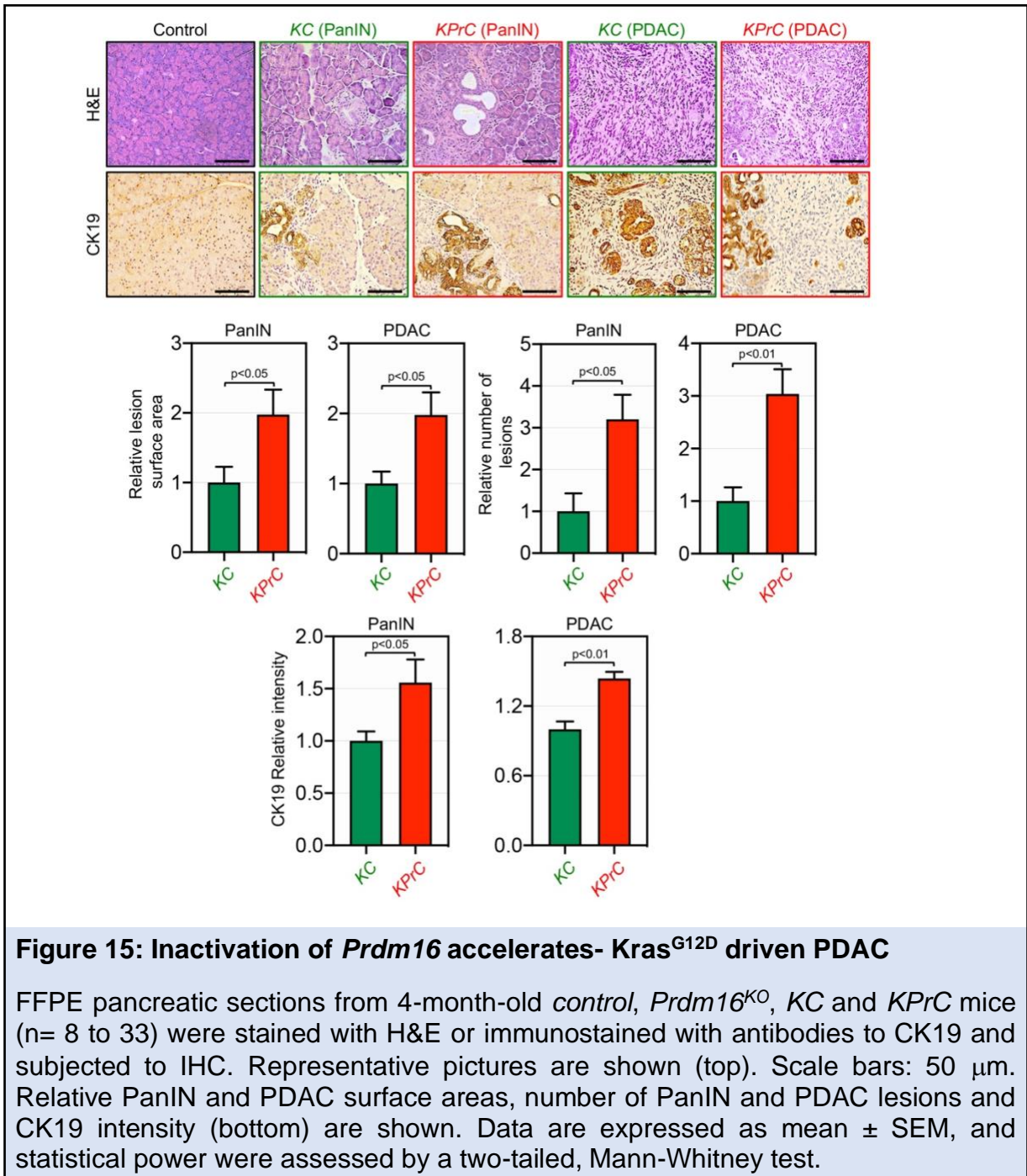
Next, we sought to investigate whether *Prdm16* could influence PDAC progression initiated through activation of *Kras* signaling. The salient genetic features of PDAC originate with the near-ubiquitous gain of function mutations in *KRAS* in their incipient stage. However, progression to invasive PDAC in *Kras*<sup>G12D</sup>-bearing mice has proved to be either a protracted or unachieved process, as a small fraction of mice succumb directly to PDAC following a very long latency period ([Hingorani et al., 2005](#); [Parajuli et al., 2020](#); [Parajuli et al., 2019](#); [Tuveson et al., 2004](#)). It is widely believed that the acquisition of secondary mutations in certain tumor suppressors can endow transformed cells with the growth advantage needed for disease progression. For instance, combining *Kras*<sup>G12D</sup> with deletion of *Smad4* or *TβRII* has been shown to accelerate the progression of PDAC, which was thought to be conferred through disruption of TGF-β cytostatic signaling ([Bardeesy et al., 2006b](#); [Ijichi et al., 2006](#); [Izeradjene et al., 2007](#)). Given its role as an inhibitor of Smad signaling, we surmised that *Prdm16* inactivation might suppress PDAC development and/or progression owing to the de-repression of TGF-β/Smad signaling. To probe this possibility, we generated mice harboring *Kras*<sup>G12D</sup> alone (*KC*) or in combination with conditional deletion of both alleles of *Prdm16* (*KPrC*) and conducted comparative studies to analyze their PDAC phenotypes. Consistent with previous studies ([Parajuli et al., 2020](#); [Parajuli et al., 2019](#); [Tuveson et al., 2004](#)), *KC* mice maintained uniformly good health until around the age of 20 weeks, and thereafter a fraction of mice became suddenly morbid and succumbed within days to an aggressive PDAC. Contrary to our prediction, combining *Prdm16* deletion with *Kras*<sup>G12D</sup> instead resulted in a marked acceleration of PDAC. Kaplan-Meyer analysis showed a significant decrease in the

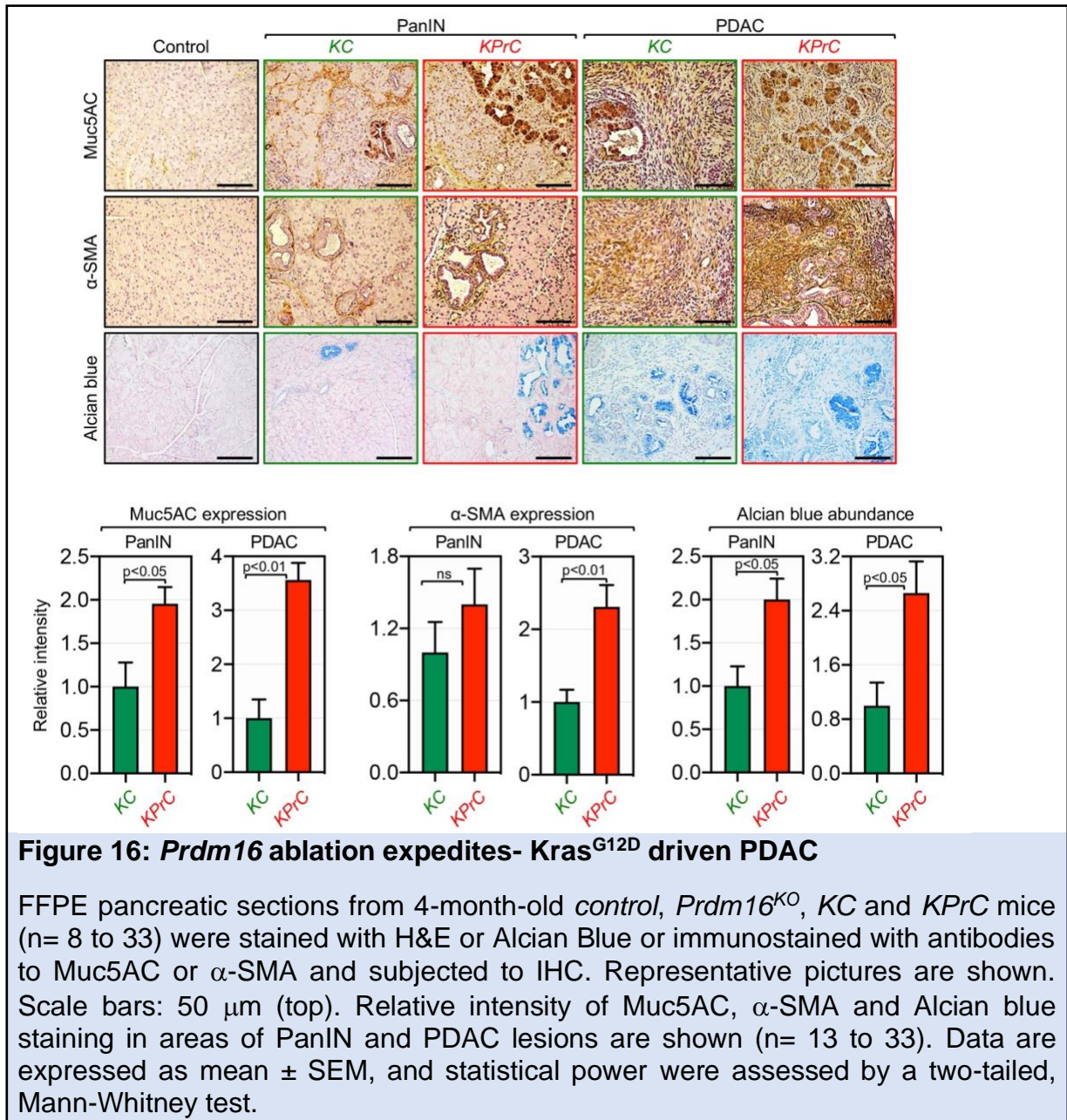
median survival of *KPrC* mice as compared to *KC* mice (Fig. 14). During an observation period of 6 months, 70% of *KPrC* mice succumbed to PDAC, whereas more than 76% of *KC* mice survived and remained free of invasive PDAC (Fig. 14).



To confirm this finding, we conducted histopathological analysis with pancreatic sections from *KPrC* and *KC* mice of the same age that showed either relatively healthy appearance or signs of morbidity characteristic of invasive PDAC at the time of necropsy. At early stages of tumorigenesis, *KPrC* mice displayed a significant increase in PanIN lesions compared to *KC* mice, as assessed by H&E and IHC using anti-CK19 antibody (Fig. 15). A similar conclusion could be drawn while analyzing another ductal marker, MUC5AC, either by IHC or Alcian blue staining (Fig. 16). *KPrC* and *KC* mice with invasive PDAC also showed clear difference in both tumor architecture and reactivity to the anti-CK19 and anti-Mu5AC antibodies as well as to Alcian blue (Figs. 15 and 16). Moreover, IHC analysis using anti- $\alpha$ -SMA antibody showed more extensive stroma both within and outside PDAC lesions in

*KPrC* mice relative to *KC* mice (Fig. 16). An automatic-guided quantification confirmed the increase in the surface areas of PanIN and PDAC lesions in *KPrC* mice as compared to *KC* mice (Fig. 15). Thus, *Prdm16* inactivation appeared to accelerate PDAC once it has been initiated through activation of oncogenic *Kras*<sup>G12D</sup> signaling.

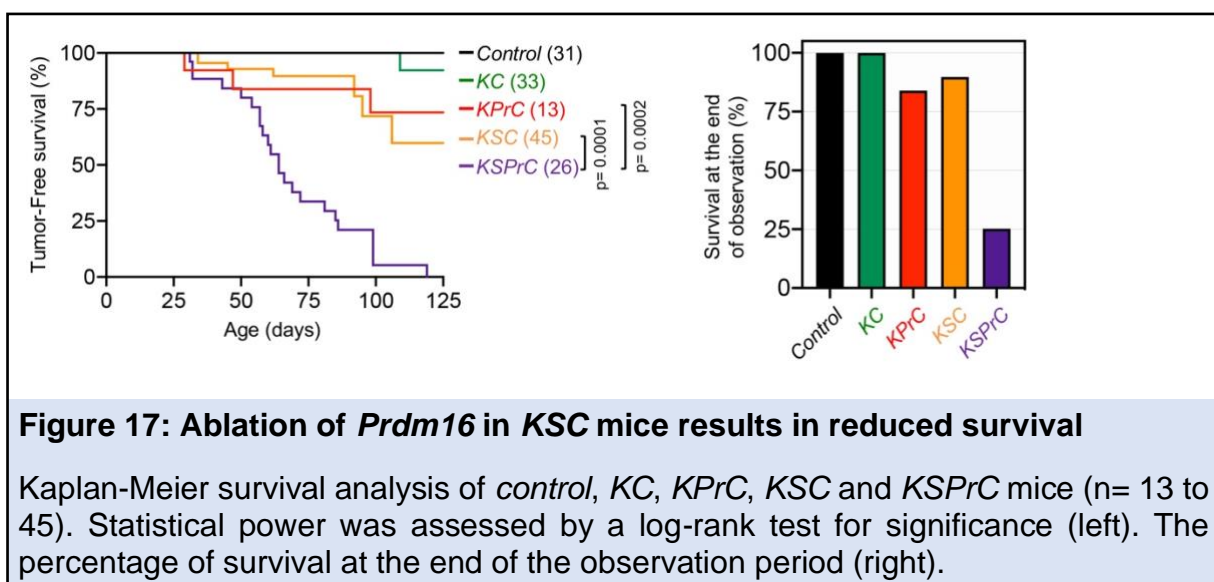




#### 2.4.3 Requirement of *Prdm16* for IPMN-to-PDAC progression

Given the inverse association between *Smad4* and *Prdm16* that we noticed earlier during PDAC progression (Figs. 6 and 8 B), we sought to extend our genetic approaches to explore whether *Prdm16* could play a role, if any, in PDAC that depends on its function in TGF- $\beta$ /Smad signaling. Accordingly, we generated mice

with the combined deletion of *Prdm16* and *Smad4* in a *Kras*<sup>G12D</sup> background (*KSPrC*). *KPrC*, *KSC*, *KC* and wild-type mice were used as controls. *KSPrC* mice were born with Mendelian frequencies and no phenotypic differences between *KSPrC* and *KSC* mice were observed. Strikingly, however, the vast majority of *KSPrC* mice became stunted and morbid in appearance within two to three weeks of weaning, and only 25% of them survived beyond 3 months (Fig. 17). During this period, most of *KPrC* and *KSC* mice (84% and 90%, respectively) did not develop or succumb to PDAC.



To elucidate the mechanism causing the acceleration of PDAC in *KSPrC* mice, we conducted histopathological analyses to study different stages of PDAC from the premalignant lesions to invasive adenocarcinomas. We found that *KSC* pancreas displayed predominantly macroscopic cystic lesions reminiscent of IPMN, as evidenced by the overall architecture as well as the high reactivity to the anti-Muc5AC and anti-CK19 antibodies as well as Alcian blue (Figs. 18 and 19). In contrast, *KSPrC* pancreas displayed none to very few IPMN lesions (Figs. 18 and 19).



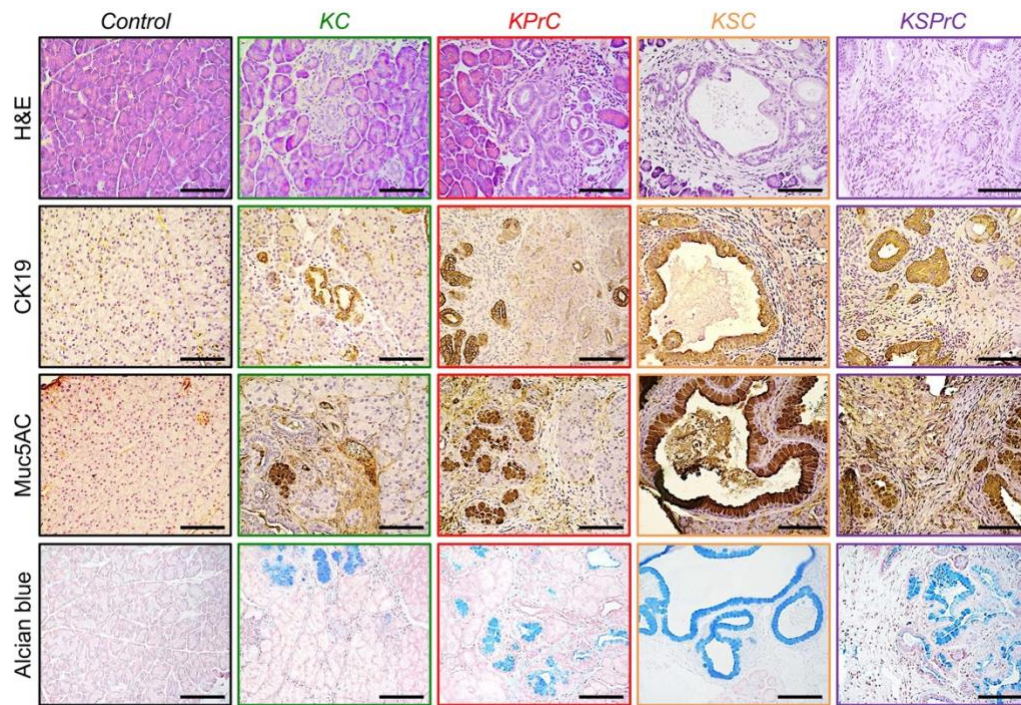


**Figure 18: Inactivation of *Prdm16* dramatically accelerates PDAC progression in *KSC* mice**

FFPE pancreatic sections from 4-month-old *control*, *KC*, *KPrC*, *KSC* and *KSPrC* mice (n= 13 to 45) were stained with H&E or Alcian blue or immunostained with antibodies to CK19 or Muc5AC and subjected to IHC. Representative pictures are shown. Scale bars: 50  $\mu$ m.

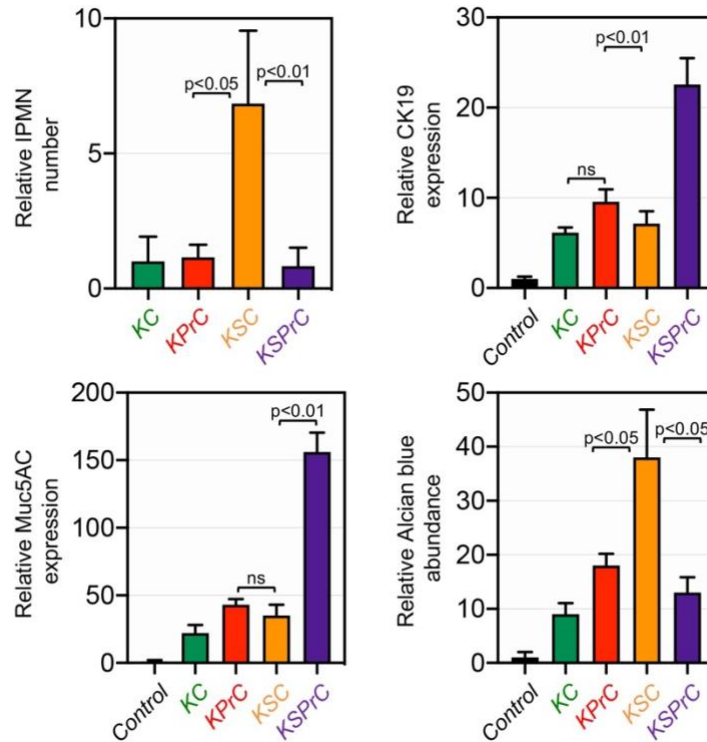


**Figure 19: Prdm16 is required for the IPMN-to-PDAC progression**

FFPE pancreatic sections from 4-month-old *control*, *KC*, *KPrC*, *KSC* and *KSPrC* mice (n= 13 to 45) were stained with H&E or Alcian blue or immunostained with antibodies to CK19 or Muc5AC and subjected to IHC. Relative abundance of IPMN lesions (top left) or intensity of CK19 (top right), Muc5AC (bottom left) or Alcian blue (bottom right) are shown. Data are expressed as mean  $\pm$  SEM, and statistical power was assessed by a two-tailed, unpaired Mann-Whitney test.

At the stage of full PDAC, *KSPrC* tumors were poorly differentiated adenocarcinomas, characterized by loss of the epithelial marker E-cadherin and acquisition of the mesenchymal marker vimentin (Fig. 20), which could be due either to increased accumulation of cancer associated fibroblasts or EMT, the latter being a general hallmark of metastasis (Pei et al., 2019). In marked contrast, *KSC* tumors were well differentiated with little or no change in E-cadherin or vimentin expression (Fig. 20), in line with previous studies that *KSC* mice are resistant to metastasis (Bardeesy et al., 2006b; Izeradjene et al., 2007; Whittle et al., 2015).

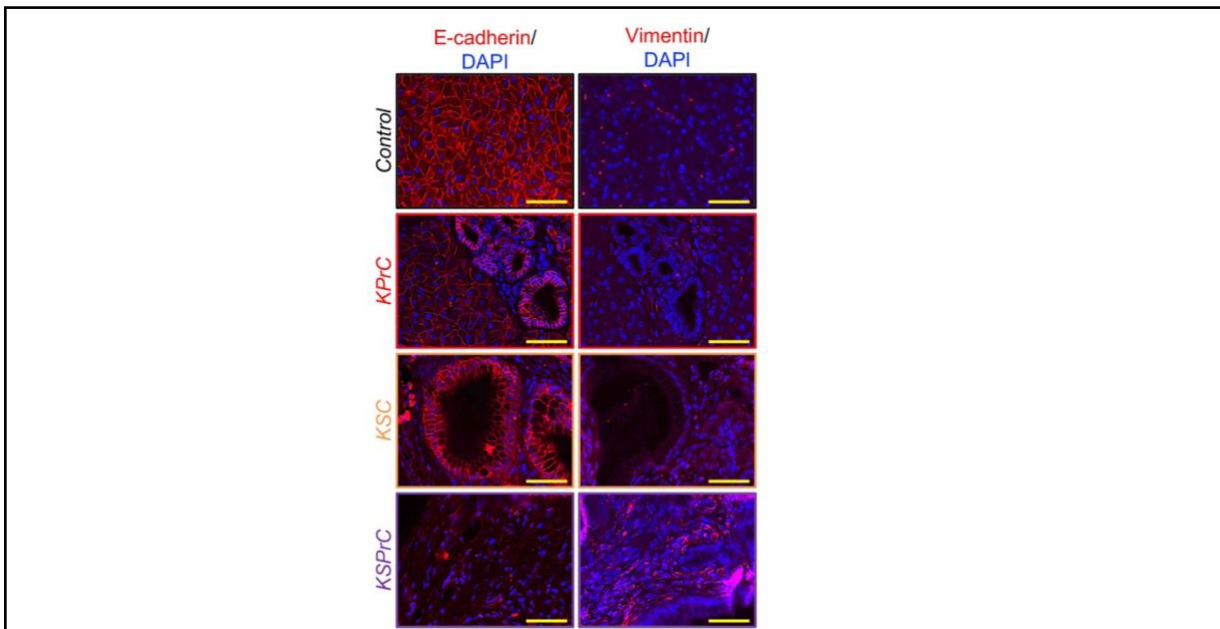
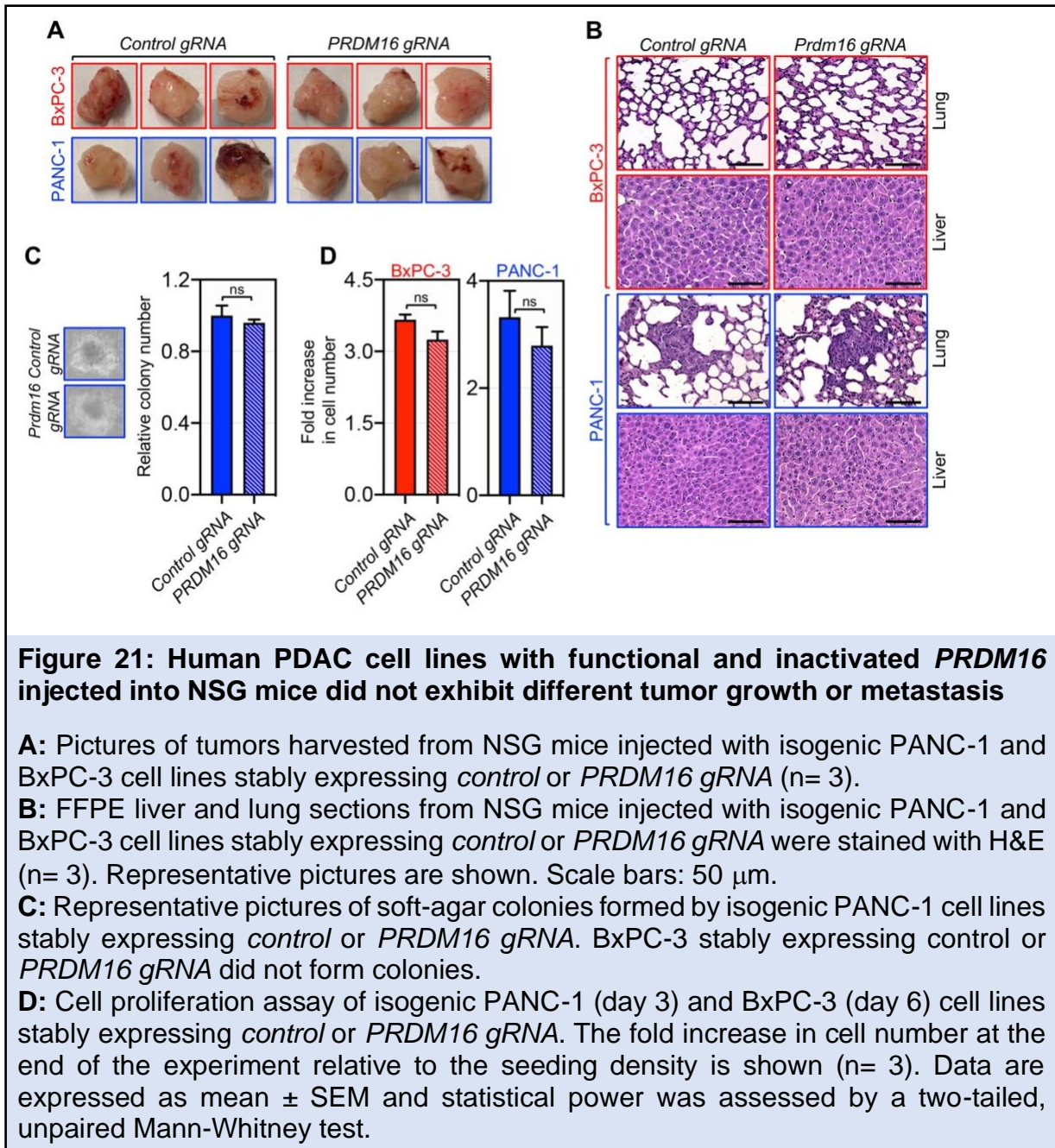


**Figure 20: *KSPrC* tumors present elevated metastatic potential**

FFPE pancreatic sections from *control*, *KPrC*, *KSC* and *KSPrC* mice (n= 13 to 45) were subjected to IF using antibodies to E-cadherin or vimentin. Representative pictures are shown. Scale bars: 50  $\mu$ m.

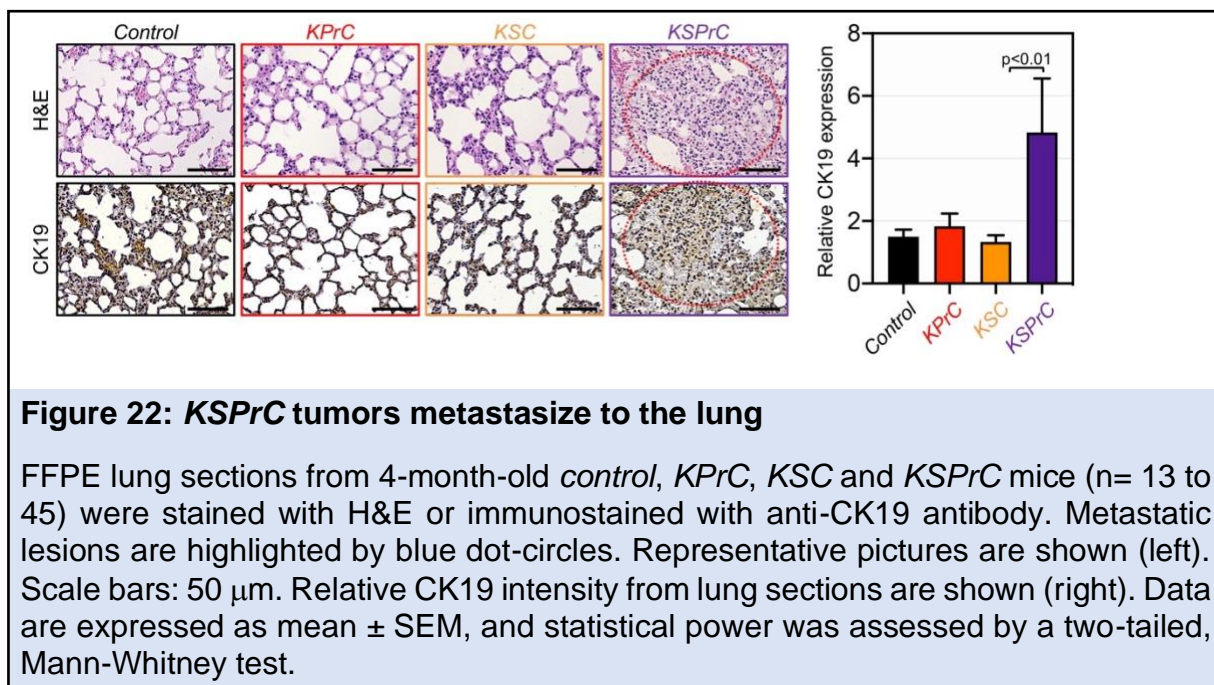
As concomitant inactivation of *Prdm16* appeared to shift the evolution of the IPMN-to-PDAC progression sequence towards the PanIN-to-PDAC progression sequence, it is tempting to speculate that *Prdm16* might function at the stage of early preneoplastic lesions to influence PDAC development and progression. In support of this notion, deleting *PRDM16* in two fully-transformed human PDAC cell lines (i.e., PANC-1, sufficient for *SMAD4* and BxPC-3, deficient for *SMAD4*) did not affect their proliferative or invasive behaviors, as gauged by a combination of in vivo and in vitro assays (Fig. 21 A-D).





The poor prognosis for human PDAC is mainly due to quasi-inevitable metastasis affecting the liver and lung at the time of diagnosis (Connor and Gallinger, 2022; Hidalgo, 2010). Due to the severity of PDAC in *KSPrc* mice, we wondered whether concomitant deletion of *Prdm16* could confer metastatic ability to the otherwise non-metastasizing PDAC tumors that typically develop in *KSC* mice

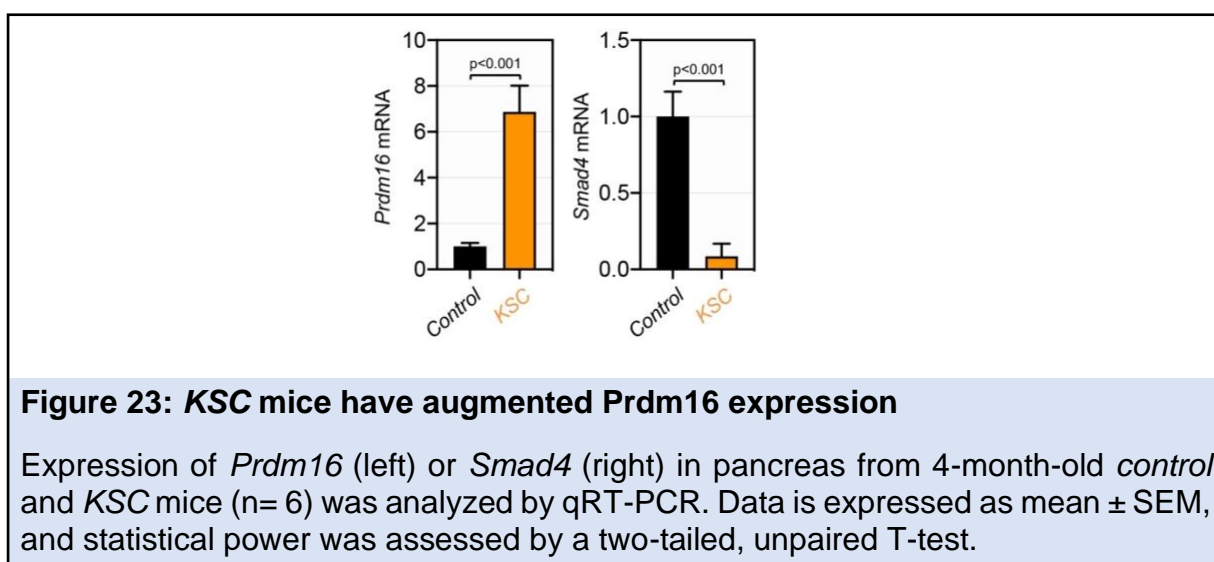
(Bardeesy et al., 2006b; Izeradjene et al., 2007; Whittle et al., 2015). Indeed, we consistently observed the presence of metastatic lesions in the lung in all *KSPrC* mice that developed invasive tumors but survived until necropsy (Fig. 22). In contrast, no metastatic lesions were detected in *KSC* mice even with terminal PDAC (Fig. 22), as previously described (Bardeesy et al., 2006b; Izeradjene et al., 2007; Whittle et al., 2015). Confirmation of these results was obtained by IHC using an antibody to the PDAC marker CK19 (Fig. 22). Collectively, these data demonstrate that concomitant inactivation of *Prdm16* was sufficient to confer metastatic properties on non-metastatic *KSC* tumors, a phenomenon that is associated with a shift from the IPMN-to-PDAC phenotype to the PanIN-to-PDAC phenotype.



#### 2.4.4 Repression of *Prdm16* expression by *Smad4*

To investigate the molecular mechanisms by which *Prdm16* controls PDAC progression and metastasis in the context of a *Smad4* null background, we took

advantage of our earlier IHC analysis showing that *Smad4* deficiency in *KSC* mice was associated with a persistent de-repression of *Prdm16* during the progression from IPMN to PDAC (Fig. 6). We surmised that *Smad4* might function either directly or indirectly to repress *Prdm16* expression, which in turn impacts the progression trajectory of PDAC. We initially conducted qRT-PCR experiments using *KSC* mice and found that the increase in *Prdm16* expression was mediated at least via gene expression (Fig. 23).



Because *Smad4* functions as an essential component of TGF- $\beta$  signaling (David and Massague, 2018; Feng and Derynck, 2005; Massague, 2008), we next wondered whether activation of TGF- $\beta$  signaling could repress *Prdm16* expression, as does *Smad4*. To our surprise, treating mouse PDAC cells KPC1 or human PDAC cells PANC-1 with TGF- $\beta$ 1 instead elicited a marked increase in *Prdm16* expression (Figs. 24 A-C). As a specificity control, TGF- $\beta$ 1 treatment failed to induce *Prdm16* expression in the human PDAC cell line MIA-PaCa-2 (Fig. 24 D), which lacks a functional TGF- $\beta$  receptor (Freeman et al., 1995).

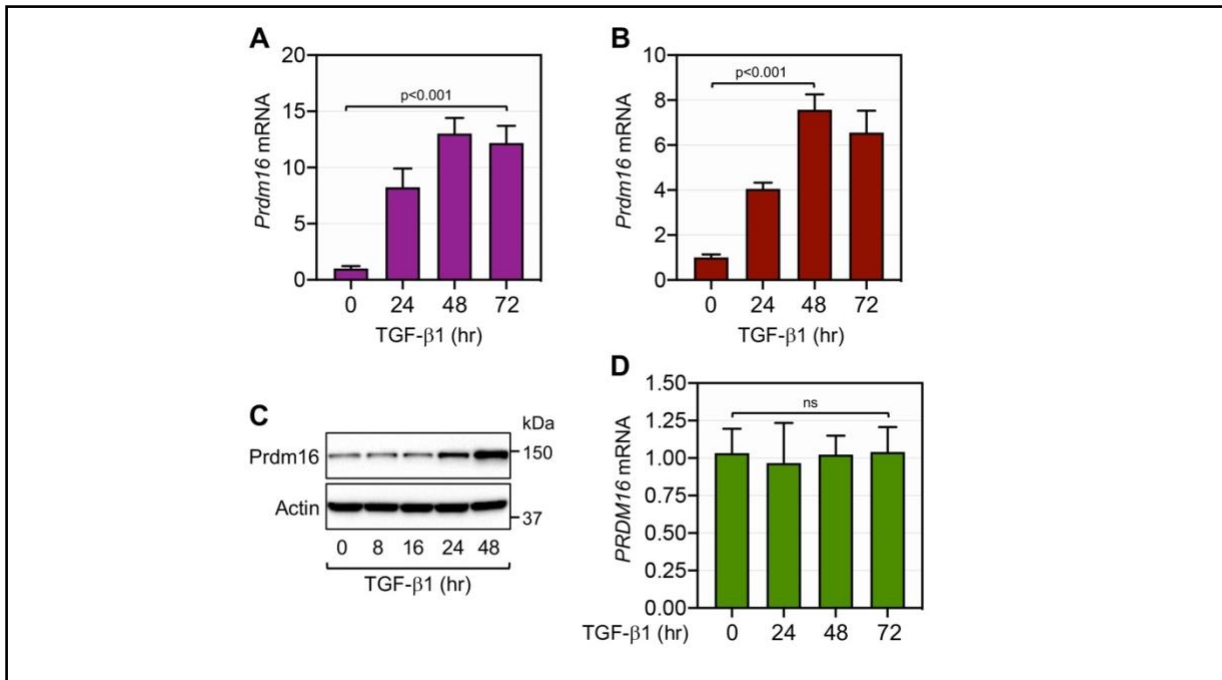


**Figure 24: Treatment of TGF-β1 in mouse and human PDAC cell lines induces Prdm16 expression**

**A:** Expression of *PRDM16* mRNA in KPC1 cells cultured in the presence or absence of TGF-β1 for various times was analyzed by qRT-PCR (n= 6).

**B:** Expression of *PRDM16* mRNA in PANC-1 cells treated with TGF-β1 for various times was analyzed by qRT-PCR (n= 6).

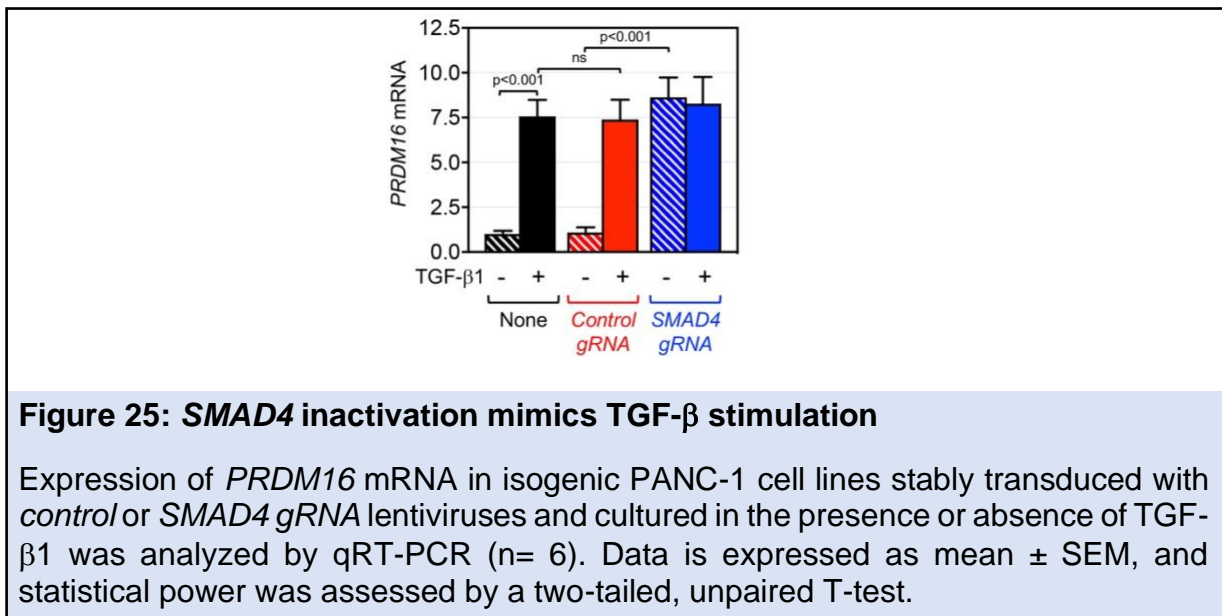
**C:** Expression of Prdm16 protein in PANC-1 cells treated with TGF-β1 for various times was analyzed by immunoblotting.

**D:** Expression of *PRDM16* mRNA in MIA-PaCa-2 cells cultured in the presence or absence of TGF-β1 for various times was analyzed by qRT-PCR (n= 6).

Data in A, B, and D are expressed as mean ± SEM, and statistical power was assessed by a two-tailed, unpaired T-test.

To determine whether the effect of TGF-β1 is mediated via Smad4, we conducted comparative experiments using PANC-1 cells deleted of *SMAD4* by CRISPR/CAS9. We found that ablating *SMAD4* resulted in a marked increase in the steady-state expression of Prdm16 mRNA and protein (Fig. 25, see also Fig. 29), confirming the ability of endogenous Smad4 to repress *PRDM16* expression in human cells. Intriguingly, challenging cells with TGF-β1 did not further increase Prdm16 expression in cells deleted of *SMAD4* as compared to cells expressing the control

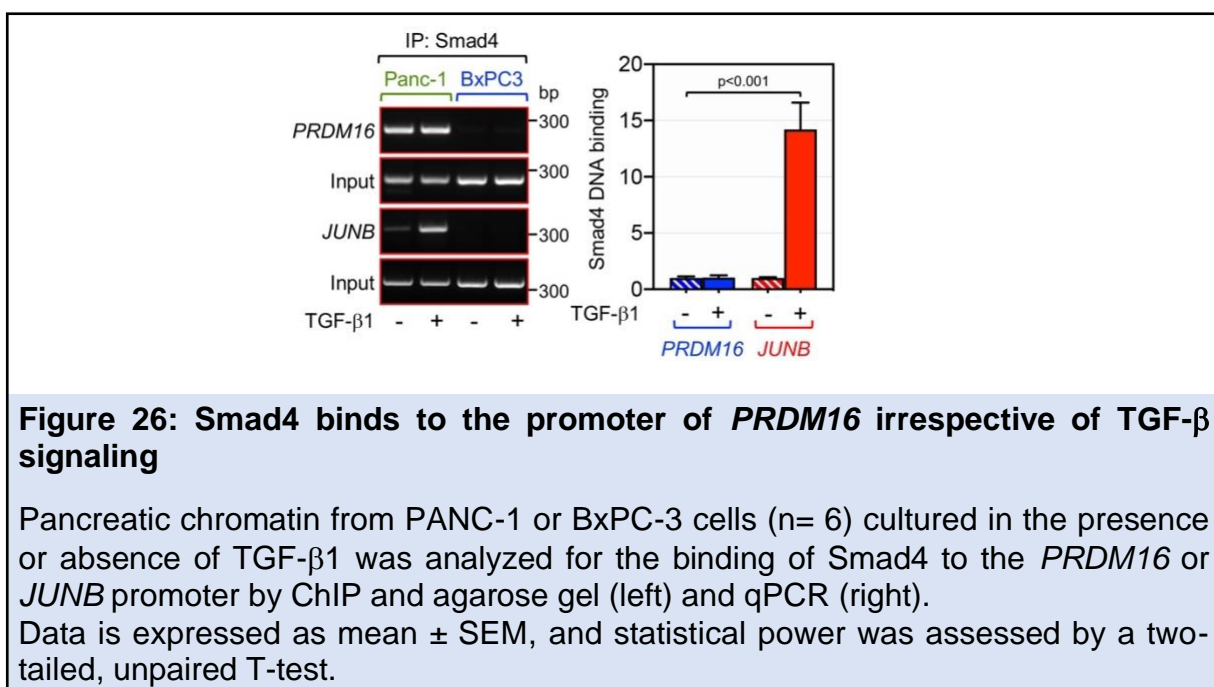
gRNA (Fig. 25, see also Fig. 29), implying that *SMAD4* inactivation is sufficient to mimic the effects of TGF- $\beta$ 1 stimulation.



Previous studies have shown that Smad proteins can stimulate or repress expression of TGF- $\beta$  responsive genes through direct binding to their promoter (David and Massague, 2018; Feng and Derynck, 2005; Massague, 2008). In addition, a substantial fraction of Smad4 has been shown to localize in the nucleus in the absence TGF- $\beta$  stimulation, but the physiopathological significance of this phenomenon remains unknown (Pierreux et al., 2000). Because *SMAD4* ablation in PANC-1 cells was sufficient to recapitulate the stimulatory effects of TGF- $\beta$  signaling on *PRDM16* expression, we initially reasoned that Smad4 might bind to and repress the *PRDM16* promoter at steady state, and that TGF- $\beta$  signaling activation might displace Smad4 from the *PRDM16* promoter. Accordingly, we conducted ChIP experiments, focusing on Smad conserved binding elements (SBE) within the *PRDM16* promoter that we identified through an *in-silico* analysis. Using chromatin

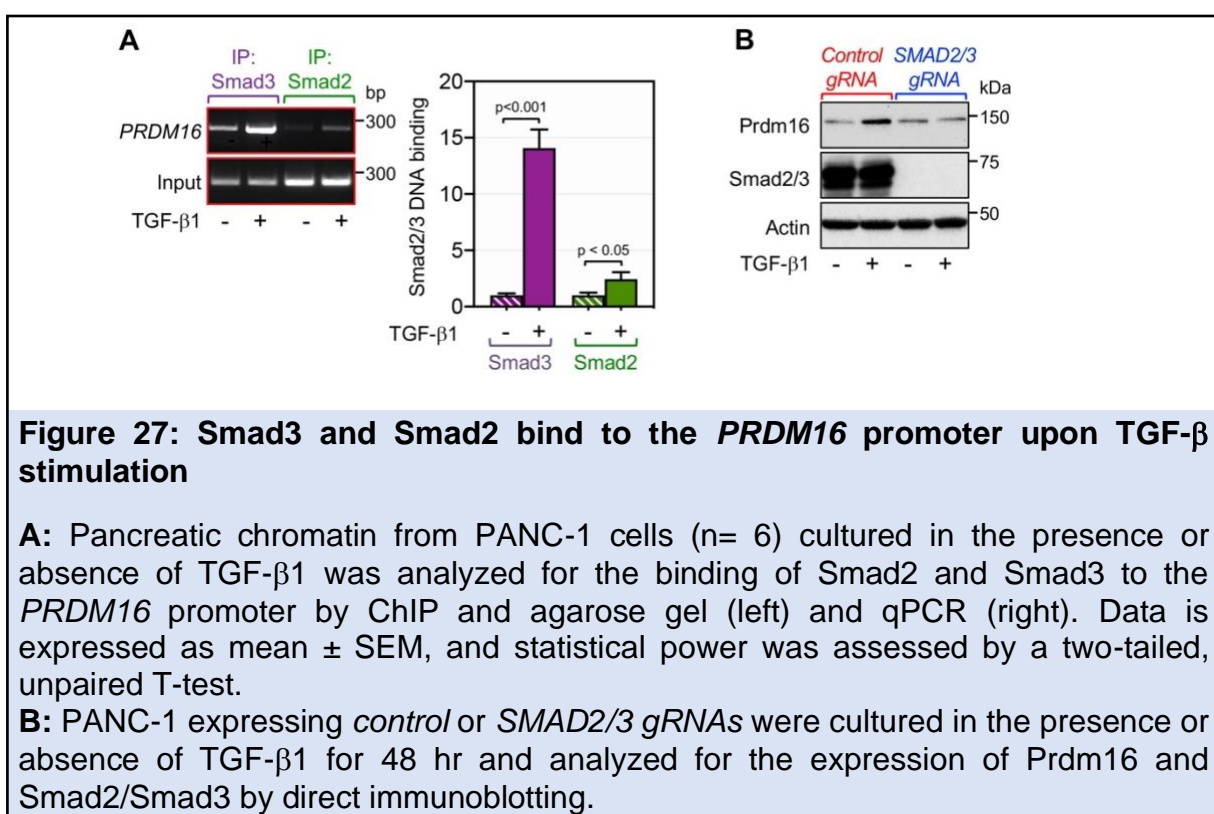


from PANC-1 cells, we detected a strong binding of Smad4 to the *PRDM16* promoter at steady state (Fig. 26). This binding is specific, as there was no signal in the human PDAC cell line BxPC-3 (Fig. 26), which bears natural homozygous deletion of *SMAD4* (Duda et al., 2003). Interestingly, treating PANC-1 cells with TGF- $\beta$ 1 had little or no effect on the binding of Smad4 to the *PRDM16* promoter despite eliciting a strong activation of this pathway, as assessed by the increased binding of Smad4 to the promoter of *JUNB* (Fig. 26), a well-characterized TGF- $\beta$  target gene (Sundqvist et al., 2018).



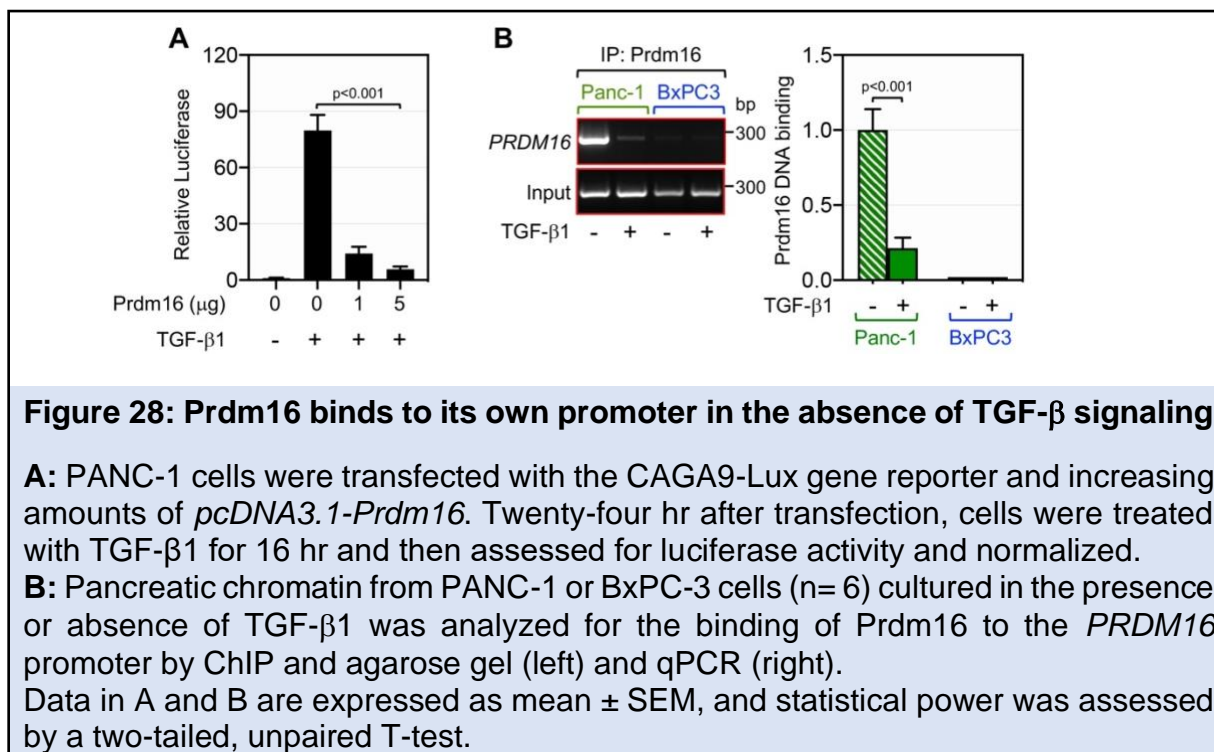
This observation, together with our gene expression experiments, strongly suggest that TGF- $\beta$  signaling might involve other players that act in partnership with Smad4 to repress *Prdm16* expression. To explore this possibility, we conducted ChIP experiments using antibodies to Smad2 and Smad3, as both transcription factors are known to interact with Smad4 in response to TGF- $\beta$  signaling (David and Massague,

2018; Feng and Derynck, 2005; Massague, 2008; Massague et al., 2005). We detected a slight but significant increase in the binding to Smad2 to the *PRDM16* promoter in PANC-1 cells upon stimulation with TGF- $\beta$ 1 (Fig. 27 A). In contrast, TGF- $\beta$ 1 stimulation induced a massive increase in the binding of Smad3 to the *PRDM16* promoter (Fig. 27 A). Concomitant deletion of *SMAD2* and *SMAD3* in PANC-1 cells resulted in almost complete blockade in TGF- $\beta$ -induced *Prdm16* expression (Fig. 27 B).



Although this finding provides a potential mechanism by which TGF- $\beta$  signaling could induce *Prdm16* expression, it failed to explain why deletion of *Smad4* in *KSC* mice leads to the derepression of *Prdm16*. Based on the literature (Chuikov et al., 2010; Stine et al., 2019; Takahata et al., 2009) and our data that *Prdm16* can repress Smad

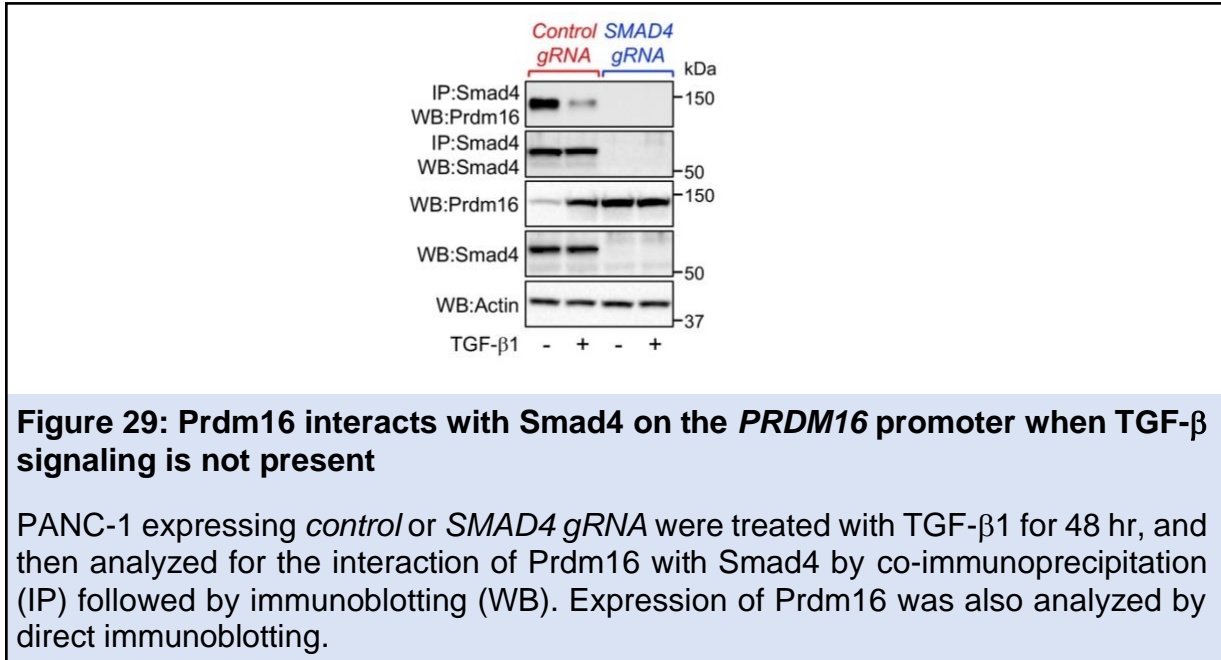
transcriptional activity in human PANC-1 cells (Fig. 28 A), we considered the possibility that Smad4 might recruit Prdm16 to its own promoter, thereby leading to *Prdm16* repression. Indeed, we detected a strong binding of Prdm16 to its promoter in PANC-1 cells at steady state, and this was almost completely suppressed upon TGF- $\beta$ 1 stimulation (Fig. 28 B), strongly suggesting that TGF- $\beta$  signaling activation might dislodge Prdm16 from its promoter. In comparison, we were not able to detect any binding of Prdm16 to its promoter in BxPC-3 cells (Fig. 28 B), attesting to the specificity of our experiments, and further providing strong evidence supporting the notion that Smad4 functions to recruit Prdm16 to its promoter to repress its expression.



To corroborate these findings, we conducted co-immunoprecipitation assays using PANC-1 cells, and detected a strong interaction between Prdm16 and Smad4, which



was inhibited upon treatment of cells with TGF- $\beta$ 1 (Fig. 29). Such interaction was not detected in PANC-1 cells deleted of *SMAD4* (Fig. 29), attesting to the specificity of the approach.



Finally, we generated a reporter construct in which luciferase expression is under the control of either wild-type or mutated (SBE) *PRDM16* promoter (Prdm16-Lux). We found that Smad4 was able to repress expression from the wild-type *PRDM16* promoter in PANC-1 cells (Fig. 30 A). More importantly, expression of Prdm16 was also able to suppress luciferase expression from the wild-type *PRDM16* promoter, and this effect was completely lost when the SBE mutated promoter was used in the assay (Fig. 30 A). Finally, expression of Prdm16 was able to repress the wild-type *PRDM16* promoter in BxPC-3 cells only when Smad4 was co-expressed (Fig. 30 B). Overall, these findings revealed that Smad4 functions as a potent repressor of *Prdm16*, therefore providing a mechanistic explanation as to why *KSC* mice display high expression of Prdm16.

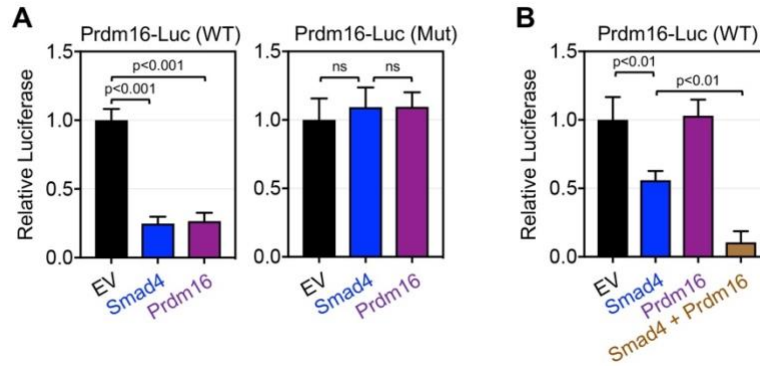


**Figure 30: Prdm16 represses its own transcription via Smad4**

**A:** PANC-1 cells were transfected with the *wild-type* (left) or *mutated Prdm16-Lux* (right) reporter together with *empty vector*, *pcDNA3.1-Prdm16* or *pCMV5-HA-Smad4*. Forty-eight hr after transfection, cells were assessed for luciferase activity and normalized (n= 6).

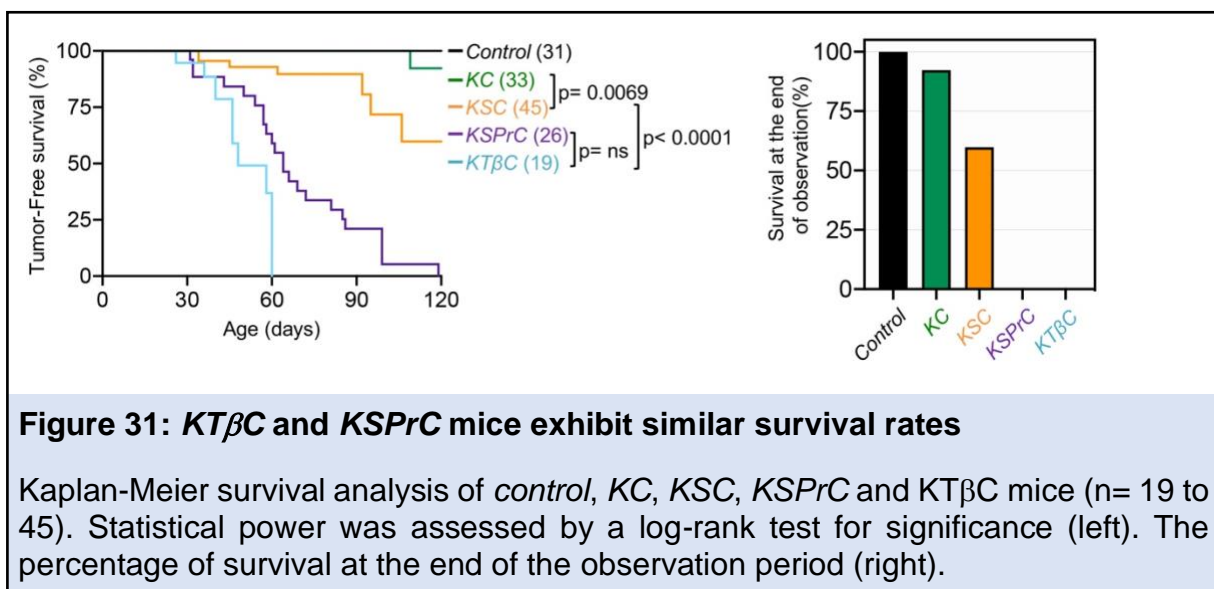
**B:** BxPC-3 cells were transfected with the *wild-type Prdm16-Lux* reporter together with the indicated combinations of *empty vector* (EV), *pcDNA3.1-Prdm16* and *pCMV5-HA-Smad4*. Forty-eight hr after transfection, cells were assessed for luciferase activity and normalized (n= 6).

Data in A and B are expressed as mean  $\pm$  SEM, and statistical power was assessed by a two-tailed, unpaired T-test.

#### 2.4.5 Concomitant inactivation of Prdm16 and Smad4 recapitulates the global inactivation of TGF- $\beta$ signaling

Both *SMAD4* and *T $\beta$ RII* are frequently inactivated in human PDAC, and landmark genetic experiments have shown that inactivation of either *Smad4* or *T $\beta$ RII* accelerates *Kras*<sup>G12D</sup>-driven PDAC (Bardeesy et al., 2006b; Ijichi et al., 2006; Izeradjene et al., 2007). To date, it remains largely unknown whether inactivation of *Smad4* or *T $\beta$ RII* could differentially impact the dynamics or trajectory of PDAC progression. Our mechanistic data that inactivation of *Smad4* recapitulates the effects of TGF- $\beta$  signaling on Prdm16 expression provided us with a unique platform to address this issue. To do so, we conducted an in-depth comparative analysis of the PDAC phenotypes in mice with homozygous deletion of *T $\beta$ RII* (*KT $\beta$ C*), *KSC* and

*KSPrC* mice side-by-side. *KC* and wild-type mice were used as controls. Kaplan-Meier analysis showed that *KTβC* mice developed lethal PDAC much earlier than *KSC* mice, often succumbing to the disease within four weeks of age and none survived beyond 17 weeks, whereas 60% of *KSC* mice survived within this observation period (Fig. 31). This observation indicates that global inactivation of TGF-β signaling through *TβRII* ablation is more efficient at deepening PDAC progression than inactivation of canonical TGF-β/Smad signaling through *Smad4* ablation. More importantly, we found that *KSPrC* mice succumbed to lethal PDAC with kinetics approaching that of *KTβC* mice (Fig. 31), suggesting that simultaneous inactivation of *Smad4* and *Prdm16* might be sufficient to recapitulate the global inactivation of TGF-β signaling.



Next, in light of our earlier findings that concomitant inactivation of *Prdm16* was able to shift the evolution of the IPMN-to-PDAC phenotype in *KSC* mice towards the PanIN-to-PDAC phenotype, we wondered whether ablation of *TβRII* or *Smad4* could differentially affect the nature of the premalignant lesions leading to PDAC, and

if so, whether this event depends on *Prdm16*. Thus, we conducted histopathological analyses to compare the PDAC phenotypes in *KSP<sup>PrC</sup>*, *KT $\beta$ C* and *KSC* mice both at the levels of pre-malignant and full-blown PDAC lesions. H&E staining showed that *KT $\beta$ C* tumors displayed uniformly poorly differentiated architecture, which is consistent with the rapid development of invasive PDAC in these mice (Fig. 32). Nevertheless, using *KT $\beta$ C* mice before displaying signs of invasive PDAC, we consistently noticed the presence of premalignant lesions that display the classical features of PanINs, as gauged by IHC using antibodies to CK19 and Muc5AC (Fig. 33). Interestingly, *KSP<sup>PrC</sup>* mice displayed similar cancerous phenotype as *KT $\beta$ C* mice, both in terms of PanIN and PDAC lesions (Figs. 32 and 33). In contrast, *KSC* mice consistently showed abundant and large IPMN lesions that exhibit high reactivity to the anti-Muc5AC antibody and Alcian blue (Fig. 33), which is in agreement with previous studies that *KSC* mice develop IPMN premalignant lesions rather than PanIN lesions (Bardeesy et al., 2006b; Izeradjene et al., 2007; Whittle et al., 2015). Taken together, these findings strongly suggest that inactivation of the entire TGF- $\beta$ /Smad pathway promotes PanIN-to-PDAC progression, whereas inactivation of Smad4 promotes IPMN-to-PDAC progression. In addition, since concomitant ablation of *Prdm16* and *Smad4* resulted in highly aggressive PDAC similar to what was observed in *KT $\beta$ C* mice, we suggest that global inactivation of TGF- $\beta$  signaling might simultaneously inactivate both Smad4 and *Prdm16*.

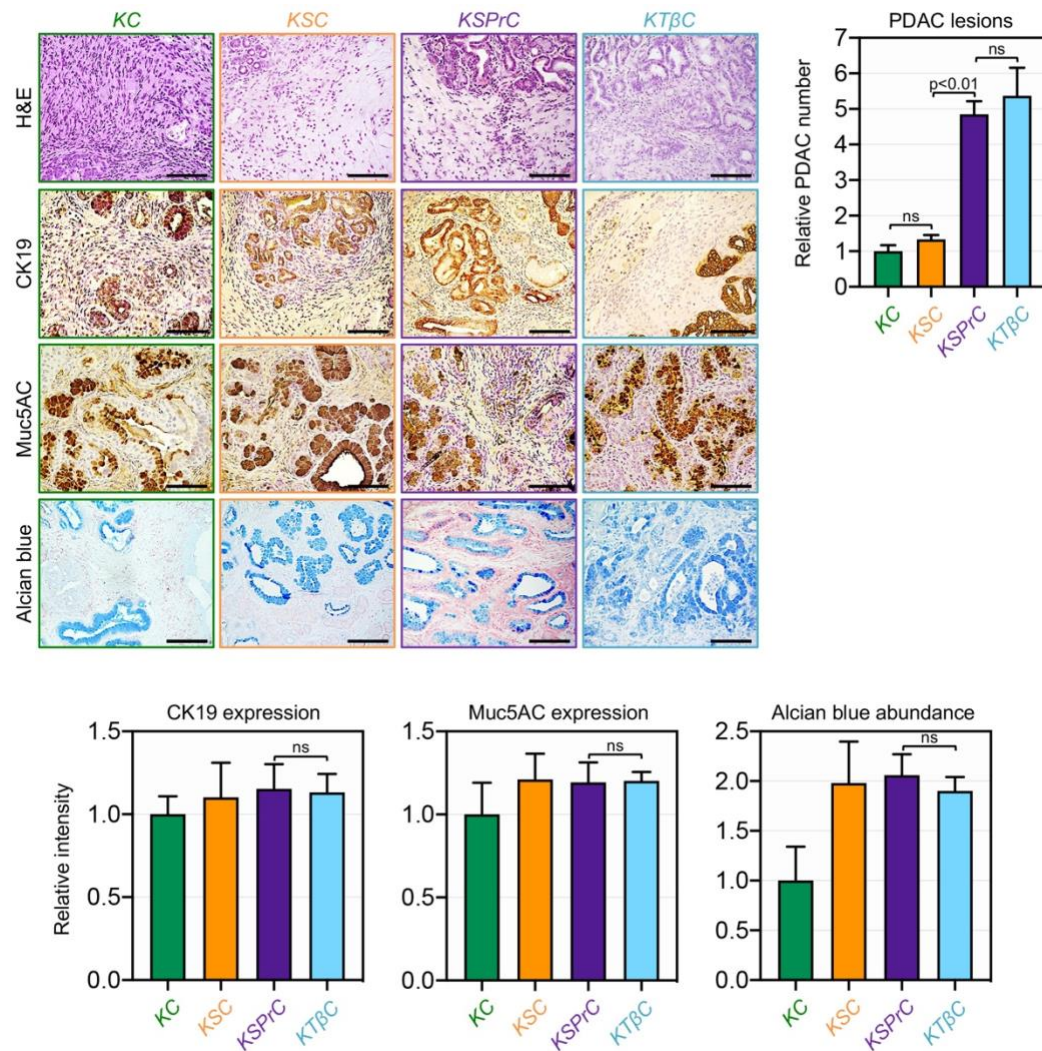
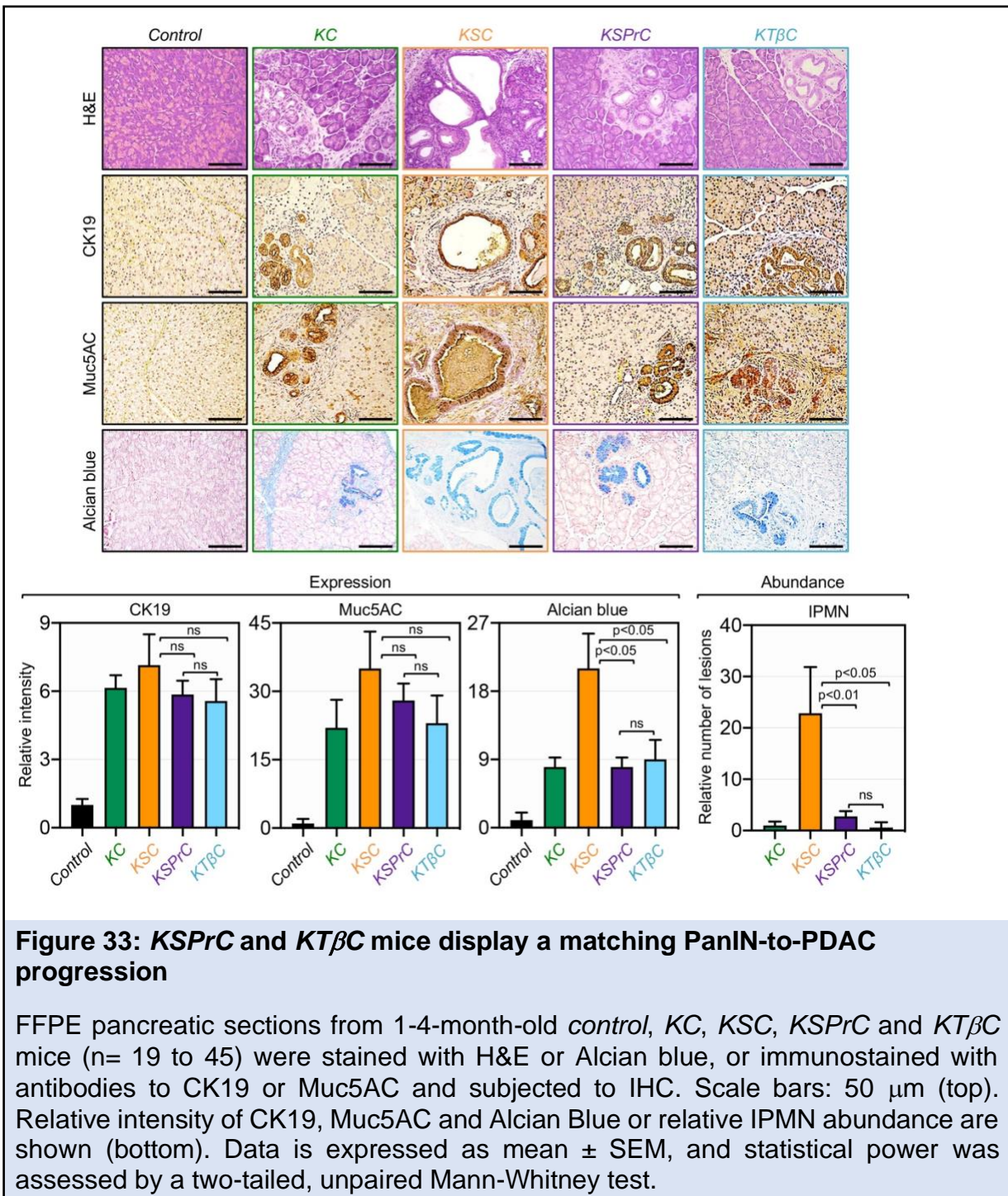


**Figure 32: *KSPrC* and *KTβC* mice exhibit a PDAC phenotype that mimic each other**

FFPE pancreatic sections from 1-4-month-old *KC*, *KSC*, *KSPrC* and *KTβC* mice (n= 19 to 45) with full-blown PDAC were stained with H&E or Alcian blue, or immunostained with antibodies to CK19 or Muc5AC and subjected to IHC. Representative pictures are shown. Scale bars: 50  $\mu$ m (top left). Relative number of PDAC lesions (top right). Relative intensity of CK19, Muc5AC and Alcian blue staining in PDAC lesions (bottom). Data is expressed as mean  $\pm$  SEM, and statistical power was assessed by a two-tailed, unpaired Mann-Whitney test.





## 2.5 Discussion

Prdm16 belongs to the PR domain-containing protein family of transcription factors, which control a plethora of essential cellular processes, including specification of cell

lineage during development (Chi and Cohen, 2016). Prdm16 was first identified in leukemia, where truncation mutants lacking functional domains behaved as oncogenic (Zhou et al., 2016), providing the first indication that Prdm16 might function as a tumor suppressor. Besides its involvement in leukemia, several studies have subsequently shown that Prdm16 controls brown fat cell differentiation as well as dedifferentiation of white fat to beige fat (Harms et al., 2015; Hiraie et al., 2017; Seale et al., 2008; Seale et al., 2007). Moreover, Prdm16 is required for stemness in multiple tissues, including hematopoietic and nervous systems (Chi and Cohen, 2016). Germline deletion of *Prdm16* in mice impairs the maintenance of neural and hematopoietic stem cells during fetal development, resulting in neonatal death (Shimada et al., 2017). As such, this lethal phenotype hampered any further investigation to delineate a possible role of Prdm16 in cell fate determination in other organ systems, such as pancreas, where the same progenitor cells give rise to all pancreas lineages, e.g., ductal, acinar and islet (Gu et al., 2003). In this study, we found that conditional deletion of *Prdm16* in early pancreatic progenitor cells had no discernible impact on animal health or pancreas physiology, indicating that Prdm16 is dispensable for pancreas development and function. Because mutational inactivation of *PRDM16* has been shown to be associated with leukemia (Zhou et al., 2016), we went on to explore whether Prdm16 could contribute to the pathogenesis and/or progression of PDAC, in which acquisition of oncogenic *KRAS* endows acinar cells with stemness traits that facilitate their differentiation towards a ductal-like lineage, thereby culminating in acinar-to-ductal metaplasia and attendant emergence of premalignant lesions (Bardeesy et al., 2006a; Gu et al., 2003; Park et al., 2008;

Tuveson et al., 2004). Progression of premalignant lesions either follows the PanIN-to-PDAC sequence, MCN-to-PDAC or IPMN-to-PDAC sequence, depending on the nature of the secondary genetic events (Bardeesy et al., 2006a; Bardeesy et al., 2006b; Gu et al., 2003; Tuveson et al., 2004). Yet, among the most studied secondary genetic alterations in PDAC, only *Smad4* inactivation stood out as the main mechanism that enables progression through the IPMN-to-PDAC sequence (Bardeesy et al., 2006b; Whittle et al., 2015). To the best of our knowledge, how *Smad4* inactivation facilitates this IPMN-to-PDAC transition phenotype has never been addressed experimentally. Using the *Kras*<sup>G12D</sup>-based mouse model of PDAC, we confirmed that *KSC* mice develop mostly IPMN lesions as described initially (Bardeesy et al., 2006b) rather MCN lesions described in a subsequent study (Izeradjene et al., 2007). Most importantly, we found that concomitant ablation of *Prdm16* and *Smad4* (*KSPrC*) resulted in highly aggressive tumors, which develop with very short latencies to the full-blown PDAC and frequently metastasize to the lung, a site associated with the human disease (Connor and Gallinger, 2022; Hidalgo, 2010). Comprehensive histopathological analyses revealed that these tumors follow the PanIN-to-PDAC progression route rather than the IPMN-to-PDAC progression route that proceeds with ablation of *Smad4* alone. Because inactivating *Smad4* led to the increased expression of *Prdm16*, we propose a model in which *Prdm16* functions as a molecular switch to dictate whether the malignant transformation process follows the IPMN-to-PDAC route or the PanIN-to-PDAC route (Fig. 34).



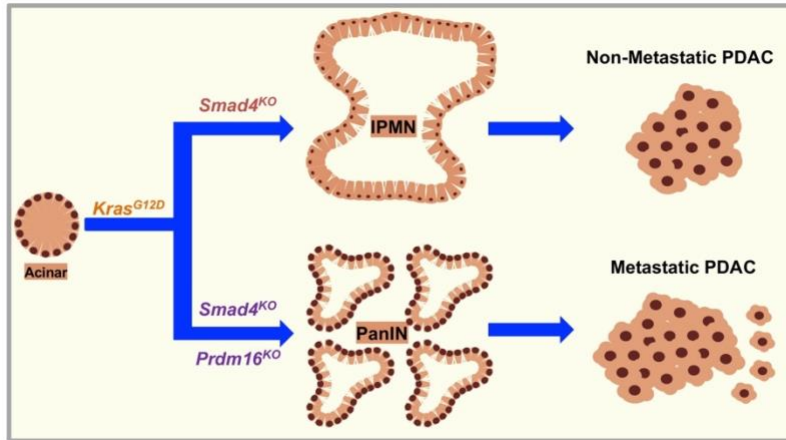


**Figure 34: Model for the functional interaction between Smad4 and Prdm16 during PDAC formation and progression**

This model also posits that Prdm16 might function to suppress PDAC pathogenesis at very early stages of the malignancy. In further support of this notion, we found that ablating *PRDM16* in the human PDAC cancer cell lines BxPC-3 and PANC-1 did not influence their proliferative or metastatic behaviors, as evidenced using a variety of in vivo and in vitro tumor growth and invasion assays. In light of these findings, a more comprehensive investigation using genetic and histological approaches are needed to firmly establish whether Prdm16 indeed elicits its tumor suppressor activity at early stages, and if so, whether this occurs through direct effects on cancer cell growth or tumor microenvironment reprogramming. As such, our findings open up unique frameworks that would ultimately leverage general efforts to unravel mechanistic paradigms of PDAC, for which very limited therapeutic interventions are currently available.

Accumulating evidence suggests that Prdm16 functions as a potent inhibitor of TGF- $\beta$ /Smad signaling under various physiological contexts ([Chuikov et al., 2010](#);

Stine et al., 2019; Takahata et al., 2009). TGF- $\beta$ /Smad signaling is well known to play a dual role during cancer progression, functioning at early stages as a tumor suppressor to restrict the malignant transformation, and at late stages as a tumor promoter to facilitate cell invasion and metastasis (Feng and Derynck, 2005). To date, the most appealing speculations as to TGF- $\beta$  dual function during PDAC progression have been that loss of the TGF- $\beta$  cytostatic function enables cells to escape growth-inhibitory regulation, which would ultimately culminate in malignant transformation (David et al., 2016; Feng and Derynck, 2005; Massague, 2008). Once the tumor has developed, other TGF- $\beta$  responses unrelated to its cytostatic function then supposedly prevail presumably in a manner that facilitates PDAC invasion and metastasis (Bardeesy et al., 2006b; Feng and Derynck, 2005; Ijichi et al., 2006; Massague, 2008). Interestingly, high levels of TGF- $\beta$  expression in human PDAC strongly correlates with poor prognosis (Friess et al., 1993; Parajuli et al., 2019), which raises a conundrum as to whether activation of TGF- $\beta$  signaling could contribute directly to malignant transformation in addition to driving cell invasion and metastasis. However, subsequent studies have shown that *Smad4* inactivation in the context of Kras<sup>G12D</sup> (*KSC*) led to the acceleration of PDAC (Bardeesy et al., 2006b; Izeradjene et al., 2007), unequivocally confirming the tumor suppressor role of TGF- $\beta$  signaling in PDAC. Nevertheless, the tumors deficient for *Smad4* retained epithelial differentiation and manifested an attenuated metastatic potential (Bardeesy et al., 2006b; Whittle et al., 2015), which is also in favor of a tumor promoter role of TGF- $\beta$  signaling. So far, definitive experimental evidence on whether inactivation of canonical TGF- $\beta$ /Smad signaling per se is sufficient to suppress PDAC invasion and

metastasis in an irreversible manner is still lacking. Here, we found that ablating *Prdm16* in a *Smad4* null-background was sufficient to render the PDAC tumors again highly invasive and metastatic. Intriguingly, concomitant ablation of *Prdm16* in *KSC* mice also resulted in a shift from IPMN to PanIN, which could conceivably contribute to metastasis in *KSPrc* mice, as the vast majority of PDAC GEMMs that develop PanINs also develop highly metastatic PDAC, including *KSPC* mice (*Smad4* deletion and p53.R172H expression), which behave similarly to our *KSPrc* mice ([Bardeesy et al., 2006a](#); [Bardeesy et al., 2006b](#); [Tuveson et al., 2004](#); [Whittle et al., 2015](#)). These findings, together with the observation that *Prdm16* expression is lost during late stages of PDAC, highlight *Prdm16* as a key player in PDAC progression and metastasis when *Smad4* is inactivated. Because TGF- $\beta$  signaling activation leads to the accumulation of *Prdm16* through the suppression of *Smad4* inhibitory effects, one would speculate that *Smad4* and *Prdm16* might function in the same signaling network that integrates the TGF- $\beta$  tumor promoter effects during PDAC progression. However, it is also conceivable that *Prdm16* might function to suppress metastasis induced by other TGF- $\beta$  superfamily members, such as Activins and BMPs, which are known to signal through *Smad4*, and can enhance malignancy and promote cancer metastasis in a variety of human malignancies ([Attisano and Wrana, 2000](#); [Feng and Derynck, 2005](#); [Pickup et al., 2017](#)). As such, a comprehensive investigation of the mechanisms by which *Smad4* and *Prdm16* interact to influence PDAC progression may uncover the existence of additional key players and/or pathways that are amenable to therapeutic interventions.

Perhaps the most intriguing finding in this study was the persistent increase in *Prdm16* expression during the progression from IPMN to PDAC in *KSC* mice, which at first glance seems to support a hypothesis in which *Smad4* might function as a repressor of *Prdm16* during PDAC progression, and hence conceivably that canonical TGF- $\beta$ /*Smad* signaling might also repress *Prdm16* expression. Quite unexpectedly, we found that activation of TGF- $\beta$  signaling did not repress *Prdm16* expression, but rather resulted in a strong accumulation of both *Prdm16* mRNA and protein both in *KSC* mice and human PANC-1 cells. Noteworthy, we also detected relatively high expression in the stromal compartment, which likely occurs because of the increased TGF- $\beta$  signaling, which is known to take place during PDAC progression and contribute to the desmoplastic stroma of this malignancy ([Friess et al., 1993](#)). In efforts to probe the underlying mechanisms, we found that inactivating *Smad4* was sufficient to recapitulate the effects of TGF- $\beta$  signaling, inducing *Prdm16* expression to an extent similar to that elicited by TGF- $\beta$ 1. Based on these observations, we reasoned that activation of TGF- $\beta$  signaling might relieve the transcriptional repression imposed by *Smad4* on the *Prdm16* promoter. However, although we found that *Smad4* associated strongly with the *PRDM16* promoter at steady state, this binding was not affected by the activation of TGF- $\beta$ 1 signaling, indicating that other factors are involved in TGF- $\beta$ -mediated *Prdm16* expression. Probing this possibility, we detected a strong binding of *Prdm16* to its own promoter at steady state, which was almost completely abolished by TGF- $\beta$  stimulation, suggesting that activation of TGF- $\beta$  signaling might dislodge *Prdm16* from its own promoter. Of note, *Prdm16* failed to bind to its promoter in cells deficient for *SMAD4*,

suggesting that Smad4 might associate with and recruit Prdm16 to the *PRDM16* promoter. Because Prdm16 has been shown to function as a potent transcriptional repressor in various contexts ([Pinheiro et al., 2012](#); [Seale et al., 2008](#); [Seale et al., 2007](#); [Stine et al., 2019](#); [Takahata et al., 2009](#)), we propose a model in which Prdm16 mediates its own repression once it has been recruited to its promoter by Smad4. While these data demonstrate for the first time that Prdm16 can repress its own expression, we cannot exclude the possibility that other mechanisms might also contribute to this phenomenon. Despite this limitation, our study sheds light on a previously uncharacterized interplay between Smad4 and Prdm16, which appears to dictate the progression trajectory of PDAC. Going forward, we anticipate that our discovery will guide forthcoming studies seeking to understand mechanistic paradigms of PDAC, which could ultimately pave the way for innovative therapeutic breakthroughs to curb this deadly disease.

ARTICLE

# Antagonism between Prdm16 and Smad4 specifies the trajectory and progression of pancreatic cancer

Eric Hurwitz<sup>1</sup>, Parash Parajuli<sup>1</sup>, Seval Ozkan<sup>2</sup>, Celine Prunier<sup>3</sup>, Thien Ly Nguyen<sup>1,2</sup>, Deanna Campbell<sup>1</sup>, Creighton Friend<sup>1</sup>, Allyn Austin Bryan<sup>1</sup>, Ting-Xuan Lu<sup>1</sup>, Steven Christopher Smith<sup>4</sup>, Mohammed Shawkat Razzaque<sup>5</sup>, Keli Xu<sup>2</sup>, and Azeddine Atfi<sup>1,3</sup>

The transcription factor Prdm16 functions as a potent suppressor of transforming growth factor-beta (TGF- $\beta$ ) signaling, whose inactivation is deemed essential to the progression of pancreatic ductal adenocarcinoma (PDAC). Using the KrasG12D-based mouse model of human PDAC, we surprisingly found that ablating Prdm16 did not block but instead accelerated PDAC formation and progression, suggesting that Prdm16 might function as a tumor suppressor in this malignancy. Subsequent genetic experiments showed that ablating Prdm16 along with Smad4 resulted in a shift from a well-differentiated and confined neoplasm to a highly aggressive and metastatic disease, which was associated with a striking deviation in the trajectory of the premalignant lesions. Mechanistically, we found that Smad4 interacted with and recruited Prdm16 to repress its own expression, therefore pinpointing a model in which Prdm16 functions downstream of Smad4 to constrain the PDAC malignant phenotype. Collectively, these findings unveil an unprecedented antagonistic interaction between the tumor suppressors Smad4 and Prdm16 that functions to restrict PDAC progression and metastasis.

## Introduction

Pancreatic ductal adenocarcinoma (PDAC) is the most aggressive type of pancreatic cancer, currently ranked as the fourth leading cause of cancer-related deaths in the United States (Connor and Gallinger, 2021; Hidalgo, 2010). Most of PDAC patients present with both locally invasive tumors and widespread metastasis, thus rendering ineffective the resection of the primary tumor as well as the applicability of the dismal therapeutic options available (Hidalgo, 2010; Stathis and Moore, 2010). Consequently, the outcome of PDAC patients remains extremely poor, with an overall 5-yr survival rate of less than 11%.

PDAC tumors emerge through three types of distinct precursor lesions called pancreatic intraepithelial neoplasia (PanIN), intraductal papillary mucinous neoplasia (IPMN), and mucinous cystic neoplasia (MCN), respectively (Connor and Gallinger, 2021; Yonezawa et al., 2008). These early-stage lesions harbor various genetic alterations, the earliest and most pervasive of which are activating mutations in KRAS, occurring in ~90% of PDAC tumors (Hayashi et al., 2021). The current model posits that mutational activation of KRAS represents an essential initiating event, whereas subsequent accumulation of inactivating mutations in the tumor suppressor genes p16INK4a, SMAD4, and TP53 is necessary for PDAC to progress and metastasize (Hayashi et al., 2021; Iacobuzio-Donahue, 2012).

Significant efforts have been made over the past two decades to create genetically engineered mouse models (GEMMs) that faithfully recapitulate the prominent features of human PDAC. For instance, pancreas-specific expression of KrasG12D in mice is sufficient to initiate PanINs, which occasionally progress into invasive PDAC following a long latency period, supporting the general notion that oncogenic activation of KRAS represents the main initiating genetic event in PDAC (Buscail et al., 2020; Hingorani et al., 2005; Tuveson et al., 2004; Westphalen and Olive, 2012). Concomitant expression of KrasG12D and deletion of any of the three cardinal tumor suppressors, e.g., Trp53, p16INK4a, Smad4, accelerate PDAC progression, though the nature and final outcome of the tumors might differ. Indeed, while mice with the combined expression of KrasG12D and deletion of Trp53 (KPC) or p16INK4a (KIC) develop PanINs that progress very rapidly to highly aggressive and metastatic PDAC, mice with the combined expression of KrasG12D and deletion of Smad4 (KSC) develop mostly IPMNs, which also progress to invasive PDAC, but the terminal disease develops with a much slower onset and manifests an attenuated metastatic phenotype (Bardeesy et al., 2006a; Bardeesy et al., 2006b; Hingorani et al., 2005; Izeradjene et al., 2007). Other examples of PDAC GEMMs include KTRC mice, which harbor KrasG12D and deletion of the

<sup>1</sup>Department of Biochemistry and Molecular Biology, Massey Cancer Center, Virginia Commonwealth University, Richmond, VA, USA; <sup>2</sup>Cancer Institute, University of Mississippi Medical Centre, Jackson, MS, USA; <sup>3</sup>Sorbonne Université, Inserm, Centre de Recherche Saint-Antoine, CRSA, Paris, France; <sup>4</sup>Department of Pathology, Virginia Commonwealth University, Richmond, VA, USA; <sup>5</sup>Department of Pathology, Lake Erie College of Osteopathic Medicine, Erie, PA, USA.

Correspondence to Azeddine Atfi: [azeddine.atfi@vcuhealth.org](mailto:azeddine.atfi@vcuhealth.org).

© 2023 Hurwitz et al. This article is available under a Creative Commons License (Attribution 4.0 International, as described at <https://creativecommons.org/licenses/by/4.0/>).

Rockefeller University Press

J. Cell Biol. 2023 Vol. 222 No. 4 e202203036



<https://doi.org/10.1083/jcb.202203036>

1 of 19



transforming growth factor-beta (TGF- $\beta$ ) type II receptor (T $\beta$ RII) gene, the latter being inactivated by mutations or deletions in 4% of PDAC (Iacobuzio-Donahue, 2012; Ijichi et al., 2006).

TGF- $\beta$  signaling regulates a wide array of biological processes vital for normal cell growth, function, and homeostasis (David and Massagué, 2018; Massagué, 2008). TGF- $\beta$  initiates signaling by inducing the assembly of a receptor complex composed of two types of transmembrane serine/threonine kinases called T $\beta$ RI and T $\beta$ RII. In that complex, the constitutive kinase of T $\beta$ RII phosphorylates and activates the kinase activity of T $\beta$ RI, which then propagates the signal to the nucleus through phosphorylation of Smad2 and Smad3 (David and Massagué, 2018; Feng and Derynck, 2005; Massagué et al., 2005). Once phosphorylated, Smad2 or Smad3 associates with Smad4, and the two complexes accumulate in the nucleus to regulate the expression of TGF- $\beta$  target genes through cooperative interactions with transcriptional cofactors or corepressors (David and Massagué, 2018; Feng and Derynck, 2005; Massagué, 2008; Massagué et al., 2005).

Because of the widespread roles of TGF- $\beta$  signaling in cellular functions, there must be multiple levels of positive and negative regulations to fine-tune initiation, magnitude, or termination of the response depending on the cell type or physiological context. One example of the mechanisms that limit TGF- $\beta$  signaling involves the transcription factor PR domain containing 16 (Prdm16). Upon accumulation in the nucleus, the Smad3/Smad4 complex associates with the general transcriptional coactivators CBP and p300 to activate transcription of TGF- $\beta$  target genes (David and Massagué, 2018; Feng and Derynck, 2005; Massagué, 2008; Massagué et al., 2005). Conversely, the Smad complex can also associate with Prdm16 and its partner c-Ski, which leads to the recruitment of general transcriptional corepressor complexes containing histone deacetylases and concomitant displacement of CBP and p300, thereby resulting in transcriptional repression (Takahata et al., 2009).

In addition to its function as a suppressor of TGF- $\beta$  signaling, Prdm16 has been shown to play key roles in a number of biological processes, including differentiation of brown fat and specification of hematopoietic and neuronal stem cell fate (Chi and Cohen, 2016; Seale et al., 2007; Shimada et al., 2017). Prdm16 possesses a methyltransferase activity that catalyzes the methylation of Lysine-9 on histone-3 (H3K9), a mark associated with heterochromatin formation and gene expression (Jambhekar et al., 2019; Pinheiro et al., 2012). Recently, Prdm16 loss-of-function has been shown to play an instrumental role in leukemia driven by the MLL fusion oncoprotein (Zhou et al., 2016). Because the MLL gene encodes a histone-3 Lysine-4 (H3K4) methyltransferase that is critical in promoting gene expression during hematopoiesis (Xue et al., 2019), it has been postulated that Prdm16 might suppress leukemia pathogenesis owing to its ability to drive heterochromatin formation (Pinheiro et al., 2012; Zhou et al., 2016). At present, whether Prdm16 has any role in cancer pathogenesis and progression that is linked to its function in TGF- $\beta$  signaling is still unknown. Here, we combined several orthogonal approaches and GEMMs to demonstrate that Prdm16 functions downstream of Smad4 to suppress PDAC

progression and metastasis. As such, our findings unveil a previously uncharacterized mechanism that orchestrates Prdm16 tumor-suppressive function, and further shed new insights into the molecular etiology of PDAC, a fatal disease for which no effective therapeutics are currently available.

## Results

### Transient expression of Prdm16 during PDAC progression

To explore the possible involvement of Prdm16 in PDAC, we conducted Kaplan-Meier analysis using The Cancer Genome Atlas (TCGA) dataset. As shown in Fig. 1 A, low PRDM16 expression is associated with poor survival, providing an initial hint that Prdm16 might function as a tumor suppressor in PDAC. To substantiate this finding, we analyzed Prdm16 expression by immunohistochemistry (IHC) using large human tissue microarrays (TMAs) comprising samples with tumor lesions at various stages (e.g., PanIN1, PanIN2, PanIN3, PDAC) and normal tissues. Using a highly specific antibody to Prdm16 (see Fig. S2 A), we detected Prdm16 expression in both cancerous lesions and stromal areas (Fig. 1 B). Interestingly, Prdm16 expression appeared to fluctuate significantly during PDAC progression, commencing with a relatively low level in normal tissue, then rising in early PanINs, and finally declining to the background level in invasive PDAC (Fig. 1 B). Although this finding fits well with the notion that Prdm16 expression might be downregulated because of the accumulation of late genetic or epigenetic alterations, it did not shed light on the mechanisms leading to its transient expression during PDAC progression. To address this issue rigorously, we sought to utilize GEMMs that faithfully recapitulate the human PDAC in a uniform genetic background (Bardeesy et al., 2006a; Bardeesy et al., 2006b; Hingorani et al., 2005; Izeradjene et al., 2007; Tuveson et al., 2004). We initially utilized mice with pancreas-specific expression of KrasG12D alone (KC) and detected transient expression of the Prdm16 protein during PDAC progression, similar to what was observed in human PDAC, being relatively high in PanINs and very modest to low in normal tissue and invasive PDAC (Fig. 1 C). Confirmation of this result was obtained by comparative qRT-PCR experiments using cohorts of KC mice at the age of 3 mo when they experience mostly PanINs and 10 mo when they display visible signs of terminal PDAC (Fig. 1 D; Parajuli et al., 2020; Parajuli et al., 2019). To understand this phenomenon more deeply, we generated mice with KrasG12D together with deletion of Trp53 (KPC), p16Ink4a (KIC), or Smad4 (KSC). Noteworthy, we found that KSC mice had a longer survival rate than KIC and KPC mice, while the two latter had almost similar survival (Fig. S1 A). With regard to Prdm16 expression, we found that KIC and KPC mice behaved similarly to KC mice (Fig. S1, B and C), suggesting that transient expression of Prdm16 might take place even under the presence of the most common and aggressive genetic alterations that facilitate PDAC progression (Hayashi et al., 2021; Iacobuzio-Donahue, 2012). But most appealing was the fact that Prdm16 expression in KSC mice did not follow this transient pattern of Prdm16 expression, increasing markedly in IPMN lesions but thereafter remaining constant in PDAC lesions (Fig. 1 E), suggesting that Smad4 might influence



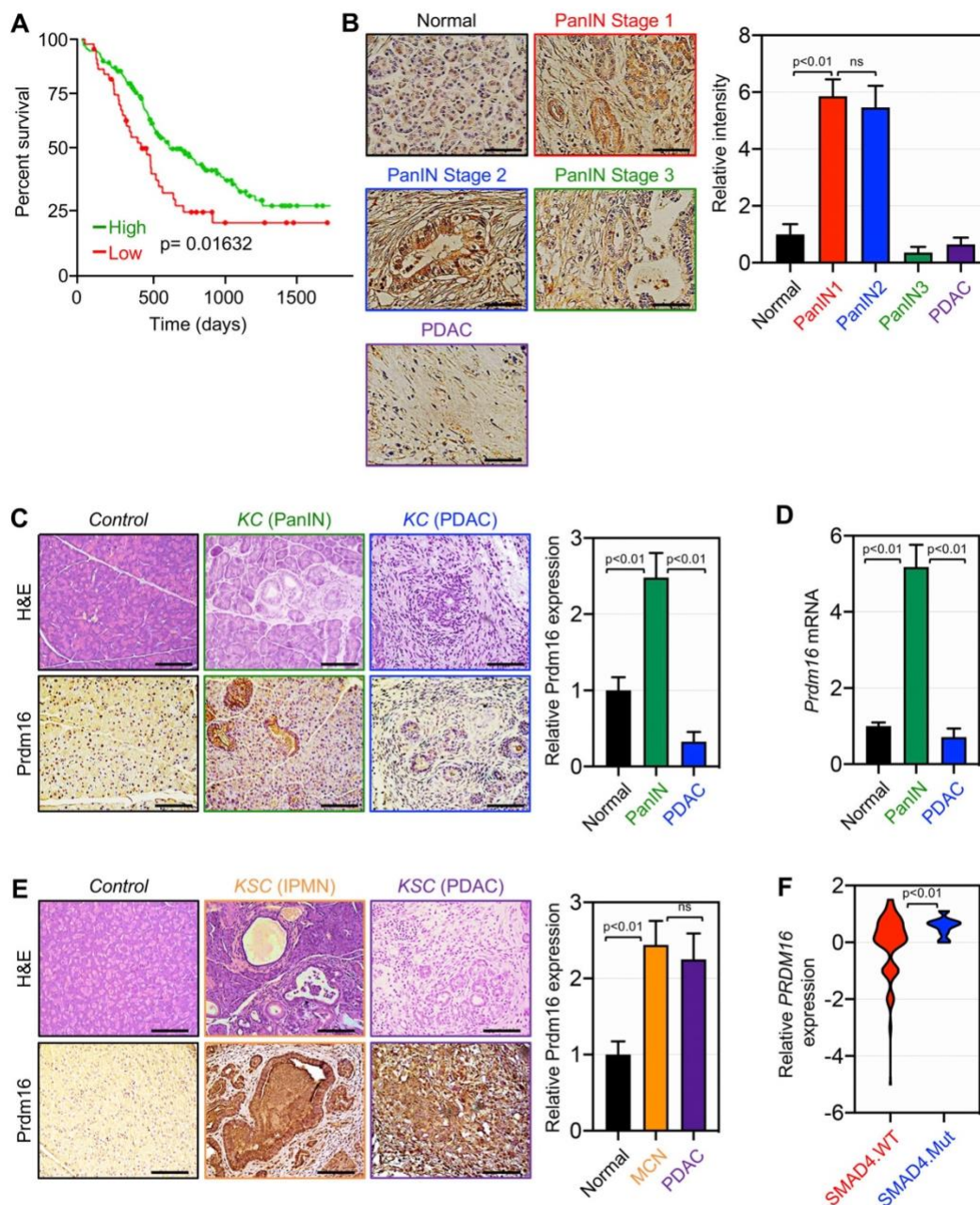


**Figure 1. Transient expression of Prdm16 during PDAC progression.** (A) Kaplan-Meier survival of PDAC patients based on high versus low PRDM16 expression was conducted using the TCGA dataset. Statistical power was assessed by log-rank test for significance. (B) Prdm16 protein expression was analyzed by IHC using human PDAC TMAs containing both normal tissues and PanIN/PDAC lesions ( $n = 152$ ). Representative pictures of normal, PanIN, and PDAC areas are shown. Scale bars: 50  $\mu$ m (left). Relative Prdm16 expression in normal, PanIN, and PDAC areas (right). Data are expressed as mean  $\pm$  SEM. (C) FFPE pancreatic sections from 4-mo-old control and KC mice ( $n = 31$  to 33) were stained with H&E or immunostained with anti-Prdm16 antibody and subjected to IHC. Representative pictures of normal, PanIN, and PDAC areas are shown. Scale bars: 50  $\mu$ m (left). Relative Prdm16 expression in normal, PanIN, and PDAC areas (right). Data are expressed as mean  $\pm$  SEM. (D) Expression of Prdm16 mRNA in pancreas from 3-mo-old control or KC mice ( $n = 6$ ) with PanIN or 10-mo-old KC mice with terminal PDAC was analyzed by qRT-PCR. Data are expressed as mean  $\pm$  SEM. (E) FFPE pancreatic sections from 4-mo-



old control and KSC mice ( $n = 31-45$ ) were stained with H&E or immunostained with anti-Prdm16 antibody and subjected to IHC. Representative pictures of normal, IPMN and PDAC areas are shown. Scale bars: 50  $\mu\text{m}$  (left). Relative Prdm16 expression in normal, IPMN and PDAC areas are shown (right). Data are expressed as mean  $\pm$  SEM. (F) Relative expression of PRDM16 in human samples with wild-type or mutated SMAD4 was conducted using the TCGA dataset. Data are presented as a violin plot. Statistical power in B–F was assessed by a two-tailed, unpaired Mann–Whitney test.

Prdm16 expression during the progression from IPMN to full-blown PDAC. Co-immunofluorescence assays using anti-Prdm16 antibody together with antibodies to E-cadherin (epithelial marker) or vimentin (mesenchymal marker) showed that Prdm16 expression remained very high in E-cadherin + cells as compared to vimentin + cells (Fig. S1 D). Consistent with these findings, we found that patients with low expression of Prdm16 had the worst survival if they carry SMAD4 mutations (Fig. S1 E). Moreover, interrogating the TCGA dataset revealed that samples with deleterious genetic alterations in SMAD4 display higher expression of PRDM16 as compared to samples with wild-type SMAD4 (Fig. 1 F). As such, these data hint at the existence of an antagonistic association between Smad4 and Prdm16 during PDAC progression; we will return to this notion later.

#### Prdm16 accelerates KrasG12D-driven PDAC

The aforementioned data prompted us to investigate whether Prdm16 could contribute to PDAC initiation, progression, or both. To do so, we generated mice with pancreas-specific deletion of Prdm16 (Prdm16KO) by crossing mice bearing a floxed allele of Prdm16 with Pdx1-Cre mice, which express Cre recombinase in all pancreatic progenitor cells that give rise to ductal, acinar, and islet compartments very early (E8.5) during development (Gu et al., 2003). Prdm16KO mice were born with the normal Mendelian frequency, develop normally without any signs of anatomic abnormalities, and were fertile. Effective deletion of Prdm16 in the pancreatic epithelium was confirmed by RT-PCR and IHC (Fig. 2 A and Fig. S2 A). To investigate whether Prdm16 deficiency could affect pancreas histology or function, we conducted a comprehensive analysis of pancreatic sections either by hematoxylin and eosin (H&E) staining, IHC or immunofluorescence (IF) encompassing all major tissue compartments, including duct (cytokeratin 19, CK19), acini (amylase), stroma ( $\alpha$ -SMA), and islet (insulin, glucagon, chromogranin-A). We were not able to detect any noticeable changes in all three compartments irrespective of the age of mice analyzed (Fig. 2, B–D; and Fig. S2, B and C). Congruently, there was also no difference in fasting blood glucose between wild-type and Prdm16KO mice (Fig. S2 D). Thus, inactivation of Prdm16 throughout embryonic development and postnatal life was insufficient to perturb pancreas homeostasis or drive sporadic pancreatic cancers.

Next, we sought to investigate whether Prdm16 could influence PDAC progression initiated through activation of Kras signaling. The salient genetic features of PDAC originate with the near-ubiquitous gain of function mutations in KRAS in their incipient stage. However, progression to invasive PDAC in KrasG12D-bearing mice has proved to be either a protracted or unachieved process, as a small fraction of mice succumb directly to PDAC following a very long latency period (Hingorani et al., 2005; Parajuli et al., 2020; Parajuli et al., 2019; Tuveson et al.,

2004). It is widely believed that the acquisition of secondary mutations in certain tumor suppressors can endow transformed cells with the growth advantage needed for disease progression. For instance, combining KrasG12D with deletion of Smad4 or TP53 has been shown to accelerate the progression of PDAC, which was thought to be conferred through disruption of TGF- $\beta$  cytoskeletal signaling (Bardeesy et al., 2006b; Ijichi et al., 2006; Izeradjene et al., 2007). Given its role as an inhibitor of Smad signaling, we surmised that Prdm16 inactivation might suppress PDAC development and/or progression owing to the de-repression of TGF- $\beta$ /Smad signaling. To probe this possibility, we generated mice harboring KrasG12D alone (KC) or in combination with conditional deletion of both alleles of Prdm16 (KPrC) and conducted comparative studies to analyze their PDAC phenotypes. Consistent with previous studies (Parajuli et al., 2020; Parajuli et al., 2019; Tuveson et al., 2004), KC mice maintained uniformly good health until around the age of 20 wk, and thereafter a fraction of mice became suddenly morbid and succumbed within days to an aggressive PDAC. Contrary to our prediction, combining Prdm16 deletion with KrasG12D instead resulted in a marked acceleration of PDAC. Kaplan–Meyer analysis showed a significant decrease in the median survival of KPrC mice as compared to KC mice (Fig. 3 A). During an observation period of 6 mo, 70% of KPrC mice succumbed to PDAC, whereas more than 76% of KC mice survived and remained free of invasive PDAC (Fig. 3 A). To confirm this finding, we conducted histopathological analysis with pancreatic sections from KPrC and KC mice of the same age that showed either relatively healthy appearance or signs of morbidity characteristic of invasive PDAC at the time of necropsy. At early stages of tumorigenesis, KPrC mice displayed a significant increase in PanIN lesions compared to KC mice, as assessed by H&E and IHC using anti-CK19 antibody (Fig. 3 B). A similar conclusion could be drawn while analyzing another ductal marker, MUC5AC, either by IHC or Alcian blue staining (Fig. S3). KPrC and KC mice with invasive PDAC also showed clear difference in both tumor architecture and reactivity to the anti-CK19 and anti-MUC5AC antibodies as well as to Alcian blue (Fig. 3 B and Fig. S3). Moreover, IHC analysis using anti- $\alpha$ -SMA antibody showed more extensive stroma both within and outside PDAC lesions in KPrC mice relative to KC mice (Fig. S3). An automatic-guided quantification confirmed the increase in the surface areas of PanIN and PDAC lesions in KPrC mice as compared to KC mice (Fig. 3 B). Thus, Prdm16 inactivation appeared to accelerate PDAC once it has been initiated through activation of oncogenic KrasG12D signaling.

#### Requirement of Prdm16 for IPMN-to-PDAC progression

Given the inverse association between Smad4 and Prdm16 that we noticed earlier during PDAC progression (Fig. 1, E and F), we sought to extend our genetic approaches to explore whether



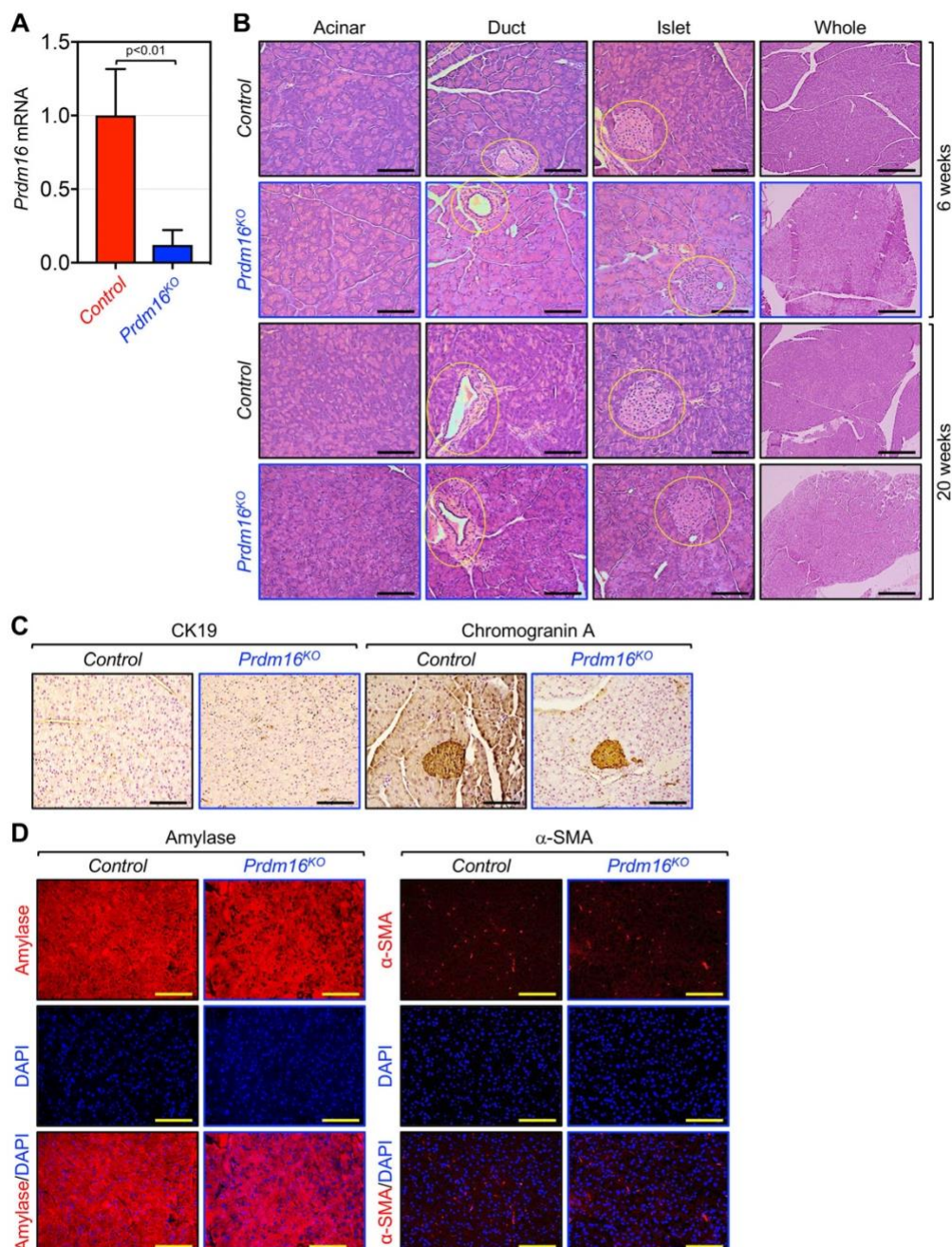


**Figure 2. Prdm16 inactivation did not affect pancreas histology or function.** (A) Prdm16 mRNA expression in 3-mo-old control and Prdm16KO mice was measured by qRT-PCR (*n* = 6). Data are expressed as mean ± SEM, and statistical power was assessed by a two-tailed, unpaired *t* test. (B) FFPE pancreatic sections from control or Prdm16KO mice (*n* = 8) at 6 or 20 wk-old were stained with H&E. Scale bars: 200 μm for “whole” pictures and 50 μm for all other pictures. (C) FFPE pancreatic sections from 15-wk-old control and Prdm16KO mice (*n* = 8 to 31) were immunostained with anti-CK19 or anti-Chromogranin A antibody and subjected to IHC. Scale bars: 50 μm. (D) FFPE pancreatic sections from 15-wk-old control and Prdm16KO mice (*n* = 8) were immunoreacted with antibodies to amylase or α-SMA before being subjected to immunofluorescence. Scale bars: 50 μm.

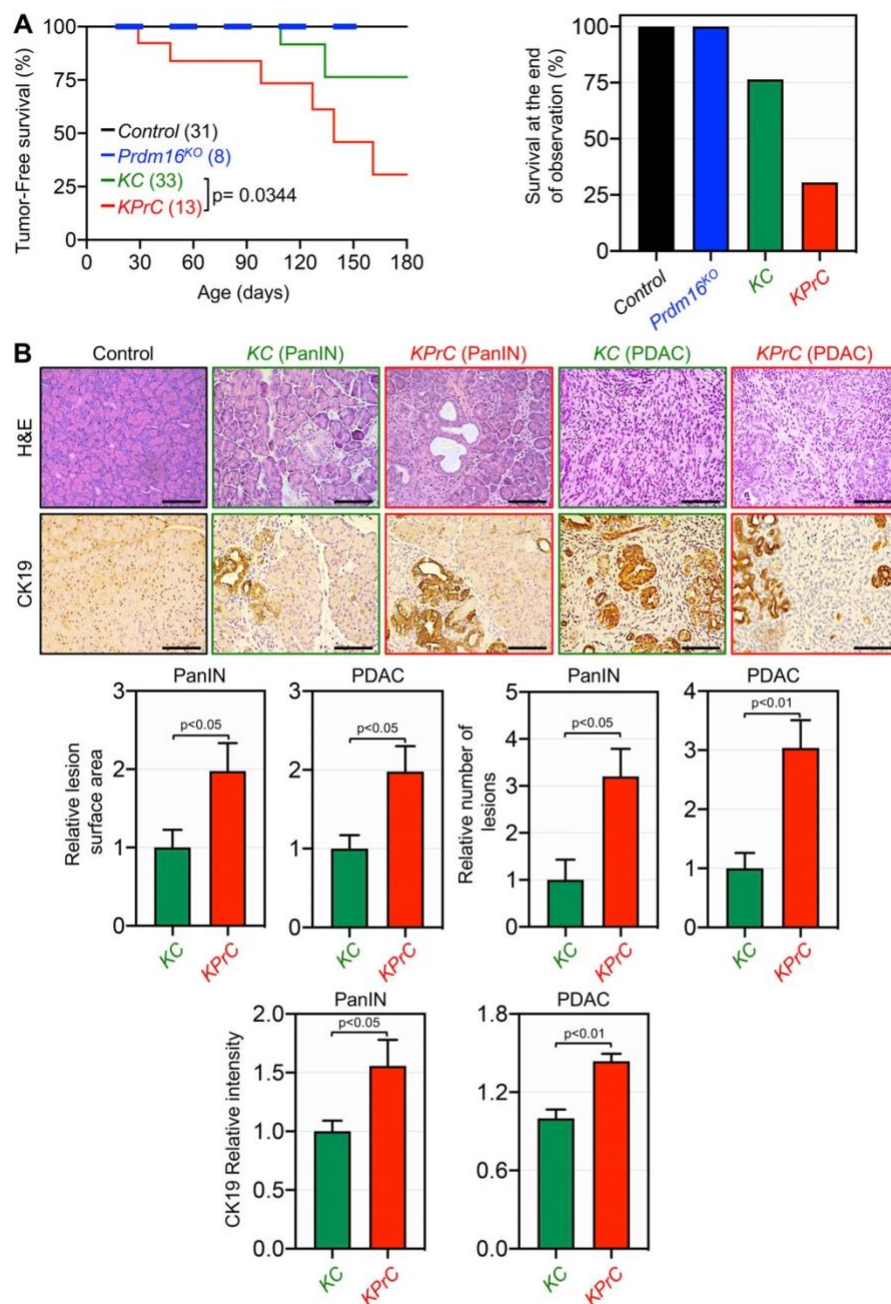


**Figure 3. Prdm16 inactivation accelerates KrasG12D-driven PDAC.** (A) Kaplan-Meier survival of control, *Prdm16*<sup>KO</sup>, KC and KPrC mice. A two-color line (black and blue bold) was used to differentiate between control and *Prdm16*<sup>KO</sup> mice. Statistical power was assessed by log-rank test for significance (left). The percentage of survival at the end of the observation period (right). (B) FFPE pancreatic sections from 4-m-old control, *Prdm16*<sup>KO</sup>, KC, and KPrC mice ( $n = 8-33$ ) were stained with H&E or immunostained with antibodies to CK19 and subjected to IHC. Representative pictures are shown (top). Scale bars: 50  $\mu$ m. Relative PanIN and PDAC surface areas, number of PanIN and PDAC lesions and CK19 intensity (bottom) are shown. Data are expressed as mean  $\pm$  SEM, and statistical power was assessed by a two-tailed, Mann-Whitney test.



Prdm16 could play a role, if any, in PDAC that depends on its function in TGF- $\beta$ /Smad signaling. Accordingly, we generated mice with the combined deletion of Prdm16 and Smad4 in a KrasG12D background (KSPrc). KPrC, KSC, KC, and wild-type mice were used as controls. KSPrc mice were born with Mendelian frequencies, and no phenotypic differences between KSPrc and KSC mice were observed. Strikingly, however, the vast majority of KSPrc mice became stunted and morbid in appearance within 2 to 3 wk of weaning, and only 25% of them survived beyond 3 mo (Fig. 4 A). During this period, most of KPrC and KSC mice (84 and 90%, respectively) did not develop or succumb to PDAC. To elucidate the mechanism causing the acceleration of PDAC in KSPrc mice, we conducted histopathological analyses to study different stages of PDAC from the premalignant lesions to invasive adenocarcinomas. We found that KSC pancreas displayed predominantly macroscopic cystic lesions reminiscent of IPMN, as evidenced by the overall architecture as well as the high reactivity to the anti-Muc5AC and anti-CK19 antibodies as well as Alcian blue (Fig. 4 B and Fig. S4 A). In contrast, KSPrc pancreas displayed none to very few IPMN lesions (Fig. 4 B and Fig. S4 A). At the stage of full PDAC, KSPrc tumors were poorly differentiated adenocarcinomas, characterized by loss of the epithelial marker E-cadherin and acquisition of the mesenchymal marker vimentin (Fig. S3 B), which could be due either to increased accumulation of cancer associated fibroblasts or epithelial to mesenchymal transition (EMT), the latter being a general hallmark of metastasis (Pei et al., 2019). In marked contrast, KSC tumors were well differentiated with little or no change in E-cadherin or vimentin expression (Fig. S4 B), in line with previous studies that KSC mice are resistant to metastasis (Bardeesy et al., 2006b; Izeradjene et al., 2007; Whittle et al., 2015). As concomitant inactivation of Prdm16 appeared to shift the evolution of the IPMN-to-PDAC progression sequence toward the PanIN-to-PDAC progression sequence, it is tempting to speculate that Prdm16 might function at the stage of early preneoplastic lesions to influence PDAC development and progression. In support of this notion, deleting PRDM16 in two fully-transformed human PDAC cell lines (i.e., PANC-1, sufficient for SMAD4 and BxPC-3, deficient for SMAD4) did not affect their proliferative or invasive behaviors, as gauged by a combination of in vivo and in vitro assays (Fig. S4, C-F).

The poor prognosis for human PDAC is mainly due to quasi-inevitable metastasis affecting the liver and lung at the time of diagnosis (Connor and Gallinger, 2021; Hidalgo, 2010). Due to the severity of PDAC in KSPrc mice, we wondered whether concomitant deletion of Prdm16 could confer metastatic ability to the otherwise non-metastasizing PDAC tumors that typically develop in KSC mice (Bardeesy et al., 2006b; Izeradjene et al., 2007; Whittle et al., 2015). Indeed, we consistently observed the presence of metastatic lesions in the lung in all KSPrc mice that developed invasive tumors but survived until necropsy (Fig. 4 C). In contrast, no metastatic lesions were detected in KSC mice even with terminal PDAC (Fig. 4 C), as previously described (Bardeesy et al., 2006b; Izeradjene et al., 2007; Whittle et al., 2015). Confirmation of these results was obtained by IHC using an antibody to the PDAC marker CK19 (Fig. 4 C). Collectively,

these data demonstrate that concomitant inactivation of Prdm16 was sufficient to confer metastatic properties on non-metastatic KSC tumors, a phenomenon that is associated with a shift from the IPMN-to-PDAC phenotype to the PanIN-to-PDAC phenotype.

#### Repression of Prdm16 expression by Smad4

To investigate the molecular mechanisms by which Prdm16 controls PDAC progression and metastasis in the context of a Smad4 null background, we took advantage of our earlier IHC analysis showing that Smad4 deficiency in KSC mice was associated with a persistent de-repression of Prdm16 during the progression from IPMN to PDAC (Fig. 1 E). We surmised that Smad4 might function either directly or indirectly to repress Prdm16 expression, which in turn impacts the progression trajectory of PDAC. We initially conducted qRT-PCR experiments using KSC mice, and found that the increase in Prdm16 expression was mediated at least via gene expression (Fig. 5 A). Because Smad4 functions as an essential component of TGF- $\beta$  signaling (David and Massagué, 2018; Feng and Derynck, 2005; Massagué, 2008), we next wondered whether activation of TGF- $\beta$  signaling could repress Prdm16 expression, as does Smad4. To our surprise, treating mouse PDAC cells KPC1 or human PDAC cells PANC-1 with TGF- $\beta$ 1 instead elicited a marked increase in Prdm16 expression (Fig. 5, B-D). As a specificity control, TGF- $\beta$ 1 treatment failed to induce Prdm16 expression in the human PDAC cell line MIA-PaCa-2 (Fig. 5 E), which lacks a functional TGF- $\beta$  receptor (Freeman et al., 1995). To determine whether the effect of TGF- $\beta$ 1 is mediated via Smad4, we conducted comparative experiments using PANC-1 cells deleted of SMAD4 by CRISPR/CAS9. We found that ablating SMAD4 resulted in a marked increase in the steady-state expression of Prdm16 mRNA and protein (Fig. 5 F, see also Fig. 6 F), confirming the ability of endogenous Smad4 to repress PRDM16 expression in human cells. Intriguingly, challenging cells with TGF- $\beta$ 1 did not further increase Prdm16 expression in cells deleted of SMAD4 as compared to cells expressing the control gRNA (Fig. 5 F; see also Fig. 6 F), implying that SMAD4 inactivation is sufficient to mimic the effects of TGF- $\beta$ 1 stimulation.

Previous studies have shown that Smad proteins can stimulate or repress expression of TGF- $\beta$  responsive genes through direct binding to their promoter (David and Massagué, 2018; Feng and Derynck, 2005; Massagué, 2008). In addition, a substantial fraction of Smad4 has been shown to localize in the nucleus in the absence TGF- $\beta$  stimulation, but the physiopathological significance of this phenomenon remains unknown (Pierreux et al., 2000). Because SMAD4 ablation in PANC-1 cells was sufficient to recapitulate the stimulatory effects of TGF- $\beta$  signaling on PRDM16 expression, we initially reasoned that Smad4 might bind to and repress the PRDM16 promoter at steady state, and that TGF- $\beta$  signaling activation might displace Smad4 from the PRDM16 promoter. Accordingly, we conducted ChIP experiments, focusing on Smad conserved binding elements (SBE) within the PRDM16 promoter that we identified through an in-silico analysis. Using chromatin from PANC-1 cells, we detected a strong binding of Smad4 to the PRDM16 promoter at steady state (Fig. 6 A). This binding is specific, as there was no signal in the human PDAC cell line BxPC-3 (Fig. 6



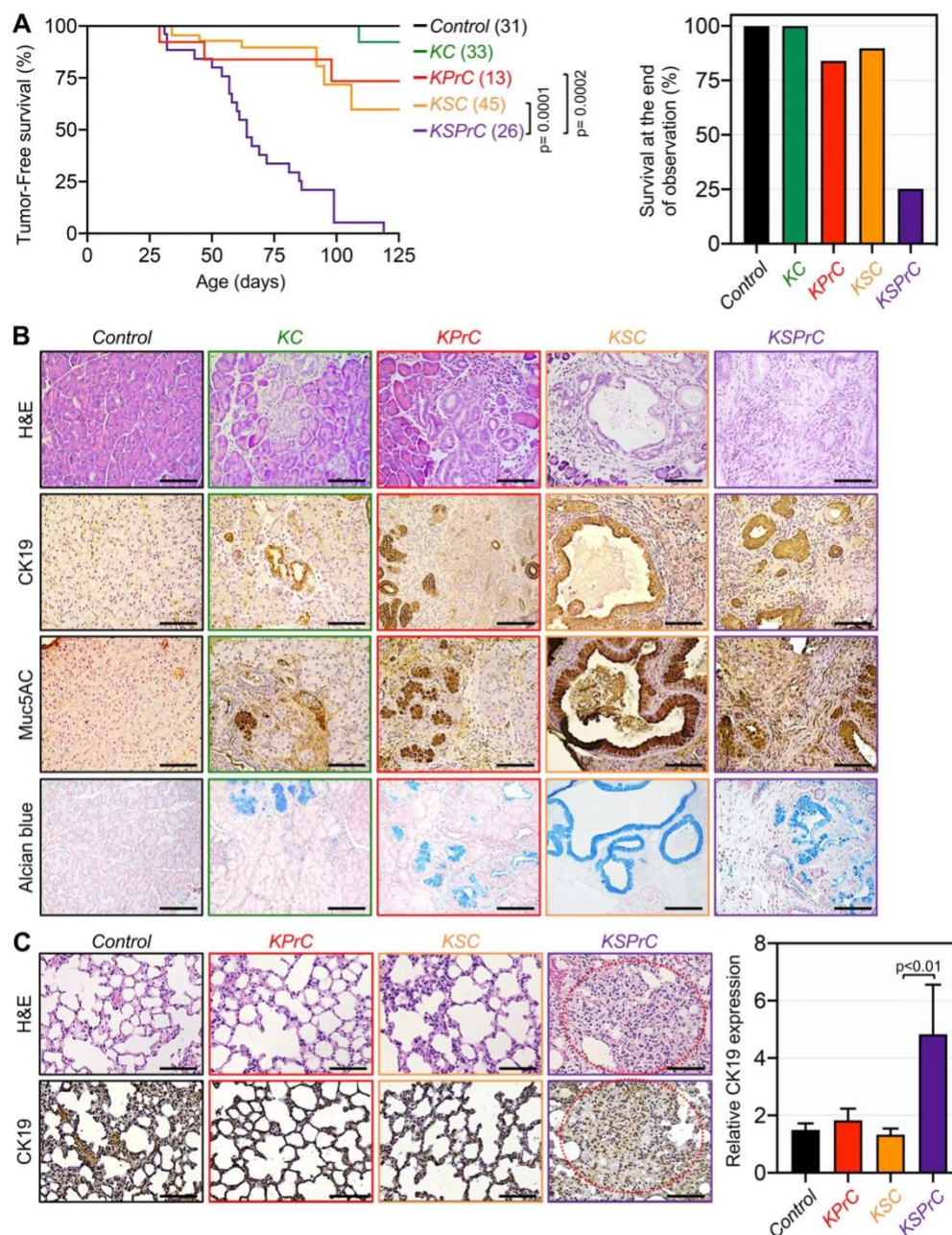


**Figure 4. Concomitant inactivation of Prdm16 and Smad4 shifts the progression trajectory of PDAC.** (A) Kaplan-Meier survival analysis of control, KC, KPrC, KSC, and KSPrC mice ( $n = 13-45$ ). Statistical power was assessed by a log-rank test for significance (left). The percentage of survival at the end of the observation period (right). (B) FFPE pancreatic sections from 4-m-old control, KC, KPrC, KSC, and KSPrC mice ( $n = 13-45$ ) were stained with H&E or Alcian blue or immunostained with antibodies to CK19 or Muc5AC and subjected to IHC. Representative pictures are shown. Scale bars: 50  $\mu$ m. (C) FFPE lung sections from 4-mo-old control, KPrC, KSC and KSPrC mice ( $n = 13-45$ ) were stained with H&E or immunostained with anti-CK19 antibody. Metastatic lesions are highlighted by blue dot-circles. Representative pictures are shown (left). Scale bars: 50  $\mu$ m. Relative CK19 intensity from lung sections are shown (right). Data are expressed as mean  $\pm$  SEM, and statistical power was assessed by a two-tailed Mann-Whitney test.

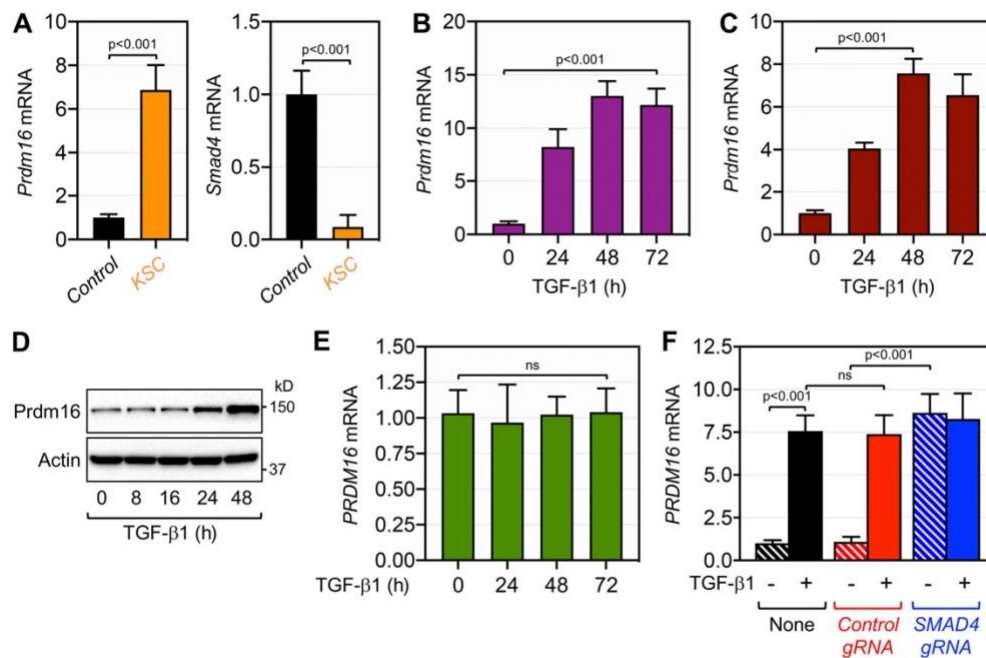


**Figure 5. Smad4 represses Prdm16 expression.** (A) Expression of Prdm16 (left) or Smad4 (right) in pancreas from 4-mo-old control and KSC mice ( $n = 6$ ) was analyzed by qRT-PCR. (B) Expression of Prdm16 mRNA in KPC1 cells cultured in the presence or absence of TGF- $\beta$ 1 for various times was analyzed by qRT-PCR ( $n = 6$ ). (C) Expression of PRDM16 mRNA in PANC-1 cells treated with TGF- $\beta$ 1 for various times was analyzed by qRT-PCR ( $n = 6$ ). (D) Expression of Prdm16 protein in PANC-1 cells treated with TGF- $\beta$ 1 for various times was analyzed by immunoblotting. (E) Expression of PRDM16 mRNA in MIA-PaCa-2 cells cultured in the presence or absence of TGF- $\beta$ 1 for various times was analyzed by qRT-PCR ( $n = 6$ ). (F) Expression of PRDM16 mRNA in isogenic PANC-1 cell lines stably transduced with control or SMAD4 gRNA lentiviruses and cultured in the presence or absence of TGF- $\beta$ 1 was analyzed by qRT-PCR ( $n = 6$ ). Data in A–C, E, and F are expressed as mean  $\pm$  SEM, and statistical power was assessed by a two-tailed, unpaired  $t$  test. Source data are available for this figure: SourceData F5.

A), which bears natural homozygous deletion of SMAD4 (Duda et al., 2003). Interestingly, treating PANC-1 cells with TGF- $\beta$ 1 had little or no effect on the binding of Smad4 to the PRDM16 promoter despite eliciting a strong activation of this pathway, as assessed by the increased binding of Smad4 to the promoter of JUNB (Fig. 6 A), a well-characterized TGF- $\beta$  target gene (Sundqvist et al., 2018). This observation, together with our gene expression experiments, strongly suggests that TGF- $\beta$  signaling might involve other players that act in partnership with Smad4 to repress Prdm16 expression. To explore this possibility, we conducted ChIP experiments using antibodies to Smad2 and Smad3, as both transcription factors are known to interact with Smad4 in response to TGF- $\beta$  signaling (David and Massagué, 2018; Feng and Derynck, 2005; Massagué, 2008; Massagué et al., 2005). We detected a slight but significant increase in the binding to Smad2 to the PRDM16 promoter in PANC-1 cells upon stimulation with TGF- $\beta$ 1 (Fig. 7 B). In contrast, TGF- $\beta$ 1 stimulation induced a massive increase in the binding of Smad3 to the PRDM16 promoter (Fig. 6 B). Concomitant deletion of SMAD2 and SMAD3 in PANC-1 cells resulted in almost complete blockade in TGF- $\beta$ -induced Prdm16 expression (Fig. 6 C). Although this finding provides a potential mechanism by which TGF- $\beta$  signaling could induce Prdm16 expression, it failed to

explain why deletion of Smad4 in KSC mice leads to the derepression of Prdm16. Based on the literature (Chuiikov et al., 2010; Stine et al., 2019; Takahata et al., 2009) and our data that Prdm16 can repress Smad transcriptional activity in human PANC-1 cells (Fig. 6 D), we considered the possibility that Smad4 might recruit Prdm16 to its own promoter, thereby leading to Prdm16 repression. Indeed, we detected a strong binding of Prdm16 to its promoter in PANC-1 cells at steady state, and this was almost completely suppressed upon TGF- $\beta$ 1 stimulation (Fig. 6 E), strongly suggesting that TGF- $\beta$  signaling activation might dislodge Prdm16 from its promoter. In comparison, we were not able to detect any binding of Prdm16 to its promoter in BxPC-3 cells (Fig. 6 E), attesting to the specificity of our experiments, and further providing strong evidence supporting the notion that Smad4 functions to recruit Prdm16 to its promoter to repress its expression. To corroborate these findings, we conducted co-immunoprecipitation assays using PANC-1 cells, and detected a strong interaction between Prdm16 and Smad4, which was inhibited upon treatment of cells with TGF- $\beta$ 1 (Fig. 6 F). Such interaction was not detected in PANC-1 cells deleted of SMAD4 (Fig. 6 F), attesting to the specificity of the approach. Finally, we generated a reporter construct in which luciferase expression is under the control of either wild-type or



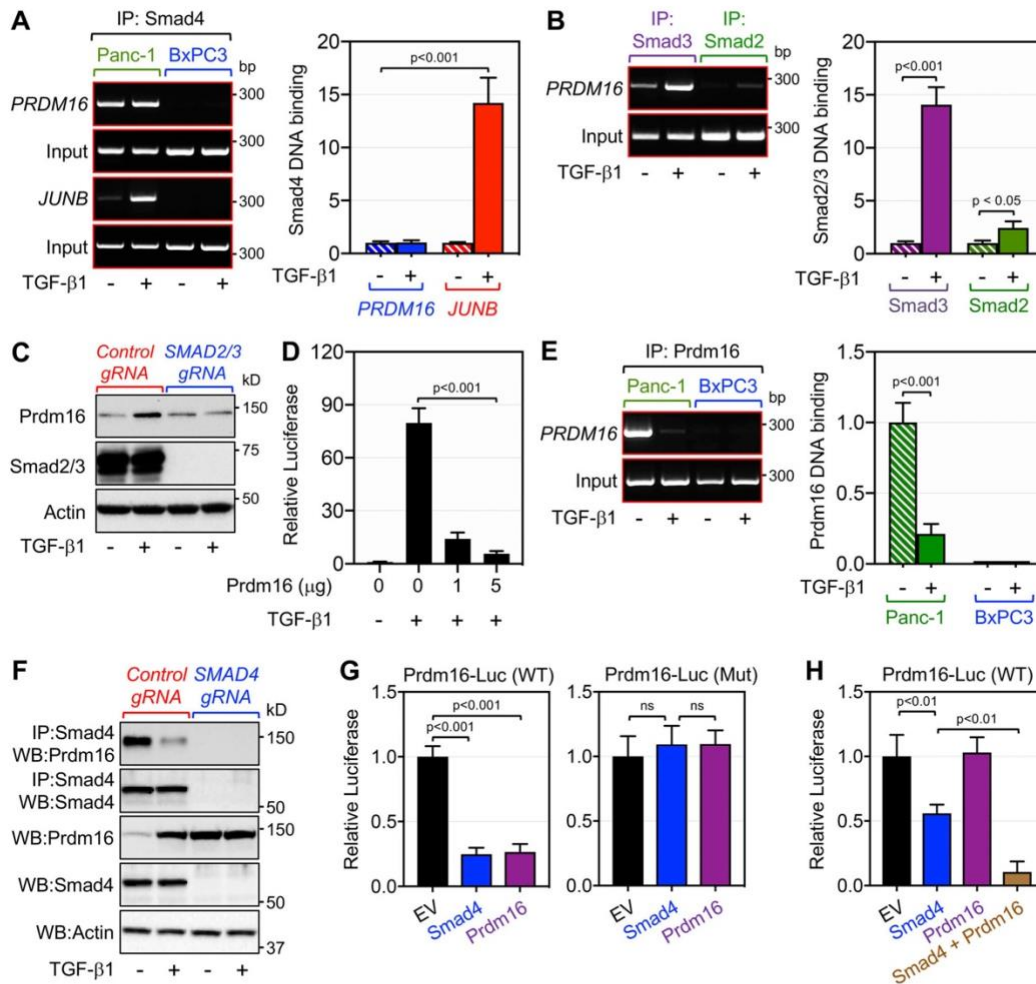


**Figure 6. Smad4 interacts with Prdm16 on the PRDM16 promoter to repress its own expression.** (A) Pancreatic chromatin from PANC-1 or BxPC-3 cells ( $n = 6$ ) cultured in the presence or absence of TGF- $\beta$ 1 was analyzed for the binding of Smad4 to the PRDM16 or JUNB promoter by ChIP and agarose gel (left) and qPCR (right). (B) Pancreatic chromatin from PANC-1 cells ( $n = 6$ ) cultured in the presence or absence of TGF- $\beta$ 1 was analyzed for the binding of Smad2 and Smad3 to the PRDM16 promoter by ChIP and agarose gel (left) and qPCR (right). (C) PANC-1 expressing control or SMAD2/3 gRNAs were cultured in the presence or absence of TGF- $\beta$ 1 for 48 h and analyzed for the expression of Prdm16 and Smad2/Smad3 by direct immunoblotting. (D) PANC-1 cells were transfected with the CAGA9-Luc gene reporter and increasing amounts of pcDNA3.1-Prdm16. 24 h after transfection, cells were treated with TGF- $\beta$ 1 for 16 h and then assessed for luciferase activity and normalized. (E) Pancreatic chromatin from PANC-1 or BxPC-3 cells ( $n = 6$ ) cultured in the presence or absence of TGF- $\beta$ 1 was analyzed for the binding of Prdm16 to the PRDM16 promoter by ChIP and agarose gel (left) and qPCR (right). (F) PANC-1 expressing control or SMAD4 gRNA were treated with TGF- $\beta$ 1 for 48 h and then analyzed for the interaction of Prdm16 with Smad4 by co-immunoprecipitation (IP) followed by immunoblotting (WB). Expression of Prdm16 was also analyzed by direct immunoblotting. (G) PANC-1 cells were transfected with the wild-type (left) or mutated Prdm16-Luc (right) reporter together with empty vector, pcDNA3.1-Prdm16 or pCMV5-HA-Smad4. 48 h after transfection, cells were assessed for luciferase activity and normalized ( $n = 6$ ). (H) BxPC-3 cells were transfected with the wild-type Prdm16-Luc reporter together with the indicated combinations of empty vector (EV), pcDNA3.1-Prdm16, and pCMV5-HA-Smad4. 48 h after transfection, cells were assessed for luciferase activity and normalized ( $n = 6$ ). Data in A, B, D, E, G, and H are expressed as mean  $\pm$  SEM, and statistical power was assessed by a two-tailed, unpaired t test. Source data are available for this figure: SourceData F6.

mutated (SBE) PRDM16 promoter (Prdm16-Luc). We found that Smad4 was able to repress expression from the wild-type PRDM16 promoter in PANC-1 cells (Fig. 6 G). More importantly, expression of Prdm16 was also able to suppress luciferase

expression from the wild-type PRDM16 promoter, and this effect was completely lost when the SBE mutated promoter was used in the assay (Fig. 6 G). Finally, expression of Prdm16 was able to repress the wild-type PRDM16 promoter in BxPC-3 cells only

when Smad4 was co-expressed (Fig. 6 H). Overall, these findings revealed that Smad4 functions as a potent repressor of Prdm16, therefore providing a mechanistic explanation as to why KSC mice display high expression of Prdm16.

#### Concomitant inactivation of Prdm16 and Smad4 recapitulates the global inactivation of TGF- $\beta$ signaling

Both SMAD4 and T $\beta$ RII are frequently inactivated in human PDAC, and landmark genetic experiments have shown that inactivation of either Smad4 or T $\beta$ RII accelerates KrasG12D-driven PDAC (Bardeesy et al., 2006b; Ijichi et al., 2006; Izeradjene et al., 2007). To date, it remains largely unknown whether inactivation of Smad4 or T $\beta$ RII could differentially impact the dynamics or trajectory of PDAC progression. Our mechanistic data that inactivation of Smad4 recapitulates the effects of TGF- $\beta$  signaling on Prdm16 expression provided us with a unique platform to address this issue. To do so, we conducted an in-depth comparative analysis of the PDAC phenotypes in mice with homozygous deletion of T $\beta$ RII (KT $\beta$ C), KSC, and KSPrC mice side-by-side. KC and wild-type mice were used as controls. Kaplan-Meier analysis showed that KT $\beta$ C mice developed lethal PDAC much more earlier than KSC mice, often succumbing to the disease within 4 wk of age and none survived beyond 17 wk, whereas 60% of KSC mice survived within this observation period (Fig. 7 A). This observation indicates that global inactivation of TGF- $\beta$  signaling through T $\beta$ RII ablation is more efficient at deepening PDAC progression than inactivation of canonical TGF- $\beta$ /Smad signaling through Smad4 ablation. More importantly, we found that KSPrC mice succumbed to lethal PDAC with kinetics approaching that of KT $\beta$ C mice (Fig. 7 A), suggesting that simultaneous inactivation of Smad4 and Prdm16 might be sufficient to recapitulate the global inactivation of TGF- $\beta$  signaling.

Next, in light of our earlier findings that concomitant inactivation of Prdm16 was able to shift the evolution of the IPMN-to-PDAC phenotype in KSC mice toward the PanIN-to-PDAC phenotype, we wondered whether ablation of T $\beta$ RII or Smad4 could differentially affect the nature of the premalignant lesions leading to PDAC, and if so, whether this event depends on Prdm16. Thus, we conducted histopathological analyses to compare the PDAC phenotypes in KSPrC, KT $\beta$ C and KSC mice both at the levels of pre-malignant and full-blown PDAC lesions. H&E staining showed that KT $\beta$ C tumors displayed uniformly poorly differentiated architecture, which is consistent with the rapid development of invasive PDAC in these mice (Fig. S5). Nevertheless, using KT $\beta$ C mice before displaying signs of invasive PDAC, we consistently noticed the presence of premalignant lesions that display the classical features of PanINs, as gauged by IHC using antibodies to CK19 and Muc5AC (Fig. 7 B). Interestingly, KSPrC mice displayed similar cancerous phenotype as KT $\beta$ C mice, both in terms of PanIN and PDAC lesions (Fig. 7 B and Fig. S5). In contrast, KSC mice consistently showed abundant and large IPMN lesions that exhibit high reactivity to the anti-Muc5AC antibody and Alcian blue (Fig. 7 B), which is in agreement with previous studies that KSC mice develop IPMN premalignant lesions rather than PanIN lesions (Bardeesy et al., 2006b; Izeradjene et al., 2007; Whittle et al., 2015). Taken

together, these findings strongly suggest that inactivation of the entire TGF- $\beta$ /Smad pathway promotes PanIN-to-PDAC progression, whereas inactivation of Smad4 promotes IPMN-to-PDAC progression. In addition, since concomitant ablation of Prdm16 and Smad4 resulted in highly aggressive PDAC similar to what was observed in KT $\beta$ C mice, we suggested that global inactivation of TGF- $\beta$  signaling might simultaneously inactivate both Smad4 and Prdm16.

#### Discussion

Prdm16 belongs to the PR domain-containing protein family of transcription factors, which control a plethora of essential cellular processes, including specification of cell lineage during development (Chi and Cohen, 2016). Prdm16 was first identified in leukemia, where truncation mutants lacking functional domains behaved as oncogenic (Zhou et al., 2016), providing the first indication that Prdm16 might function as a tumor suppressor. In addition its involvement in leukemia, several studies have subsequently shown that Prdm16 controls brown fat cell differentiation as well as dedifferentiation of white fat to beige fat (Harms et al., 2015; Hiraike et al., 2017; Seale et al., 2008; Seale et al., 2007). Moreover, Prdm16 is required for stemness in multiple tissues, including hematopoietic and nervous systems (Chi and Cohen, 2016). Germline deletion of Prdm16 in mice impairs the maintenance of neural and hematopoietic stem cells during fetal development, resulting in neonatal death (Shimada et al., 2017). As such, this lethal phenotype hampered any further investigation to delineate a possible role of Prdm16 in cell fate determination in other organ systems, such as pancreas, where the same progenitor cells give rise to all pancreas lineages, e.g., ductal, acinar, and islet (Gu et al., 2003). In this study, we found that conditional deletion of Prdm16 in early pancreatic progenitor cells had no discernible impact on animal health or pancreas physiology, indicating that Prdm16 is dispensable for pancreas development and function. Because mutational inactivation of PRDM16 has been shown to be associated with leukemia (Zhou et al., 2016), we went on to explore whether Prdm16 could contribute to the pathogenesis and/or progression of PDAC, in which acquisition of oncogenic KRAS endows acinar cells with stemness traits that facilitate their differentiation toward a ductal-like lineage, thereby culminating in acinar-to-ductal metaplasia and attendant emergence of premalignant lesions (Bardeesy et al., 2006a; Gu et al., 2003; Park et al., 2008; Tuveson et al., 2004). Progression of premalignant lesions either follows the PanIN-to-PDAC sequence, MCN-to-PDAC, or IPMN-to-PDAC sequence, depending on the nature of the secondary genetic events (Bardeesy et al., 2006a; Bardeesy et al., 2006b; Gu et al., 2003; Tuveson et al., 2004). Yet, among the most studied secondary genetic alterations in PDAC, only Smad4 inactivation stood out as the main mechanism that enables progression through the IPMN-to-PDAC sequence (Bardeesy et al., 2006b; Whittle et al., 2015). To the best of our knowledge, how Smad4 inactivation facilitates this IPMN-to-PDAC transition phenotype has never been addressed experimentally. Using the KrasG12D-based mouse model of PDAC, we confirmed that KSC mice develop mostly IPMN lesions as described initially (Bardeesy et al.,



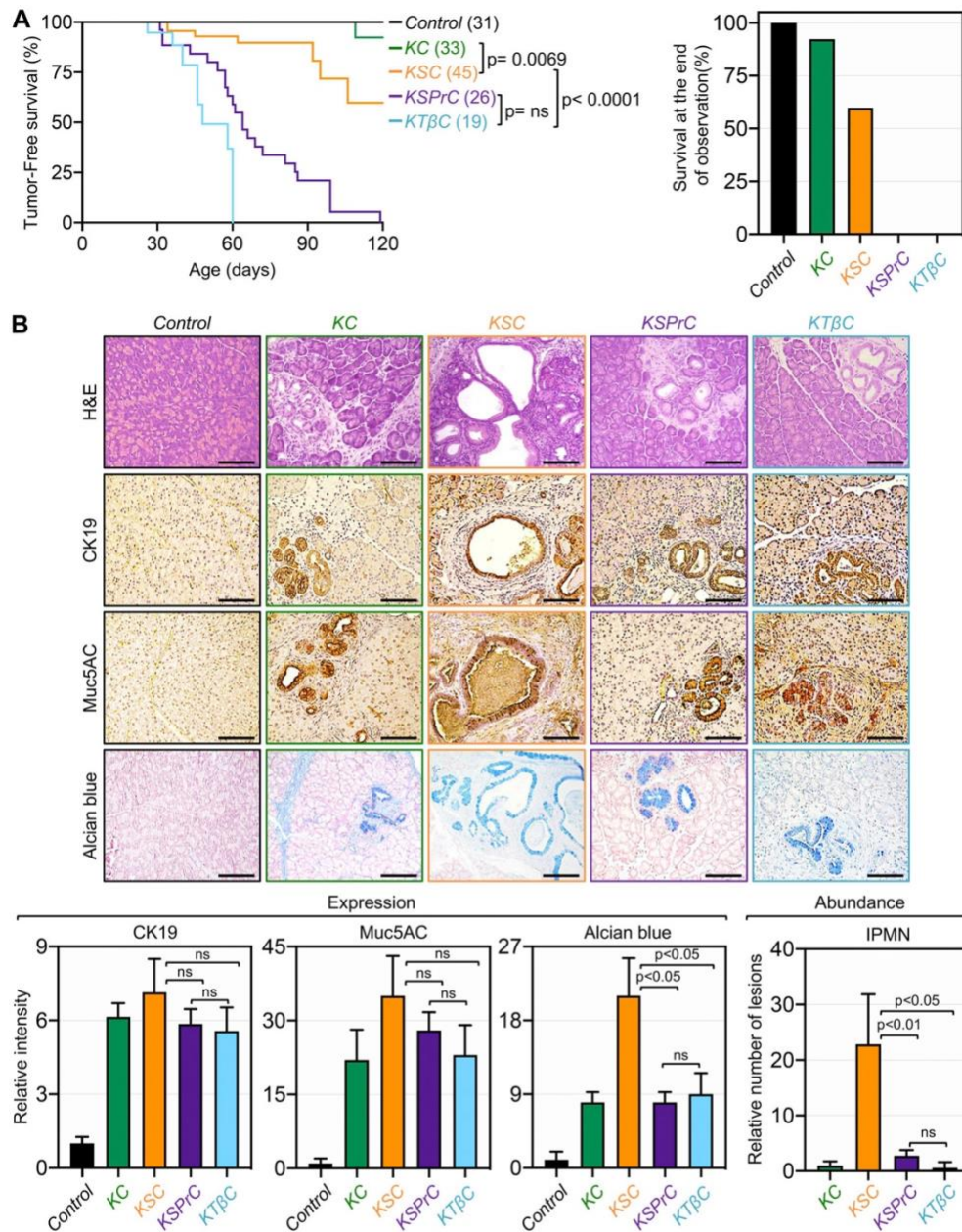


Figure 7. **Concomitant ablation of *Prdm16* and *Smad4* recapitulates the global inactivation of TGF- $\beta$  signaling through ablation of T $\beta$ RII.** (A) Kaplan-Meier survival analysis of control, KC, KSC, KSPrC, and KT $\beta$ C mice ( $n = 19-45$ ). Statistical power was assessed by a log-rank test for significance (left). The percentage of survival at the end of the observation period (right). (B) FFPE pancreatic sections from 1- to 4-mo-old control, KC, KSC, KSPrC, and KT $\beta$ C mice ( $n = 19-45$ ) were stained with H&E or Alcian blue, or immunostained with antibodies to CK19 or Muc5AC and subjected to IHC. Scale bars: 50  $\mu$ m (top). Relative intensity of CK19, Muc5AC, and Alcian blue or relative IPMN abundance are shown (bottom). Data are expressed as mean  $\pm$  SEM, and statistical power was assessed by a two-tailed, unpaired Mann-Whitney test.

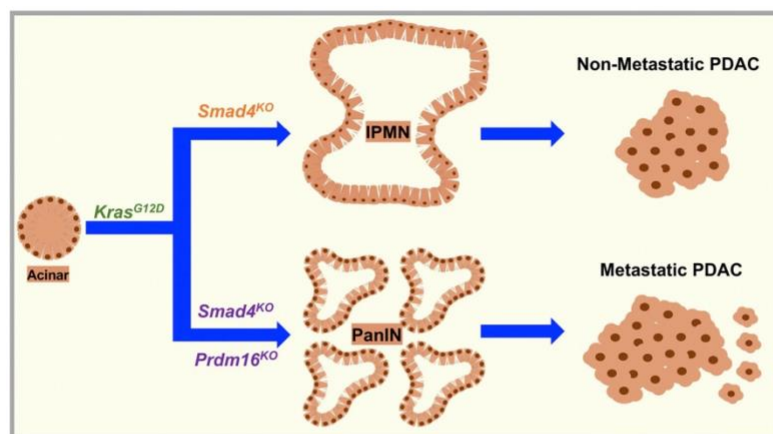


Figure 8. Model for the functional interaction between Smad4 and Prdm16 during PDAC formation and progression.

2006b) rather than MCN lesions described in a subsequent study (Izeradjene et al., 2007). Most importantly, we found that concomitant ablation of Prdm16 and Smad4 (KSPrc) resulted in highly aggressive tumors, which develop with very short latencies to the full-blown PDAC and frequently metastasize to the lung, a site associated with the human disease (Connor and Gallinger, 2021; Hidalgo, 2010). Comprehensive histopathological analyses revealed that these tumors follow the PanIN-to-PDAC progression route rather than the IPMN-to-PDAC progression route that proceeds with ablation of Smad4 alone. Because inactivating Smad4 led to the increased expression of Prdm16, we proposed a model in which Prdm16 functions as a molecular switch to dictate whether the malignant transformation process follows the IPMN-to-PDAC route or the PanIN-to-PDAC route (Fig. 8). This model also posits that Prdm16 might function to suppress PDAC pathogenesis at very early stages of the malignancy. In further support of this notion, we found that ablating PRDM16 in the human PDAC cancer cell lines BxPC-3 and PANC-1 did not influence their proliferative or metastatic behaviors, as evidenced using a variety of in vivo and in vitro tumor growth and invasion assays. In light of these findings, a more comprehensive investigation using genetic and histological approaches are needed to firmly establish whether Prdm16 indeed elicits its tumor suppressor activity at early stages, and if so, whether this occurs through direct effects on cancer cell growth or tumor microenvironment reprogramming. As such, our findings open up unique frameworks that would ultimately leverage general efforts to unravel mechanistic paradigms of PDAC, for which very limited therapeutic interventions are currently available.

Accumulating evidence suggests that Prdm16 functions as a potent inhibitor of TGF- $\beta$ /Smad signaling under various physiological contexts (Chuiikov et al., 2010; Stine et al., 2019; Takahata et al., 2009). TGF- $\beta$ /Smad signaling is well known to play a dual role during cancer progression, functioning at early stages as a tumor suppressor to restrict the malignant transformation, and at late stages as a tumor promoter to facilitate cell

invasion and metastasis (Feng and Derynck, 2005). To date, the most appealing speculations as to TGF- $\beta$  dual function during PDAC progression have been that loss of the TGF- $\beta$  cytosolic function enables cells to escape growth-inhibitory regulation, which would ultimately culminate in malignant transformation (David et al., 2016; Feng and Derynck, 2005; Massagué, 2008). Once the tumor has developed, other TGF- $\beta$  responses unrelated to its cytosolic function then supposedly prevail presumably in a manner that facilitates PDAC invasion and metastasis (Bardeesy et al., 2006b; Feng and Derynck, 2005; Ijichi et al., 2006; Massagué, 2008). Interestingly, high levels of TGF- $\beta$  expression in human PDAC strongly correlates with poor prognosis (Friess et al., 1993; Parajuli et al., 2019), which raises a conundrum as to whether activation of TGF- $\beta$  signaling could contribute directly to malignant transformation in addition to driving cell invasion and metastasis. However, subsequent studies have shown that Smad4 inactivation in the context of KrasG12D (KSC) led to the acceleration of PDAC (Bardeesy et al., 2006b; Izeradjene et al., 2007), unequivocally confirming the tumor suppressor role of TGF- $\beta$  signaling in PDAC. Nevertheless, the tumors deficient for Smad4 retained epithelial differentiation and manifested an attenuated metastatic potential (Bardeesy et al., 2006b; Whittle et al., 2015), which is also in favor of a tumor promoter role of TGF- $\beta$  signaling. So far, definitive experimental evidence on whether inactivation of canonical TGF- $\beta$ /Smad signaling per se is sufficient to suppress PDAC invasion and metastasis in an irreversible manner is still lacking. Here, we found that ablating Prdm16 in a Smad4 null-background was sufficient to render the PDAC tumors again highly invasive and metastatic. Intriguingly, concomitant ablation of Prdm16 in KSC mice also resulted in a shift from IPMN to PanIN, which could conceivably contribute to metastasis in KSPrc mice, as the vast majority of PDAC GEMMs that develop PanINs also develop highly metastatic PDAC, including KSPC mice (Smad4 deletion and p53.R172H expression), which behave similarly to our KSPrc mice (Bardeesy et al., 2006a; Bardeesy et al., 2006b; Tuveson et al., 2004; Whittle et al., 2015). These



findings, together with the observation that Prdm16 expression is lost during late stages of PDAC, highlight Prdm16 as a key player in PDAC progression and metastasis when Smad4 is inactivated. Because TGF- $\beta$  signaling activation leads to the accumulation of Prdm16 through the suppression of Smad4 inhibitory effects, one would speculate that Smad4 and Prdm16 might function in the same signaling network that integrates the TGF- $\beta$  tumor promoter effects during PDAC progression. However, it is also conceivable that Prdm16 might function to suppress metastasis induced by other TGF- $\beta$  superfamily members, such as Activins and BMPs, which are known to signal through Smad4, and can enhance malignancy and promote cancer metastasis in a variety of human malignancies (Attisano and Wrana, 2000; Feng and Derynck, 2005; Pickup et al., 2017). As such, a comprehensive investigation of the mechanisms by which Smad4 and Prdm16 interact to influence PDAC progression may uncover the existence of additional key players and/or pathways that are amenable to therapeutic interventions.

Perhaps the most intriguing finding in this study was the persistent increase in Prdm16 expression during the progression from IPMN to PDAC in KSC mice, which at first glance seems to support a hypothesis in which Smad4 might function as a repressor of Prdm16 during PDAC progression, and hence conceivably that canonical TGF- $\beta$ /Smad signaling might also repress Prdm16 expression. Quite unexpectedly, we found that activation of TGF- $\beta$  signaling did not repress Prdm16 expression, but rather resulted in a strong accumulation of both Prdm16 mRNA and protein both in KSC mice and human PANC-1 cells. Noteworthy, we also detected relatively high expression in the stromal compartment, which likely occurs because of the increased TGF- $\beta$  signaling, which is known to take place during PDAC progression and contribute to the desmoplastic stroma of this malignancy (Friess et al., 1993). In efforts to probe the underlying mechanisms, we found that inactivating Smad4 was sufficient to recapitulate the effects of TGF- $\beta$  signaling, inducing Prdm16 expression to an extent similar to that elicited by TGF- $\beta$ 1. Based on these observations, we reasoned that activation of TGF- $\beta$  signaling might relieve the transcriptional repression imposed by Smad4 on the Prdm16 promoter. However, although we found that Smad4 associated strongly with the PRDM16 promoter at steady state, this binding was not affected by the activation of TGF- $\beta$ 1 signaling, indicating that other factors are involved in TGF- $\beta$ -mediated Prdm16 expression. Probing this possibility, we detected a strong binding of Prdm16 to its own promoter at steady state, which was almost completely abolished by TGF- $\beta$  stimulation, suggesting that activation of TGF- $\beta$  signaling might dislodge Prdm16 from its own promoter. Of note, Prdm16 failed to bind to its promoter in cells deficient for SMAD4, suggesting that Smad4 might associate with and recruit Prdm16 to the PRDM16 promoter. Because Prdm16 has been shown to function as a potent transcriptional repressor in various contexts (Pinheiro et al., 2012; Seale et al., 2008; Seale et al., 2007; Stine et al., 2019; Takahata et al., 2009), we proposed a model in which Prdm16 mediates its own repression once it has been recruited to its promoter by Smad4. While these data demonstrate for the first time that Prdm16 can repress its own expression, we cannot exclude the possibility that other

mechanisms might also contribute to this phenomenon. Despite this limitation, our study sheds light on a previously uncharacterized interplay between Smad4 and Prdm16, which appears to dictate the progression trajectory of PDAC. Going forward, we anticipated that our discovery will guide forthcoming studies seeking to understand mechanistic paradigms of PDAC, which could ultimately pave the way for innovative therapeutic breakthroughs to curb this deadly disease.

## Materials and methods

### Plasmids

The CAGA9-Lux gene reporter construct was previously described (Seo et al., 2006). The expression vector pCDNA3.1-Prdm16 was a gift from Dr. Bruce Spiegelman (#15503; Addgene). The expression vector pCMV5-HA-Smad4 was a gift from Dr. Joan Massague. To generate the Prdm16-Lux reporter, genomic fragments (1,391 bp) upstream of the transcription initiation site (SST) of the PRDM16 gene (based on gene association NM\_022114 and Eukaryotic Promoter Database, epd.epfl.ch) was amplified by the Genomic-GC PCR amplification kit (BD Biosciences) using human genomic DNA obtained from PANC-1 cells. Unique KpnI and XhoI sites were incorporated at the 5' and 3' ends of the sequence, respectively, to simplify directional cloning into KpnI and XhoI sites in the reporter plasmid, pGL3-basic (Promega). Introduction of inactivating mutation into the SBE sequence (-41 bp from SST) was generated by PCR using the QuickChange Site-Directed Mutagenesis kit according to the manufacturer's instructions (Stratagene). The lentiCRISPRV2 expression vectors encoding SMAD4 and PRDM16 gRNAs were purchased from GenScript. The lentiCRISPRV2 expression vectors encoding SMAD2 and SMAD3 gRNAs were generated using lentiCRISPRV2 hygro (#98291; Addgene) and primers with sequences generated using the Synthego Design tool. All cloned cDNAs and their corresponding mutants were checked by sequencing.

### Sequences of gRNAs

**SMAD4.** 5'-TCTCTCCTAAGGTTGCACAT-3'; 5'-AATACACTTACCAGGATGAT-3'.

**PRDM16.** 5'-CTCGTACGGCGAGCCCTCT-3'; 5'-AGGGGTCTTACCGTCCAGGC-3'.

**SMAD2.** 5'-TGGCGGCGTGAATGGCAAGA-3'; 5'-TTCACAAGTGGCGGCGTGAA-3'.

**SMAD3.** 5'-CACCTGCAACCGGCCATCCA-3'; 5'-ACACCTGCAACCGGCCATCC-3'.

### Antibodies

Chromatin immunoprecipitation (ChIP), immunoblotting, immunofluorescence, or immunohistochemistry were performed using the following antibodies: anti- $\alpha$ -SMA (#19245T; Cell Signaling); anti- $\beta$ -Actin (#64225332; Bio-Rad), anti-amylase (#ab21156; Abcam), anti-chromogranin-A (#ab45179; Abcam), anti-cytokeratin 19 (#ab52625; Abcam), anti-E-cadherin (#3195S; Cell Signaling), anti-glucagon (#2760; Cell Signaling), anti-insulin (#4590; Cell Signaling), anti-JunB (#3753; Cell Signaling), anti-Muc5AC (#ab3649; Abcam), anti-Prdm16 (#ab202344 and #ab106410; Abcam), anti-Smad2 (#5339; Cell Signaling),



anti-Smad3, (#9523; Cell Signaling), anti-Smad4, (#46535; Cell Signaling), anti-Smad4 (#sc-7966; Santa Cruz), anti-Smad2/3 (#8685; Cell Signaling), and anti-vimentin (#5741S; Cell Signaling).

#### Cell lines and culture

HEK293T, MIA-PaCa-2, BxPC-3, and PANC-1 cell lines were obtained from the American Type Culture Collection (ATCC). They were cultured in Dulbecco's modified Eagle's medium (DMEM) supplemented with 10% fetal bovine serum (#S11150; FBS, Atlanta Biologicals), antibiotics (#P4458; Gibco) and L-glutamine (#17921004; Corning). The murine pancreatic cancer cell line KPC1 was originally described in our recent publication (Parajuli et al., 2018). The cell line was established from a KP53 mouse, which harbored KrasG12D and one conditional allele of Trp53 (LSL-KrasG12D;LSL-Trp53fl/+;Pdx1-Cre). Freshly isolated specimen from the KP53 mouse with terminal PDAC was gently dissected, minced with scissors, and digested with Dispase II at 2.4 U/ml (#4942078001; Sigma-Aldrich) and Collagenase D at 0.5 mg/ml (#11088858001; Sigma-Aldrich) for 1 h at 37°C in an atmosphere of 5% CO<sub>2</sub>. Then, cells were washed three times with PBS, suspended in RPMI 1540 containing 20% FCS, and seeded on fibronectin-coated plates. Cell colonies were subsequently passaged by trypsinization, pooled, and propagated in DMEM supplemented with 10% FBS, antibiotics, and L-glutamine. To generate the PANC-1-SMAD4KO and PANC-1-SMAD2/3KO cell lines, cells were transduced with the corresponding lentiCRISPRV2-gRNA lentiviruses, selected with puromycin (for SMAD4) or hygromycin (for SMAD2/3), and all resistant clones were pooled and expanded as a single population. Lentiviruses were produced by transfecting HEK293T cells with lentiviral constructs and the One-Step Lentivirus Packaging System as described by the manufacturer (#631275; Takara). Lentiviral particles in the conditioned media were harvested after a period of 48–72 h. The conditioned media were then cleaned of cell debris by centrifugation at 5,000×g for 15 min, filtered through a 0.45-μm filter, and used immediately for cell transduction.

#### In vitro and in vivo cell proliferation assays

For the soft agar assay, cell culture dishes (p60) were first prepared using complete DMEM media containing 0.6% agarose (#16500500; Thermo Fisher Scientific) and allowed to solidify at room temperature for 2 h. Then, cells suspended in complete DMEM media containing 0.3% agarose were added to the dishes preloaded with the 0.6% agarose layer. PANC-1 and BxPC-3 stably expressing control or PRDM16 gRNA were plated at a density of 1,000 cells per dish and grown for ~2 mo. Within this time frame, PANC-1 isogenic cell lines developed small but similar colonies in size, whereas neither of the BxPC-3 isogenic cell lines developed colonies. Colonies were visualized and counted using an Olympus CKX53 microscope with the UPlanFL N 4×/0.13 IPC objective.

For the cell proliferation assay, isogenic PANC-1 (50,000 cells/well) and BxPC-3 (100,000 cells/well) cell lines stably expressing control or PRDM16 gRNA were inoculated into 6-well plates. Three (for PANC-1) and six (for BxPC-3) days after

inoculation, cells were trypsinized and mixed with equal volumes of trypan blue (#T10282; Invitrogen) before being counted using an automatic cell counter (#AMQAF2000; Invitrogen Countess 3 FL). Each well was counted twice and averaged to ensure accurate cell counts were obtained.

For the in vivo growth assay, NOD scid gamma (NSG) mice were injected subcutaneously with isogenic PANC-1 and BxPC-3 cell lines stably expressing control or PRDM16 gRNA (106 cells) under septic conditions. During the observation period of ~2 mo, mice were maintained in sterile conditions and sacrificed if they displayed any symptoms of illness. At the end of the observation period, tumors were dissected, weighted, and imaged using a 12-megapixel f/1.8 aperture camera.

#### Mice

NOD scid gamma (NSG), Prdm16fl/fl, Smad4fl/fl, TβR2fl/fl and Trp53fl/fl mice were obtained from Jackson Laboratories. Loxp-Stop-Loxp-KrasG12D (LSL-KrasG12D) and Pdx1-Cre mice were obtained from the NCI Mouse Repository. p16Ink4A-Luciferase (p16Luc) was kindly provided by Dr. Sharpless (Burd et al., 2013). All PDAC mouse models were generated through successive crossbreeding of Prdm16fl/fl, Smad4fl/fl, TβR2fl/fl, p16Luc, Trp53fl/fl, LSL-KrasG12D and Pdx1-Cre mice as appropriate. Full descriptions of the genotypes of mice used throughout the study are: KC: LSL-KrasG12D;Pdx1-Cre; Prdm16KO: Prdm16fl/fl;Pdx1-Cre; KPrC: LSL-KrasG12D;Prdm16fl/fl;Pdx1-Cre; KSC: LSL-KrasG12D;Smad4fl/fl;Pdx1-Cre; KSPrC: LSL-KrasG12D;Smad4fl/fl;Prdm16fl/fl;Pdx1-Cre; KPC: LSL-KrasG12D;LSL-Trp53fl/fl;Pdx1-Cre; KIC: LSL-KrasG12D;p16Luc+/+;Pdx1-Cre; KTβC: LSL-KrasG12D;TβR2fl/fl;Pdx1-Cre.

The Institutional Animal Care and Use Committee (IACUC) of the University of Mississippi Medical Center (UMMC) or Virginia Commonwealth University (VCU) approved all animal experiments. All experiments with transgenic mouse models (including KSPrC mice) were initiated at UMMC and continued at VCU. We did not see any significant difference in the onset of tumor formation or survival in mice generated or maintained in both sites.

All mice were maintained on a mixed C57BL/6 and FVB/N genetic background. Mice were maintained in twelve-hour light/dark cycles (6:00 AM–6:00 PM) at 22°C and fed a standard rodent chow diet. Formation of PDAC in all mice enrolled in the study was confirmed using pancreatic tissue sections stained with hematoxylin and eosin (H&E) or immunostained with an anti-cytokeratin 19 antibody. Blood glucose levels were measured with blood collected from the tail vein using the ReliON Prime blood glucose strips. The average of one measurement from 2 to 3 different blood ReliON meters was used for each mouse.

#### Clinical samples

Human tissue micro arrays for pancreatic tissues (#PA242b, n = 24; #PA483c, n = 48; #PA805c, n = 80) were purchased from US Biomax, Inc.

#### Kaplan-Meier survival analysis in patients with wild-type or mutant SMAD4

In order to compare the survival of patients with high versus low expression of PRDM16 in the context of wild-type or mutated



SMAD4, PRDM16 expression data (mRNA expression z-scores relative to all samples (log RNA Seq V2 RSEM) were first downloaded from the TCGA PanCancer Atlas in cBioPortal. Then, patients of the TCGA-PAAD cohort with wild-type ( $n = 140$ ) or mutated ( $n = 26$ ) SMAD4 were identified using the COSMIC database. Next, patients were classified as having high or low PRDM16 expression based on whether they were above or below the top and bottom quartile of PRDM16 expression of the TCGA-PAAD cohort, respectively. Lastly, each patient was matched with the corresponding expression of PRDM16 and SMAD4 mutational status as well as the time to death or to last follow up (depending on their vital status) to create a Kaplan-Meier survival curve.

#### PRDM16 expression in patients with or without SMAD4 mutations

To assess the expression of PRDM16 in patients in the context of wild-type or mutated SMAD4, PRDM16 expression data (mRNA expression z-scores relative to all samples, log RNA Seq V2 RSEM) were first downloaded from the TCGA PanCancer Atlas in cBioPortal. Then, patients of the TCGA-PAAD cohort with different types of SMAD4 mutations were identified using the cBioPortal interface. Patients were then filtered based on those with no alteration or with truncating mutations in SMAD4 in order to create a violin plot comparing the normalized PRDM16 expression between these two groups.

#### qRT-PCR

Total RNA was extracted from frozen mouse tissue samples using TRIzol (#15596018; Ambion) and purified with chloroform (#066903; Thermo Fisher Scientific) and ethanol (#BP2818; Thermo Fisher Scientific). The RNA was then reverse-transcribed using a High-Capacity cDNA Reverse Transcription kit (#4368814; Applied Biosystems). The cDNA product was analyzed by qRT-PCR. Briefly, 25 ng cDNA and 150 nmol of each primer were mixed together with the SsoFast EvaGreen Supermix (#1725200; BioRad). PCR reactions were conducted using a CFX96 Real-Time System (BioRad) in a 96-well plate. The relative mRNA levels were calculated with the comparative CT method and normalized to GAPDH mRNA.

#### Primers used for human samples

PRDM16-For 5'-CTTTGACCACACCCGAAGGT-3'; PRDM16-Rev 5'-TGTGGAGAGGAGTGTCTTCG-3'; JUNB-For 5'-CCTGGACGATCTGCACAAGA-3'; JUNB-Rev 5'-GGTTGGTGTAAACGGGAGGT-3'; GAPDH-For 5'-CCATGGGGAAGGTGAAGTC-3'; GAPDH-Rev 5'-AGTGATGGCATGGACTGTGG-3'.

#### Primers used for mouse samples

Prdm16-For 5'-TCCCACCAGACTTCGAGCTA-3'; Prdm16-Rev 5'-AAAGTCGGCCTCTTCAGTG-3'; Gapdh-For 5'-CACCATCTTCCAGGAGCGAG-3'; Gapdh-Rev 5'-CACCATCTTCCAGGAGCGAG-3'.

#### Chromatin immunoprecipitation assay (ChIP)

ChIP assays were performed using a kit following the manufacturer's instructions (#17-295; Millipore). Accordingly, cells

were first treated with 1% formaldehyde and incubated at 37°C for 10 min. Next, cells were washed twice with ice-cold PBS containing protease inhibitors. Cells were then scraped and pelleted by centrifugation at 2,000 RPM for 4 min at 4°C. Then, cells were resuspended in SDS Lysis Buffer (Millipore, #20-163) and incubated for 10 min on ice. After samples were centrifuged for 10 min at 13,000 RPM at 4°C, the supernatants were diluted 10 times by adding ChIP Dilution Buffer (#20-153; Millipore) containing protease inhibitors. The diluted supernatants were then treated with 75  $\mu$ l of a 50% slurry of Protein-A Agarose/Salmon Sperm DNA (#16-157C; Millipore) at 4°C for 30 min with agitation. After centrifugation, supernatants were immunoprecipitated with antibodies against Smad4, Smad2, Smad3, Prdm16, GAPDH or isotype-matched control IgG and 60  $\mu$ l of a 50% slurry of Protein-A Agarose/Salmon Sperm DNA at 4°C for 1 h with rotation. Agarose was pelleted using centrifugation at 1,000 RPM for 1 min at 4°C. The pellets were washed for 5 min in Low Salt Immune Complex Wash Buffer (#20-154; Millipore) once, High Salt Immune Complex Wash Buffer (#20-155; Millipore) once, LiCl Immune Complex Wash Buffer (#20-156; Millipore) once, and TE Buffer (#20-157; Millipore) twice. To amplify DNA bound to the immunoprecipitates, elution buffer (1% SDS, 0.1 M NaHCO<sub>3</sub>) was added to each sample followed by agitation and incubation for 15 min with rotation at room temperature. Eluates were then mixed with NaCl (final concentration of 0.2 M) and incubated for 4 h at 65°C followed by adding EDTA (0.01 M), Tris-HCl, pH 6.5 (0.04 M), and Proteinase K (0.04 mg/ml). Samples were then incubated for 1 h at 45°C, and DNA was recovered using phenol/chloroform extraction coupled with ethanol precipitation. Pellets were washed with 70% ethanol and air-dried. Lastly, pellets were resuspended in an appropriate buffer for PCR, and PCR products were analyzed on a 2% agarose gel. The immunoprecipitated DNA was also analyzed by qPCR using locus specific primers and normalized to input DNA. Relative fold enrichment in each locus was quantified relative to the control as described above (qRT-PCR) as well as in our published studies (Parajuli et al., 2018; Zhang et al., 2015). The following primers were used: PRDM16-For 5'-CATCTCCCCAGCATTTGTCAGT-3'; PRDM16-Rev 5'-GGAGCGCCGAACAGGAATG-3'; JUNB-For 5'-GGCAAAGCCAGGGTCAATA-3'; JUNB-Rev 5'-AAAGCTAGTAAGCGGCCTGG-3'; GAPDH-For 5'-CGGGATGTCTGCCCTAATTAT-3'; GAPDH-Rev 5'-GCACGGAAGTCCAGCATGT-3'.

#### Luciferase reporter assay

PANC-1 cells were plated in 6-well plates and transfected with the CAGA9-Lux or Prdm16-Lux reporter in the presence of pcDNA3.1-Prdm16, pCMV5-HA-Smad4, or empty vector (pcDNA3.1 or pCMV5-HA as appropriate) using X-tremeGENE9 (#0635779001; Sigma-Aldrich). The pRL-SV40 plasmid (#AF025845; Promega) was cotransfected to normalize for transfection efficiency. For CAGA9-Lux assays, cells were incubated for 24 h with the transfection mixtures and then treated with 5 ng/ml TGF- $\beta$ 1 (#7754-BH; R&D Systems) for 24 h before measuring luciferase activity using the Dual-Luciferase Reporter Assay System (#E1910; Promega). For Prdm16-Lux assays, cells were incubated for 48 h with the transfection mixtures and then processed for luciferase activity as



described for CAGA9-Lux. Firefly Luciferase activity was normalized based on Renilla luciferase expressed from pRL-SV40 plasmid.

### Co-immunoprecipitation

Cell lysates were prepared in lysis buffer (25 mM Tris-HCl, pH 7.2, 150 mM NaCl, 5 mM MgCl<sub>2</sub>, 5% glycerol and 1% NP40) supplemented with phosphatase inhibitors (#P5726; Sigma-Aldrich) and EDTA-free protease inhibitors (#P8340; Sigma-Aldrich). Cells were lysed with 1 ml of lysis buffer for 10 min on ice and protein concentrations were determined using the BCA reagent (#23227; Thermo Fisher Scientific). Then, 90% of the pre-cleared lysates were added to anti-Smad4 antibody for 1 h at 4°C under constant rocking, and then protein A magnetic beads (#G8781; Promega) were added for an additional 1 h at 4°C. The beads were subsequently pelleted and washed five times with lysis buffer and eluted for immunoblotting using 1X SDS-PAGE sample buffer (#NP0007; Thermo Fisher Scientific). The other remaining 10% of lysate was used to determine total protein levels by direct immunoblotting.

### Immunoblotting

Cell extracts were prepared in lysis buffer containing 20 mM Tris HCl (pH 7.5), 150 mM NaCl, 1 mM EDTA, 1 mM EGTA, 1% Triton, 2.5% sodium pyrophosphate, 1 mM β-glycerophosphate, 1 mM Na<sub>2</sub>VO<sub>4</sub>, 1 μg/μL leupeptin, protease inhibitors (#P8340; Sigma-Aldrich) and phosphatase inhibitors (#P5726; Sigma-Aldrich). Protein concentrations were determined using the BCA reagent as described earlier, and samples were denatured using SDS sample buffer (#1610747; BioRad). Samples were loaded into a Criterion Tris-Glycine Extended Gel (#5671124; BioRad) and separated by electrophoreses at 60 mA. The gels were then transferred onto a nitrocellulose membrane (#1620115; BioRad) by a wet transfer system (BioRad) at 100V for 1 h at room temperature. All membranes were then blocked by incubation with 5% dry milk in TBST (TBS with 0.1% Tween20) for 1 h at room temperature. Membranes were probed with the primary antibody overnight at 4°C in the blocking buffer, washed with TBST, and incubated with the peroxidase-conjugated secondary antibody. Enhanced chemiluminescence (ECL) Western blotting substrates (#170-5061; BioRad) were used for the visualization of the results. The acquisition of images was performed using the ChemiDoc MP Imaging System (BioRad).

### Histology, immunohistochemistry, and immunofluorescence

Tissue samples were fixed in 10% formalin and embedded in paraffin. For pancreatic tissue histology, paraffin sections were stained with hematoxylin and eosin (H&E) using standard techniques. Briefly, sections were deparaffinized with xylene and rehydrated in a graded series of ethanol. They were then successively immersed in a hematoxylin solution (HHS128-4L; Sigma-Aldrich) for 2 min, a clarifier solution (7402L; EpreDia) for 15 s, and blueing reagent solution (7301L; EpreDia) for 1 min. Between each of the three steps, sections were immersed in water for 1 min. Next, slides were immersed in an eosin solution (HT110280-2.5L; Sigma-Aldrich) for 3 min before being dehydrated 3 times for 3 min in 100% ethanol (89370-088; VWR)

followed by xylene (V1001; Koptec). For immunofluorescence and immunohistochemistry, tissue sections were deparaffinized with xylene and rehydrated in a graded series of ethanol. Antigen retrieval was performed for 30 min at high temperature in citrate buffer. Then, slides were blocked and incubated overnight with anti-insulin, anti-glucagon, anti-Prdm16, anti-Muc5AC, anti-chromogranin-A, anti-αSMA, anti-E-cadherin, anti-vimentin or IgG-matched isotype control antibody (negative control) at 4°C. For immunofluorescence, slides were incubated with the secondary antibodies conjugated to Alexa-Fluor568 (#A11011; Invitrogen) or Alex-Fluor488 (#A11088; Invitrogen), co-stained with DAPI (#H1800; Vector Laboratories), and viewed on a Nikon Ti-E fluorescence microscope. Immunohistochemistry was done with the VECTASTAIN Elite ABC HRP kit (rabbit, #PK6101 or mouse, #PK-6102; Vector Laboratories) as per manufacturer's instructions. Tissue sections were incubated for 30 min in the secondary antibody followed by the VECTASTAIN ABC reagent. Color development was done with the DAB Peroxidase Substrate kit (#SK-4100; Vector Laboratories) with or without Nickel added enhancement as appropriate.

To quantify Prdm16 expression in human samples, the TMA was scanned using the PlanApo 40 × 0.95/0.25–0.17 mm objective on the Keyence BZ-X810 automated microscope and characterized using the BZ-X800 Analyzer software from Keyence. The expression intensity of six images of normal areas and PanIN stages 1, 2, 3 and PDAC lesions were chosen in a random manner. The intensity of Prdm16 expression was obtained automatically using the BZ-X800 Analyzer software from Keyence and the means of each stage (normal, PanIN stage 1, 2, 3, PDAC) were calculated. Each area/lesion was individually quantified using the area directly around the lesion.

To quantify Prdm16 expression in mouse tissues, slides chosen in a random manner from all mice under study were scanned using the PlanApo 10 × 0.45/4.00 mm objective on the Keyence BZ-X810 automated microscope and characterized using the BZ-X800 Analyzer software from Keyence. Random images of PanIN and PDAC lesions were taken and quantified only using the area directly around the lesions. Each lesion was individually quantified and the mean ± SEM of six independent lesions was presented in figures.

The quantifications of Alcian blue staining or CK19, Muc5AC, and α-SMA immunostaining were conducted by first taking images of six normal areas or PanIN/PDAC lesions from all mice under study in a random manner using the PlanApo 40 × 0.95/0.25–0.17 mm objective on the Keyence BZ-X800 microscope. We then individually quantified each image using the Keyence BZ-X800 analyzer software from Keyence. Lastly, the mean ± SEM was calculated for each genotype.

To quantify the distribution of PDAC lesions, mouse tissue slides were scanned using the PlanApo 10 × 0.45/4.00 mm objective on the Keyence BZ-X810 automated microscope and characterized using the BZ-X800 Analyzer software from Keyence. PanIN and IPMN lesions were counted and characterized as either PanIN or IPMN. The surface area for each lesion was obtained from the Keyence software and the mean sum of the surface area for all PanIN or IPMN lesions were calculated for each genotype, including all mice recruited. The percentage of



stroma was identified using the BZ-X800 Analyzer software from Keyence. The distribution of PDAC lesions was then calculated by multiplying the percentage of PanIN surface area divided by the total non-PDAC surface area of the tissue. The same process was repeated for IPMN lesions.

All images were taken using the Zeiss Axio Lab.A1 upright (Zeiss EC Plan-NEOFLUAR 40×/0.9 Pol and Zeiss A-Plan 10×/0.25 objectives), Zeiss Observer.A1 inverted (Zeiss LDA-Plan 40×/0.55 Ph1 objective), or Leica DM1000LED upright microscopes (Leica HI PLAN 40×/0.65 objective). The numerical aperture of the objective lenses are 0.9 and 0.25, 0.55, and 0.65, respectively, with a temperature of 1 (10 Kelvin) with an imaging medium of air. The fluorochromes analyzed in immunofluorescence experiments were Alexa-Fluor568 (red), Alexa-Fluor488 (green) and DAPI (blue). The cameras used were the Axiocam ICc5, Axiocam503mono, and LeicaDM2900 with the acquisition software was ZEN 2 lite for both Zeiss microscopes and LAS X for the Leica microscope. Subsequent software used for incorporating images into figures was Adobe Photoshop followed Microsoft PowerPoint.

### Statistical analysis

The values are expressed as mean ± SEM. The error bars (SEM) shown for all results were derived from biological replicates, not technical replicates. Significant differences between two groups were evaluated using either a two-tailed, unpaired Mann-Whitney test or two-tailed, unpaired *t* test, which was found to be appropriate for the statistics, as the sample groups displayed a normal distribution and comparable variance. Statistical significance of survival differences was determined by log-rank test.

### Online supplemental material

**Fig. S1** shows that *Prdm16* is transiently expressed in the pre-malignant lesions. **Fig. S2** shows that *Prdm16*KO mice display normal insulin and glucagon expression and distribution as well as normal blood glucose levels. **Fig. S3** provides additional data demonstrating that inactivation of *Prdm16* accelerates *Kras*G12D-driven PDAC. **Fig. S4** displays that *Prdm16* is required for IPMN-to-PDAC progression and that *Prdm16* deletion led to the accumulation of cells with high vimentin expression. In addition, **Fig. S4** shows the effects of deleting *PRDM16* on the proliferation of PANC-1 and BxPC-3 cell lines. **Fig. S5** further expands upon the notion that concomitant inactivation of *Prdm16* and *Smad4* mimics the phenotype of complete TGF- $\beta$  signaling inactivation through *T $\beta$ RII* ablation.

### Acknowledgments

We thank Dr. N. Sharpless (University of North Carolina at Chapel Hill, Chapel Hill, NC, USA) for providing p16<sup>Ink4a</sup>-Luc mice. We thank Dr. J. Massagué (Memorial Sloan Kettering Cancer Center, New York, NY, USA) for providing the pCMV5-HA-Smad4. We thank Dr. Atfi's lab members (present and past) for help with mice maintenance, genotyping analyses, and tissue preparation and embedding. Special thanks go to the VCU Animal Imaging and Histology Cores.

### Hurwitz et al.

*Prdm16* and *Smad4* specify the trajectory of PDAC

This work was supported by grants from the National Cancer Institute (R01CA240484, R01CA210911, R01CA251405) and Department of Defense (PR162051) to A. Atfi. Services and products in support of the research project were generated by the Virginia Commonwealth University Tissue and Data Acquisition and Analysis Core Laboratory as well as the Virginia Commonwealth University Cancer Mouse Models Core Laboratory, supported, in part, with funding by the Massey Cancer Center from NIH-NCI Cancer Center Support Grant P30 CA016059. Open Access funding provided by the VIVA consortium.

**Author contributions:** E. Hurwitz, M. Razzaque, K. Xu, and A. Atfi conceived the project. E. Hurwitz, P. Parajuli, S. Ozkan, C. Prunier, T.L. Nguyen, D. Campbell, C. Friend, A. Bryan, T.-X. Lu, S. Smith, and K. Xu, performed the experiments, analyzed the data, and interpreted results. E. Hurwitz, M. Razzaque, and A. Atfi wrote the original draft and edited the manuscript. All authors reviewed the manuscript. A. Atfi acquired funding.

**Disclosures:** The authors declare no competing interests exist.

Submitted: 14 March 2022

Revised: 28 November 2022

Accepted: 23 January 2023

### References

- Attisano, L., and J.L. Wrana. 2000. Smads as transcriptional co-modulators. *Curr. Opin. Cell Biol.* 12:235–243. [https://doi.org/10.1016/S0955-0674\(99\)00081-2](https://doi.org/10.1016/S0955-0674(99)00081-2)
- Bardeesy, N., A.J. Aguirre, G.C. Chu, K.H. Cheng, L.V. Lopez, A.F. Hezel, B. Feng, C. Brennan, R. Weissleder, U. Mahmood, et al. 2006a. Both p16<sup>Ink4a</sup> and the p19(Arf)-p53 pathway constrain progression of pancreatic adenocarcinoma in the mouse. *Proc. Natl. Acad. Sci. USA* 103: 5947–5952. <https://doi.org/10.1073/pnas.0601273103>
- Bardeesy, N., K.H. Cheng, J.H. Berger, G.C. Chu, J. Pahler, P. Olson, A.F. Hezel, J. Horner, G.Y. Lauwers, D. Hanahan, and R.A. DePinto. 2006b. Smad4 is dispensable for normal pancreas development yet critical in progression and tumor biology of pancreatic cancer. *Genes Dev.* 20:3130–3146. <https://doi.org/10.1101/gad.1478706>
- Burd, C.E., J.A. Sorrentino, K.S. Clark, D.B. Darr, J. Krishnamurthy, A.M. Deal, N. Bardeesy, D.H. Castrillon, D.H. Beach, and N.E. Sharpless. 2013. Monitoring tumorigenesis and senescence in vivo with a p16<sup>Ink4a</sup>-luciferase model. *Cell* 152:340–351. <https://doi.org/10.1016/j.cell.2012.12.010>
- Buscail, L., B. Bourmet, and P. Cordelier. 2020. Role of oncogenic KRAS in the diagnosis, prognosis and treatment of pancreatic cancer. *Nat. Rev. Gastroenterol. Hepatol.* 17:153–168. <https://doi.org/10.1038/s41575-019-0245-4>
- Chi, J., and P. Cohen. 2016. The multifaceted roles of PRDM16: Adipose biology and beyond. *Trends Endocrinol. Metab.* 27:11–23. <https://doi.org/10.1016/j.tem.2015.11.005>
- Chuikov, S., B.P. Levi, M.L. Smith, and S.J. Morrison. 2010. Prdm16 promotes stem cell maintenance in multiple tissues, partly by regulating oxidative stress. *Nat. Cell Biol.* 12:999–1006. <https://doi.org/10.1038/ncb2101>
- Connor, A.A., and S. Gallinger. 2021. Pancreatic cancer evolution and heterogeneity: Integrating omics and clinical data. *Nat. Rev. Cancer* 22: 131–142. <https://doi.org/10.1038/s41568-021-00418-1>
- David, C.J., Y.H. Huang, M. Chen, J. Su, Y. Zou, N. Bardeesy, C.A. Iacobuzio-Donahue, and J. Massagué. 2016. TGF- $\beta$  tumor suppression through a lethal EMT. *Cell* 164:1015–1030. <https://doi.org/10.1016/j.cell.2016.01.009>
- David, C.J., and J. Massagué. 2018. Contextual determinants of TGF $\beta$  action in development, immunity and cancer. *Nat. Rev. Mol. Cell Biol.* 19:419–435. <https://doi.org/10.1038/s41580-018-0007-0>
- Duda, D.G., M. Sunamura, L.P. Lefter, T. Furukawa, T. Yokoyama, T. Yatsuoka, T. Abe, H. Inoue, F. Motoi, S. Egawa, et al. 2003. Restoration of SMAD4 by gene therapy reverses the invasive phenotype in pancreatic



- adenocarcinoma cells. *Oncogene*. 22:6857–6864. <https://doi.org/10.1038/sj.onc.1206751>
- Feng, X.H., and R. Derynck. 2005. Specificity and versatility in *tgf*- $\beta$  signaling through Smads. *Annu. Rev. Cell Dev. Biol.* 21:659–693. <https://doi.org/10.1146/annurev.cellbio.21.022404.142018>
- Freeman, J.W., C.A. Mattingly, and W.E. Strodel. 1995. Increased tumorigenicity in the human pancreatic cell line MIA PaCa-2 is associated with an aberrant regulation of an IGF-1 autocrine loop and lack of expression of the TGF- $\beta$  type RII receptor. *J. Cell. Physiol.* 165:155–163. <https://doi.org/10.1002/jcp.1041650118>
- Friess, H., Y. Yamanaka, M. Büchler, M. Ebert, H.G. Beger, L.I. Gold, and M. Korc. 1993. Enhanced expression of transforming growth factor  $\beta$  isoforms in pancreatic cancer correlates with decreased survival. *Gastroenterology*. 105:1846–1856. [https://doi.org/10.1016/0016-5085\(93\)91084-U](https://doi.org/10.1016/0016-5085(93)91084-U)
- Gu, G., J.R. Brown, and D.A. Melton. 2003. Direct lineage tracing reveals the ontogeny of pancreatic cell fates during mouse embryogenesis. *Mech. Dev.* 120:35–43. [https://doi.org/10.1016/S0925-4773\(02\)00330-1](https://doi.org/10.1016/S0925-4773(02)00330-1)
- Harms, M.J., H.W. Lim, Y. Ho, S.N. Shapira, J. Ishibashi, S. Rajakumari, D.J. Steger, M.A. Lazar, K.J. Won, and P. Seale. 2015. PRDM16 binds MED1 and controls chromatin architecture to determine a brown fat transcriptional program. *Genes Dev.* 29:298–307. <https://doi.org/10.1101/gad.252734.114>
- Hayashi, A., J. Hong, and C.A. Iacobuzio-Donahue. 2021. The pancreatic cancer genome revisited. *Nat. Rev. Gastroenterol. Hepatol.* 18:469–481. <https://doi.org/10.1038/s41575-021-00463-z>
- Hidalgo, M. 2010. Pancreatic cancer. *N. Engl. J. Med.* 362:1605–1617. <https://doi.org/10.1056/NEJMra0901557>
- Hingorani, S.R., L. Wang, A.S. Multani, C. Combs, T.B. Deramaudt, R.H. Hruban, A.K. Rustgi, S. Chang, and D.A. Tuveson. 2005. Trp53R172H and KrasG12D cooperate to promote chromosomal instability and widely metastatic pancreatic ductal adenocarcinoma in mice. *Cancer Cell*. 7:469–483. <https://doi.org/10.1016/j.ccr.2005.04.023>
- Hiraike, Y., H. Waki, J. Yu, M. Nakamura, K. Miyake, G. Nagano, R. Nakaki, K. Suzuki, H. Kobayashi, S. Yamamoto, et al. 2017. NFIA co-localizes with PPAR $\gamma$  and transcriptionally controls the brown fat gene program. *Nat. Cell Biol.* 19:1081–1092. <https://doi.org/10.1038/ncb3590>
- Iacobuzio-Donahue, C.A. 2012. Genetic evolution of pancreatic cancer: Lessons learnt from the pancreatic cancer genome sequencing project. *Gut*. 61:1085–1094. <https://doi.org/10.1136/gut.2010.236026>
- Iijichi, H., A. Chytil, A.E. Gorska, M.E. Aakre, Y. Fujitani, S. Fujitani, C.V. Wright, and H.L. Moses. 2006. Aggressive pancreatic ductal adenocarcinoma in mice caused by pancreas-specific blockade of transforming growth factor- $\beta$  signaling in cooperation with active Kras expression. *Genes Dev.* 20:3147–3160. <https://doi.org/10.1101/gad.1475506>
- Izeraidjane, K., C. Combs, M. Best, A. Gopinathan, A. Wagner, W.M. Grady, C.X. Deng, R.H. Hruban, N.V. Adsay, D.A. Tuveson, and S.R. Hingorani. 2007. Kras(G12D) and Smad4/Dpc4 haploinsufficiency cooperate to induce mucinous cystic neoplasms and invasive adenocarcinoma of the pancreas. *Cancer Cell*. 11:229–243. <https://doi.org/10.1016/j.ccr.2007.01.017>
- Jambhekar, A., D. Hall, and Y. Shi. 2019. Roles and regulation of histone methylation in animal development. *Nat. Rev. Mol. Cell Biol.* 20:625–641. <https://doi.org/10.1038/s41580-019-0151-1>
- Massagué J. 2008. TGF $\beta$  in cancer. *Cell*. 134:215–230. <https://doi.org/10.1016/j.cell.2008.07.001>
- Massagué, J., J. Seoane, and D. Wotton. 2005. Smad transcription factors. *Genes Dev.* 19:2783–2810. <https://doi.org/10.1101/gad.1350705>
- Parajuli, P., S. Kumar, A. Loumaye, P. Singh, S. Eragamreddy, T.L. Nguyen, S. Ozkan, M.S. Razzaque, C. Prunier, J.P. Thissen, and A. Atfi. 2018. Twist1 activation in muscle progenitor cells causes muscle loss akin to cancer cachexia. *Dev. Cell*. 45:712–725.e6. <https://doi.org/10.1016/j.devcel.2018.05.026>
- Parajuli, P., T.L. Nguyen, C. Prunier, M.S. Razzaque, K. Xu, and A. Atfi. 2020. Pancreatic cancer triggers diabetes through TGF- $\beta$ -mediated selective depletion of islet  $\beta$ -cells. *Life Sci. Alliance*. 3:3. <https://doi.org/10.26508/lsa.201900573>
- Parajuli, P., P. Singh, Z. Wang, L. Li, S. Eragamreddy, S. Ozkan, O. Ferrigno, C. Prunier, M.S. Razzaque, K. Xu, and A. Atfi. 2019. TGIF1 functions as a tumor suppressor in pancreatic ductal adenocarcinoma. *EMBO J.* 38:e101067. <https://doi.org/10.15252/embj.2018101067>
- Park, S.W., J.M. Davison, J. Rhee, R.H. Hruban, A. Maitra, and S.D. Leach. 2008. Oncogenic KRAS induces progenitor cell expansion and malignant transformation in zebrafish exocrine pancreas. *Gastroenterology*. 134:2080–2090. <https://doi.org/10.1053/j.gastro.2008.02.084>
- Pei, D., X. Shu, A. Gassama-Diagne, and J.P. Thiery. 2019. Mesenchymal-epithelial transition in development and reprogramming. *Nat. Cell Biol.* 21:44–53. <https://doi.org/10.1038/s41556-018-0195-z>
- Pickup, M.W., P. Owens, and H.L. Moses. 2017. TGF- $\beta$ , bone morphogenetic protein, and activin signaling and the tumor microenvironment. *Cold Spring Harb. Perspect. Biol.* 9:9. <https://doi.org/10.1101/cshperspect.a022285>
- Pierreux, C.E., F.J. Nicolás, and C.S. Hill. 2000. Transforming growth factor  $\beta$ -independent shuttling of Smad4 between the cytoplasm and nucleus. *Mol. Cell. Biol.* 20:9041–9054. <https://doi.org/10.1128/MCB.20.23.9041-9054.2000>
- Pinheiro, L., R. Margueron, N. Shukeir, M. Eisold, C. Fritzsche, F.M. Richter, G. Mittler, C. Genoud, S. Goyama, M. Kurokawa, et al. 2012. Prdm3 and Prdm16 are H3K9me1 methyltransferases required for mammalian heterochromatin integrity. *Cell*. 150:948–960. <https://doi.org/10.1016/j.cell.2012.06.048>
- Seale, P., B. Bjork, W. Yang, S. Kajimura, S. Chin, S. Kuang, A. Scimè, S. Devarakonda, H.M. Conroe, H. Erdjument-Bromage, et al. 2008. PRDM16 controls a brown fat/skeletal muscle switch. *Nature*. 454:961–967. <https://doi.org/10.1038/nature07182>
- Seale, P., S. Kajimura, W. Yang, S. Chin, L.M. Rohas, M. Uldry, G. Tavernier, D. Langin, and B.M. Spiegelman. 2007. Transcriptional control of brown fat determination by PRDM16. *Cell Metab.* 6:38–54. <https://doi.org/10.1016/j.cmet.2007.06.001>
- Seo, S.R., N. Ferrand, N. Faresse, C. Prunier, L. Abécassis, M. Pessah, M.F. Bourgeade, and A. Atfi. 2006. Nuclear retention of the tumor suppressor cPML by the homeodomain protein TGIF restricts TGF- $\beta$  signaling. *Mol. Cell*. 23:547–559. <https://doi.org/10.1016/j.molcel.2006.06.018>
- Shimada, I.S., M. Acar, R.J. Burgess, Z. Zhao, and S.J. Morrison. 2017. Prdm16 is required for the maintenance of neural stem cells in the postnatal forebrain and their differentiation into ependymal cells. *Genes Dev.* 31:1134–1146. <https://doi.org/10.1101/gad.291713.116>
- Stathis, A., and M.J. Moore. 2010. Advanced pancreatic carcinoma: Current treatment and future challenges. *Nat. Rev. Clin. Oncol.* 7:163–172. <https://doi.org/10.1038/nrclinonc.2009.236>
- Stine, R.R., A.P. Sakers, T. TeSlaa, M. Kissig, Z.E. Stine, C.W. Kwon, L. Cheng, H.W. Lim, K.H. Kaestner, J.D. Rabinowitz, and P. Seale. 2019. PRDM16 maintains homeostasis of the intestinal epithelium by controlling region-specific metabolism. *Cell Stem Cell*. 25:830–845.e8. <https://doi.org/10.1016/j.stem.2019.08.017>
- Sundqvist, A., M. Morikawa, J. Ren, E. Vasilaki, N. Kawasaki, M. Kobayashi, D. Koinuma, H. Aburatani, K. Miyazono, C.H. Heldin, et al. 2018. JUNB governs a feed-forward network of TGF $\beta$  signaling that aggravates breast cancer invasion. *Nucleic Acids Res.* 46:1180–1195. <https://doi.org/10.1093/nar/gkx1190>
- Takahata, M., Y. Inoue, H. Tsuda, I. Imoto, D. Koinuma, M. Hayashi, T. Ichikura, T. Yamori, K. Nagasaki, M. Yoshida, et al. 2009. SKI and MEL1 cooperate to inhibit transforming growth factor- $\beta$  signal in gastric cancer cells. *J. Biol. Chem.* 284:3334–3344. <https://doi.org/10.1074/jbc.M808989200>
- Tuveson, D.A., A.T. Shaw, N.A. Willis, D.P. Silver, E.L. Jackson, S. Chang, K.L. Mercer, R. Grochow, H. Hock, D. Crowley, et al. 2004. Endogenous oncogenic K-ras(G12D) stimulates proliferation and widespread neoplastic and developmental defects. *Cancer Cell*. 5:375–387. [https://doi.org/10.1016/S1535-6108\(04\)00085-6](https://doi.org/10.1016/S1535-6108(04)00085-6)
- Westphalen, C.B., and K.P. Olive. 2012. Genetically engineered mouse models of pancreatic cancer. *Cancer J.* 18:502–510. <https://doi.org/10.1097/PPO.0b013e31827ab4c4>
- Whittle, M.C., K. Izeraidjane, P.G. Rani, L. Feng, M.A. Carlson, K.E. DelGiorno, L.D. Wood, M. Goggins, R.H. Hruban, A.E. Chang, et al. 2015. RUNX3 controls a metastatic switch in pancreatic ductal adenocarcinoma. *Cell*. 161:1345–1360. <https://doi.org/10.1016/j.cell.2015.04.048>
- Xue, H., T. Yao, M. Cao, G. Zhu, Y. Li, G. Yuan, Y. Chen, M. Lei, and J. Huang. 2019. Structural basis of nucleosome recognition and modification by MLL methyltransferases. *Nature*. 573:445–449. <https://doi.org/10.1038/s41586-019-1528-1>
- Yonezawa, S., M. Higashi, N. Yamada, and M. Goto. 2008. Precursor lesions of pancreatic cancer. *Gut Liver*. 2:137–154. <https://doi.org/10.5009/gnl.2008.2.3.137>
- Zhang, M.Z., O. Ferrigno, Z. Wang, M. Ohnishi, C. Prunier, L. Levy, M. Razzaque, W.C. Horne, D. Romero, G. Tzivion, et al. 2015. TGIF governs a feed-forward network that empowers Wnt signaling to drive mammary tumorigenesis. *Cancer Cell*. 27:547–560. <https://doi.org/10.1016/j.ccr.2015.03.002>
- Zhou, B., J. Wang, S.Y. Lee, J. Xiong, N. Bhanu, Q. Guo, P. Ma, Y. Sun, R.C. Rao, B.A. Garcia, et al. 2016. PRDM16 suppresses MLL1 leukemia via intrinsic histone methyltransferase activity. *Mol. Cell*. 62:222–236. <https://doi.org/10.1016/j.molcel.2016.03.010>

Hurwitz et al.

Prdm16 and Smad4 specify the trajectory of PDAC

Journal of Cell Biology

<https://doi.org/10.1083/jcb.202203036>

19 of 19



## Supplemental material

Downloaded from [http://rupress.org/jcb/article-pdf/224/4/20203036/1448319/jcb\\_202203036.pdf](http://rupress.org/jcb/article-pdf/224/4/20203036/1448319/jcb_202203036.pdf) by Virginia Commonwealth University user on 06 March 2023

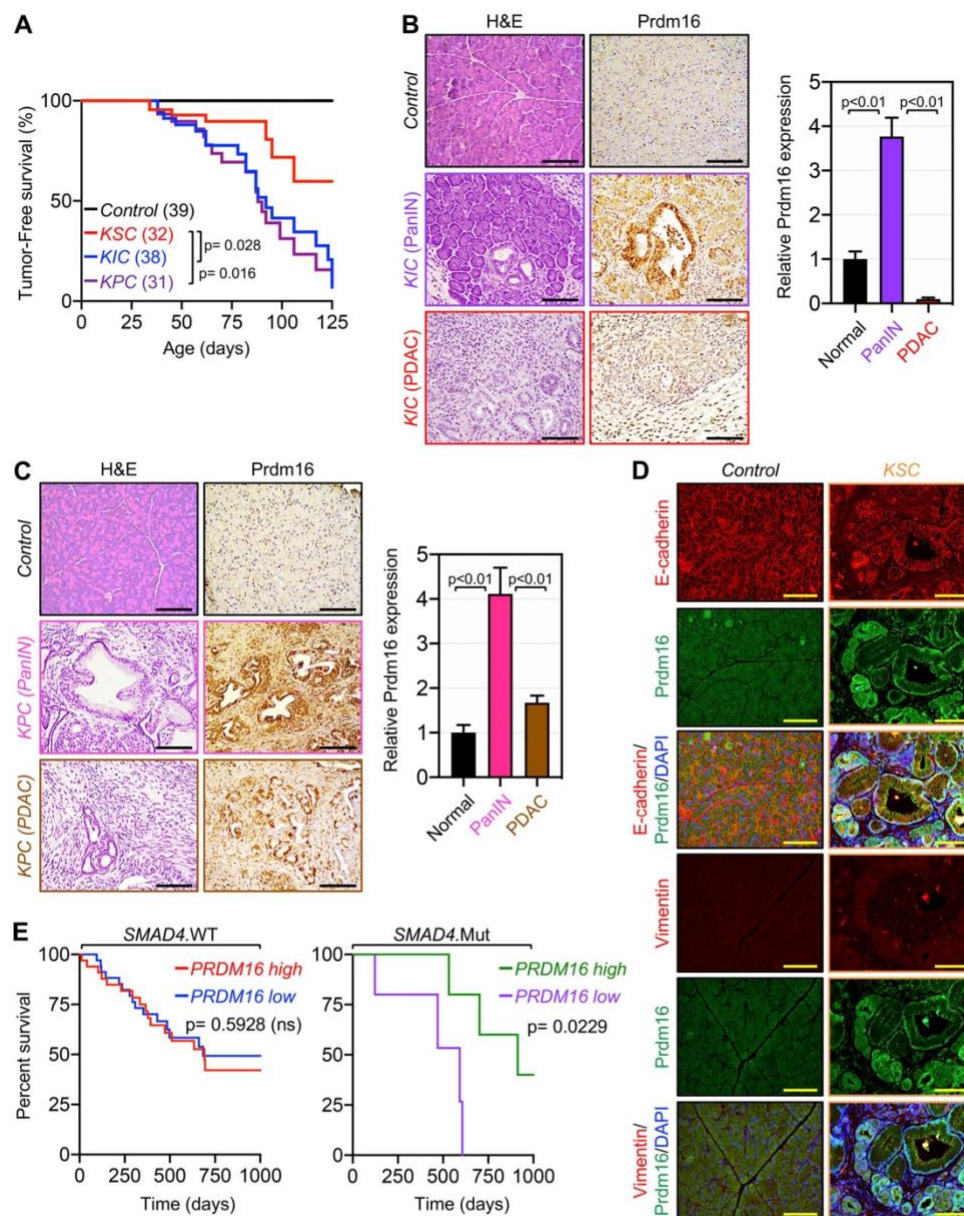


Figure S1. **Transient expression of Prdm16 during PDAC progression.** (A) Kaplan-Meier survival analysis of control, KSC, KIC, and KPC mice ( $n = 31-39$ ). Statistical power was assessed by a log-rank test for significance. (B) FFPE pancreatic sections from 4-mo-old control and KIC mice ( $n = 38-39$ ) were stained with H&E or immunostained with anti-Prdm16 antibody and subjected to IHC. Representative pictures of normal, PanIN and PDAC areas are shown. Scale bars: 50  $\mu$ m (left). Relative Prdm16 expression in normal tissue and PanIN or PDAC lesions are shown (right). Data are expressed as mean  $\pm$  SEM. (C) FFPE pancreatic sections from 3-mo-old control and KPC mice ( $n = 31-39$ ) were stained with H&E or immunostained with anti-Prdm16 antibody and subjected to IHC. Representative pictures of normal, PanIN, and PDAC areas are shown. Scale bars: 50  $\mu$ m (left). Relative Prdm16 expression in normal tissue and PanIN or PDAC lesions are shown (right). Data are expressed as mean  $\pm$  SEM. (D) FFPE pancreatic sections from control and KSC mice ( $n = 31-45$ ) were subjected to co-IF using antibodies to Prdm16 and E-cadherin or vimentin. Representative pictures of normal tissue and IPMN or PDAC areas are shown. Scale bars: 50  $\mu$ m. (E) Kaplan-Meier survival analysis of patients with wild-type or mutated SMAD4 based on high versus low PRDM16 expression was conducted using the TCGA dataset. Statistical power was assessed by log-rank test for significance. Statistical power in B and C were assessed by a two-tailed, unpaired Mann-Whitney test.

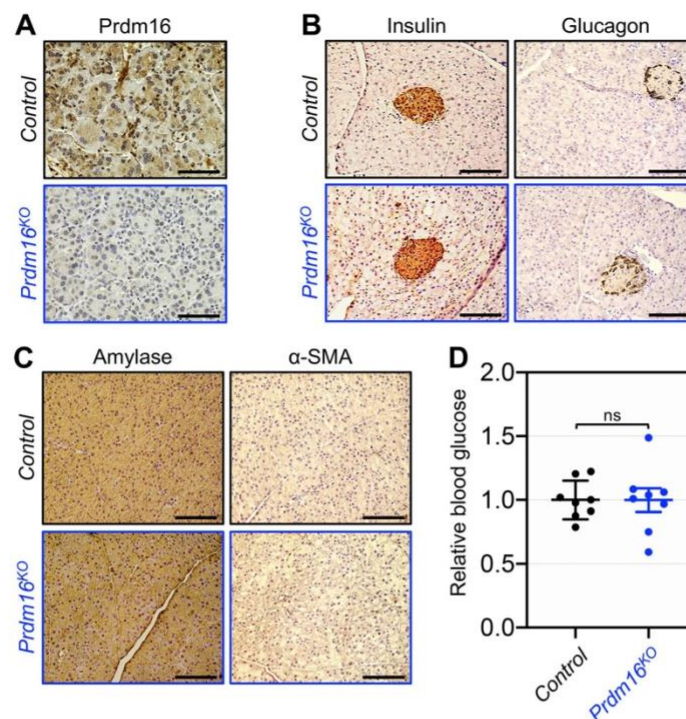


Figure S2. **Prdm16KO mice display normal pancreatic endocrine function.** (A) FFPE pancreatic sections from 15-wk-old control and Prdm16KO mice ( $n = 8-31$ ) were immunostained with anti-Prdm16 antibody and subjected to IHC. Scale bars: 50  $\mu\text{m}$ . (B) FFPE pancreatic sections from 15-wk-old control and Prdm16KO mice ( $n = 8-31$ ) were immunoreacted with antibodies to insulin or glucagon and subjected to IHC. Scale bars: 50  $\mu\text{m}$ . (C) FFPE pancreatic sections from 15-wk-old control and Prdm16KO mice were subjected to IHC using antibodies to amylase or  $\alpha$ -SMA. Scale bars: 50  $\mu\text{m}$ . (D) Blood glucose of 15-wk-old control or Prdm16KO mice ( $n = 8$ ). Statistical power was assessed by a two-tailed, unpaired Mann-Whitney test.

Downloaded from [http://rnpres.org/jcb/article-pdf/22/4/20203036/1448319/jcb\\_202203036.pdf](http://rnpres.org/jcb/article-pdf/22/4/20203036/1448319/jcb_202203036.pdf) by Virginia Commonwealth University user on 06 March 2023



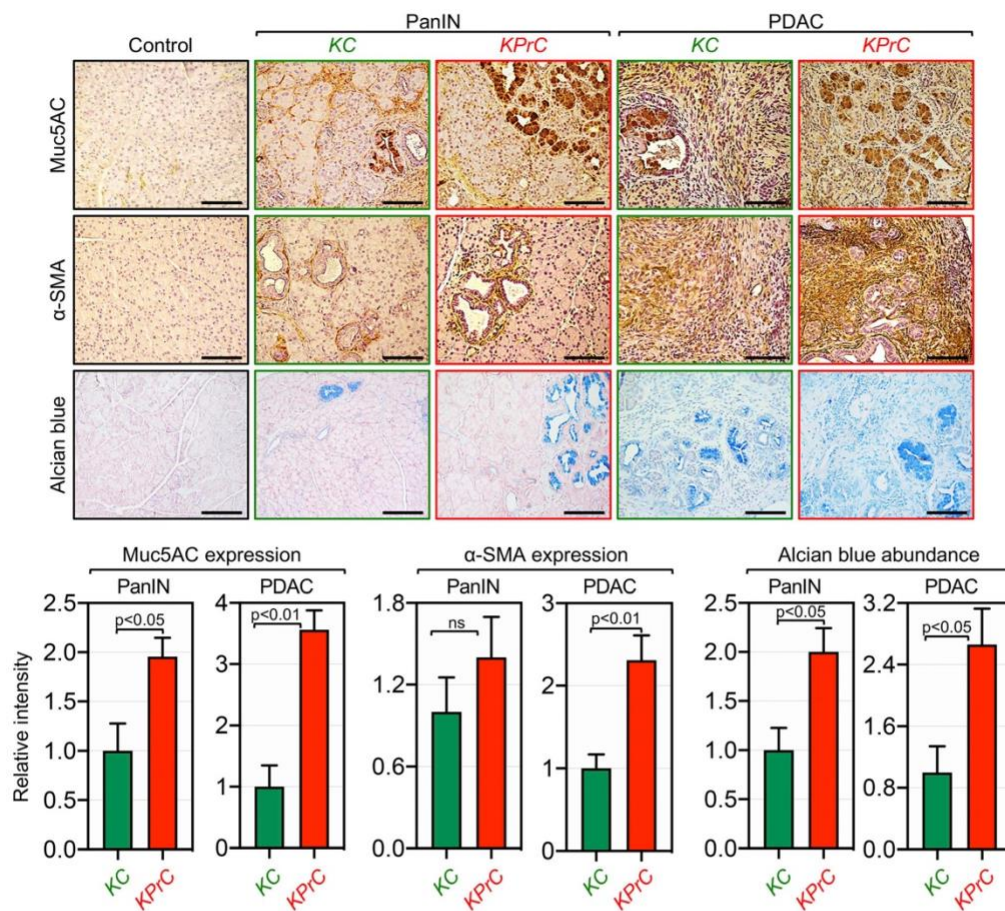
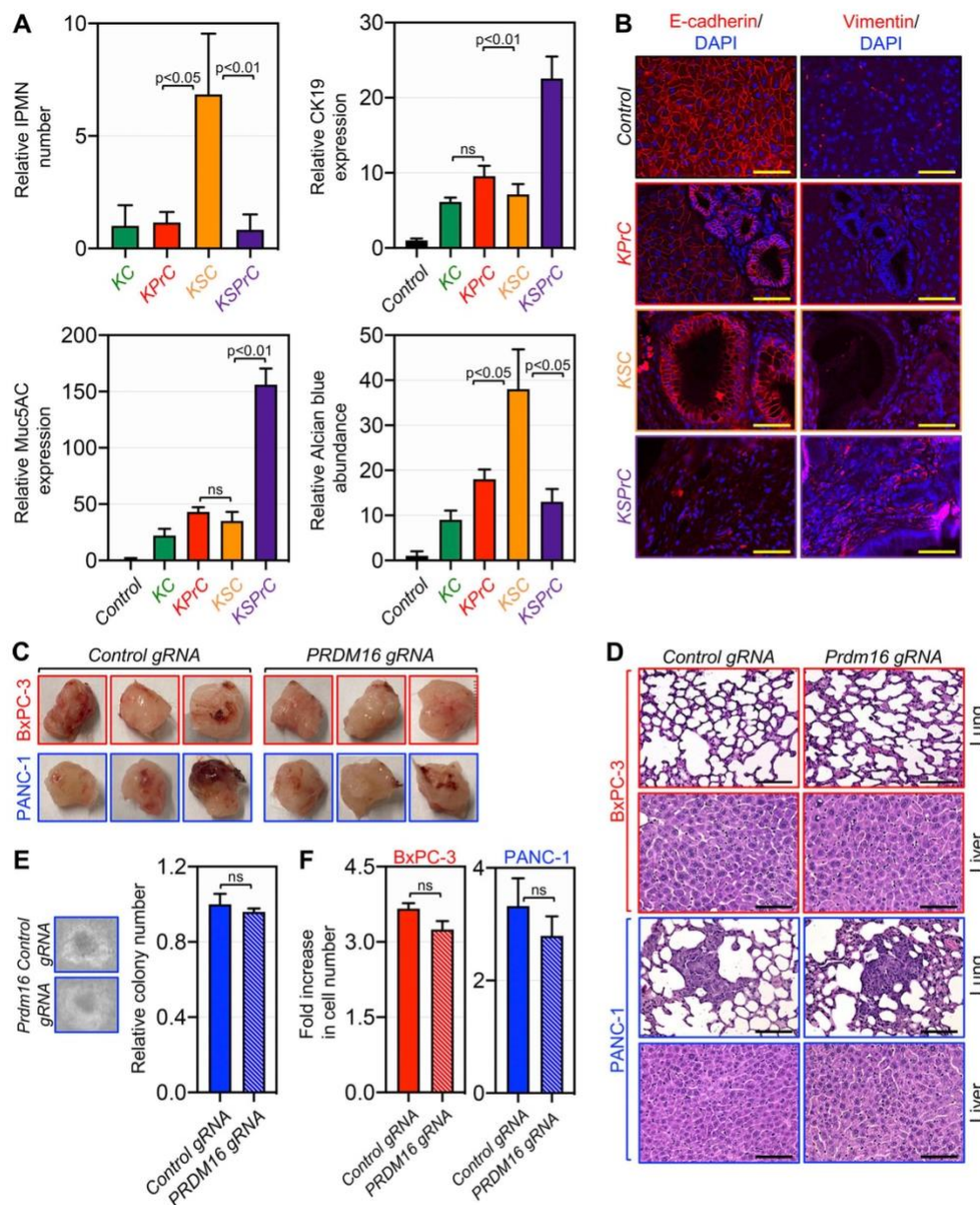


Figure S3. **Prdm16 ablation accelerates PDAC driven by KrasG12D.** FFPE pancreatic sections from 4-mo-old control, Prdm16KO, KC, and KPrC mice ( $n = 8-33$ ) were stained with H&E or Alcian Blue or immunostained with antibodies to Muc5AC or  $\alpha$ -SMA and subjected to IHC. Representative pictures are shown. Scale bars: 50  $\mu$ m (top). Relative intensity of Muc5AC,  $\alpha$ -SMA, and Alcian blue staining in areas of PanIN and PDAC lesions are shown ( $n = 13-33$ ). Data are expressed as mean  $\pm$  SEM (bottom), and statistical power was assessed by a two-tailed, unpaired Mann-Whitney test.



**Figure S4. Prdm16 inactivation in KSC mice resulted in acceleration of PDAC.** (A) FFPE pancreatic sections from 4-mo-old control, KC, KPrC, KSC, and KSPrC mice ( $n = 13-45$ ) were stained with H&E or Alcian blue or immunostained with antibodies to CK19 or Muc5AC and subjected to IHC. Relative abundance of IPMN lesions (top left) or intensity of CK19 (top right), Muc5AC (bottom left), or Alcian blue (bottom right) are shown. Data are expressed as mean  $\pm$  SEM, and statistical power was assessed by a two-tailed, unpaired Mann-Whitney test. (B) FFPE pancreatic sections from control, KPrC, KSC, and KSPrC mice ( $n = 13-45$ ) were subjected to IF using antibodies to E-cadherin or vimentin. Representative pictures are shown. Scale bars: 50  $\mu$ m. (C) Pictures of tumors harvested from NSG mice injected with isogenic PANC-1 and BxPC-3 cell lines stably expressing control or PRDM16 gRNA ( $n = 3$ ). (D) FFPE liver and lung sections from NSG mice injected with isogenic PANC-1 and BxPC-3 cell lines stably expressing control or PRDM16 gRNA were stained with H&E ( $n = 3$ ). Representative pictures are shown. Scale bars: 50  $\mu$ m. (E) Representative pictures of soft-agar colonies formed by isogenic PANC-1 cell lines stably expressing control or PRDM16 gRNA. BxPC-3 stably expressing control or PRDM16 gRNA did not form colonies. (F) Cell proliferation assay of isogenic PANC-1 (day 3) and BxPC-3 (day 6) cell lines stably expressing control or PRDM16 gRNA. The fold increase in cell number at the end of the experiment relative to the seeding density is shown ( $n = 3$ ). Data are expressed as mean  $\pm$  SEM and statistical power was assessed by a two-tailed, unpaired Mann-Whitney test.



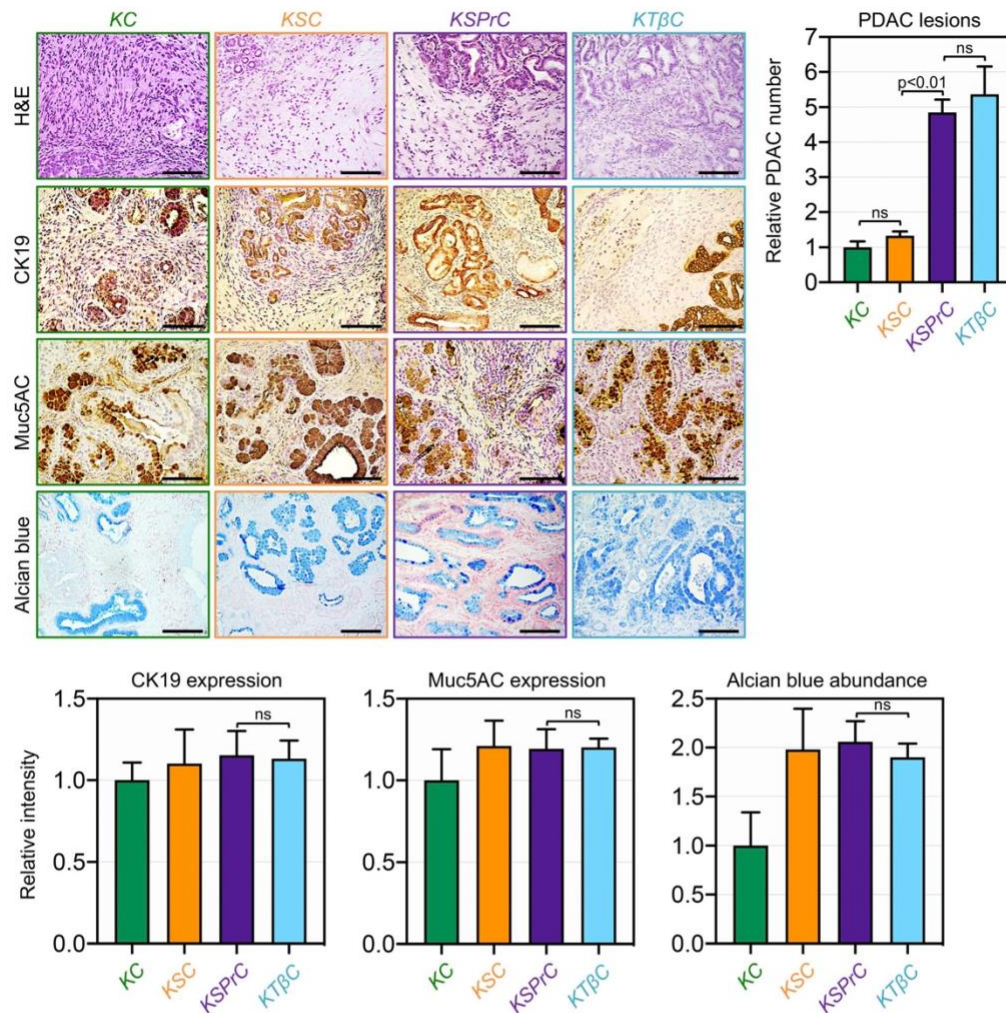


Figure S5. **Alterations in TGF- $\beta$  signaling result in different PDAC trajectories.** FFPE pancreatic sections from 1–4-mo-old KC, KSC, KSPrC, and KT $\beta$ C mice ( $n = 19$ –45) with full-blown PDAC were stained with H&E or Alcian blue, or immunostained with antibodies to CK19 or Muc5AC and subjected to IHC. Representative pictures are shown. Scale bars: 50  $\mu$ m (top left). Relative number of PDAC lesions (top right). Relative intensity of CK19, Muc5AC, and Alcian blue staining in PDAC lesions (bottom). Data are expressed as mean  $\pm$  SEM, and statistical power was assessed by a two-tailed, unpaired Mann–Whitney test.

### 3 SUMMARY AND FUTURE DIRECTIONS

This study provided the first evidence that *Prdm16* functions as a tumor suppressor gene in PDAC. Kaplan-Meier survival analysis revealed that inactivation of *Prdm16* significantly accelerated PDAC progression in both *KC* and *KSC* mice. These data also demonstrated that ablation of *Prdm16* in *KSC* mice resulted in the PanIN-to-PDAC route, suggesting that *Prdm16* required for the IPMN-to-PDAC progression that is well established in *KSC* mice. Mechanistic experiments uncovered that *Smad4* inhibits *PRDM16* transcription by recruiting *Prdm16* to the *PRDM16* promoter to repress its own transcription. These data provide an explanation as to why elevated levels of *Prdm16* expression are observed in IPMN and PDAC of *KSC* mice as opposed to the transient level of *Prdm16* expression seen in mice with the PanIN-to-PDAC progression trajectory.

Future research involving *Prdm16* in PDAC could be expanded to include a translational component in the following two ways: 1) targeting *Prdm16* therapeutically and 2) identifying downstream mechanisms as a result of *Prdm16* inactivation in PDAC. Given the unique observation that inactivation of *Prdm16* leads to significant tumor progression in the context of both *KC* and *KSC* mice, potential PDAC therapeutics could aim to promote *Prdm16* expression. One possible approach to induce *Prdm16* expression is through the use of the drug rosiglitazone. Interestingly, rosiglitazone has been shown to stimulate *Prdm16* expression and stabilize the *Prdm16* protein, which in turn can help maintain its activation in adipose tissue ([Ohno et al., 2012](#)). Furthermore, treatment with rosiglitazone in the absence

of *Prdm16* resulted in a reduced brown fat gene expression signature, as *Prdm16* is known to promote the being of fat which is metabolically similar to BAT. Based on these observations, future experiments could investigate whether rosiglitazone may serve as an effective therapeutic in PDAC tumors deficient of *Prdm16* via similar mechanisms observed in adipose tissue. To confirm that rosiglitazone is capable of inducing *Prdm16* expression in the pancreas, the expression of *Prdm16* protein could be analyzed in several human PDAC cancer cell lines (i.e., PANC-1, SUIT-2, BxPC-3, AsPC-1, and MIA-PaCa-2) by either western blot or immunostaining in the presence and absence of rosiglitazone treatment. Using similar conditions from studies in adipose tissue, the starting concentration and duration of treatment would be 1  $\mu$ M for 4 days (Ohno et al., 2012). If studies confirm that rosiglitazone can induce *Prdm16* expression in human PDAC cells, subsequent experiments could evaluate whether treatment of rosiglitazone impacts PDAC cell death using a MTT assay. A MTT assay could also be performed concurrently in *wildtype* and *PRDM16*-depleted cells to determine the impact of rosiglitazone on cell viability in a *Prdm16*-dependent manner. This experiment could be performed using multiple cell lines in parallel, such as PANC-1 and BxPC-3, which are *Smad4* sufficient and deficient, respectively. Together, these data could provide additional insight into the function of rosiglitazone as a PDAC therapeutic since *SMAD4* is inactivated in 50% of all cases of human PDAC. A strong next step would then be in vivo experimentation using *control*, *KC*, *KPrC*, *KSC*, and *KSPrC* mice at a starting dose of 10 mg/kg for 10 days based on previous studies in order to evaluate rosiglitazone treatment on PDAC tumor progression (Ohno et al., 2012). Potential experiments may consist of monitoring



tumor growth, survival rates, and tumor response at the molecular level as a result of rosiglitazone treatment. While there are a multitude of other potential experiments that could be performed to gauge whether rosiglitazone may serve as an effective PDAC therapeutic, those listed here provide a robust starting point. Overall, the development of rosiglitazone as a PDAC therapeutic may lead to a targeted treatment approach for tumors with *Prdm16* inactivation.

The second method to develop a translational component to this work could be through studying the downstream mechanisms as a result of *Prdm16* inactivation. Here, single-cell RNA sequencing (scRNA-seq) could be leveraged using *control* samples in addition to *KC*, *KPrC*, *KSC* and *KSPrC* tumors. Traditional RNA sequencing suffers from the limitation of sample heterogeneity, where studies have indicated that PDAC samples contain a high intra-tumor heterogeneity in addition to an abundance of cellular populations that make up the tumor microenvironment, such as tumor cells, immune cells, and endothelial cells ([Peng et al., 2019](#); [Tanay and Regev, 2017](#)). Therefore, scRNA-seq provides additional granularity to differentiate the gene expression between individual cells and can be better utilized to answer complex research questions regarding the function of *Prdm16* in PDAC. For example, differential gene expression analysis using scRNA-seq data could be carried out to identify genes differentially expressed between *KSPrC* and *KSC* tumors that lead to dramatic PDAC progression ([Anders and Huber, 2010](#)). This data could then be leveraged for GSEA to identify pathways that are up- and down-regulated in *KSPrC* tumors relative to those in *KSC* mice. ([Subramanian et al., 2005](#)). Upon completion

of the GSEA, these results may reveal gene targets/pathways that can be exploited therapeutically in order to ameliorate the poor prognosis of PDAC.

In summary, this work suggests that Prdm16 plays a crucial role as a tumor suppressor in PDAC. The data presented here in combination with proposed future studies not only yield additional mechanistic insights into how Prdm16 functions in PDAC, but also provides novel perception into an ideological basis for which researchers can build from to develop innovative therapeutic strategies for this insidious disease.

## REFERENCES

- Anders, S., and W. Huber. 2010. Differential expression analysis for sequence count data. *Genome Biol.* 11:R106.
- Apte, M.V., R.C. Pirola, and J.S. Wilson. 2012. Pancreatic stellate cells: a starring role in normal and diseased pancreas. *Front Physiol.* 3:344.
- Attisano, L., and J.L. Wrana. 2000. Smads as transcriptional co-modulators. *Curr Opin Cell Biol.* 12:235-243.
- Bardeesy, N., A.J. Aguirre, G.C. Chu, K.H. Cheng, L.V. Lopez, A.F. Hezel, B. Feng, C. Brennan, R. Weissleder, U. Mahmood, D. Hanahan, M.S. Redston, L. Chin, and R.A. Depinho. 2006a. Both p16(Ink4a) and the p19(Arf)-p53 pathway constrain progression of pancreatic adenocarcinoma in the mouse. *Proc Natl Acad Sci U S A.* 103:5947-5952.
- Bardeesy, N., K.H. Cheng, J.H. Berger, G.C. Chu, J. Pahler, P. Olson, A.F. Hezel, J. Horner, G.Y. Lauwers, D. Hanahan, and R.A. DePinho. 2006b. Smad4 is dispensable for normal pancreas development yet critical in progression and tumor biology of pancreas cancer. *Genes Dev.* 20:3130-3146.
- Barton, C.M., S.L. Staddon, C.M. Hughes, P.A. Hall, C. O'Sullivan, G. Kloppel, B. Theis, R.C. Russell, J. Neoptolemos, R.C. Williamson, and et al. 1991. Abnormalities of the p53 tumour suppressor gene in human pancreatic cancer. *Br J Cancer.* 64:1076-1082.
- Basso, D., E. Gnatta, A. Padoan, P. Fogar, S. Furlanello, A. Aita, D. Bozzato, C.F. Zambon, G. Arrigoni, C. Frasson, C. Franchin, S. Moz, T. Brefort, T. Laufer,

- F. Navaglia, S. Pedrazzoli, G. Basso, and M. Plebani. 2017. PDAC-derived exosomes enrich the microenvironment in MDSCs in a SMAD4-dependent manner through a new calcium related axis. *Oncotarget*. 8:84928-84944.
- Baugh, E.H., H. Ke, A.J. Levine, R.A. Bonneau, and C.S. Chan. 2018. Why are there hotspot mutations in the TP53 gene in human cancers? *Cell Death Differ*. 25:154-160.
- Bijlsma, M.F., A. Sadanandam, P. Tan, and L. Vermeulen. 2017. Molecular subtypes in cancers of the gastrointestinal tract. *Nat Rev Gastroenterol Hepatol*. 14:333-342.
- Bonner-Weir, S., and A. Sharma. 2002. Pancreatic stem cells. *J Pathol*. 197:519-526.
- Bos, J.L., H. Rehmann, and A. Wittinghofer. 2007. GEFs and GAPs: critical elements in the control of small G proteins. *Cell*. 129:865-877.
- Bournet, B., C. Buscail, F. Muscari, P. Cordelier, and L. Buscail. 2016. Targeting KRAS for diagnosis, prognosis, and treatment of pancreatic cancer: Hopes and realities. *Eur J Cancer*. 54:75-83.
- Brereton, M.F., E. Vergari, Q. Zhang, and A. Clark. 2015. Alpha-, Delta- and PP-cells: Are They the Architectural Cornerstones of Islet Structure and Coordination? *J Histochem Cytochem*. 63:575-591.
- Bryant, K.L., J.D. Mancias, A.C. Kimmelman, and C.J. Der. 2014. KRAS: feeding pancreatic cancer proliferation. *Trends Biochem Sci*. 39:91-100.
- Burd, C.E., J.A. Sorrentino, K.S. Clark, D.B. Darr, J. Krishnamurthy, A.M. Deal, N. Bardeesy, D.H. Castrillon, D.H. Beach, and N.E. Sharpless. 2013. Monitoring

- tumorigenesis and senescence in vivo with a p16(INK4a)-luciferase model. *Cell*. 152:340-351.
- Buscail, L., B. Bournet, and P. Cordelier. 2020. Role of oncogenic KRAS in the diagnosis, prognosis and treatment of pancreatic cancer. *Nat Rev Gastroenterol Hepatol*. 17:153-168.
- Calon, A., D.V. Tauriello, and E. Batlle. 2014. TGF-beta in CAF-mediated tumor growth and metastasis. *Semin Cancer Biol*. 25:15-22.
- Cancer.net. 2022. Pancreatic Cancer: Statistics.
- Cave, D.D., M. Di Guida, V. Costa, M. Sevillano, L. Ferrante, C. Heeschen, M. Corona, A. Cucciardi, and E. Lonardo. 2020. TGF-beta1 secreted by pancreatic stellate cells promotes stemness and tumourigenicity in pancreatic cancer cells through L1CAM downregulation. *Oncogene*. 39:4271-4285.
- Chela, H., B.S. Romana, M. Madabattula, A.A. Albarrak, M.H. Yousef, S. Samiullah, and V. Tahan. 2020. Stem cell therapy: a potential for the perils of pancreatitis. *Turk J Gastroenterol*. 31:415-424.
- Chen, Y.W., P.J. Hsiao, C.C. Weng, K.K. Kuo, T.L. Kuo, D.C. Wu, W.C. Hung, and K.H. Cheng. 2014. SMAD4 loss triggers the phenotypic changes of pancreatic ductal adenocarcinoma cells. *BMC Cancer*. 14:181.
- Chi, J., and P. Cohen. 2016. The Multifaceted Roles of PRDM16: Adipose Biology and Beyond. *Trends Endocrinol Metab*. 27:11-23.

- Chiaradonna, F., C. Magnani, E. Sacco, R. Manzoni, L. Alberghina, and M. Vanoni. 2005. Acquired glucose sensitivity of k-ras transformed fibroblasts. *Biochem Soc Trans.* 33:297-299.
- Chiaradonna, F., E. Sacco, R. Manzoni, M. Giorgio, M. Vanoni, and L. Alberghina. 2006. Ras-dependent carbon metabolism and transformation in mouse fibroblasts. *Oncogene.* 25:5391-5404.
- Chuikov, S., B.P. Levi, M.L. Smith, and S.J. Morrison. 2010. Prdm16 promotes stem cell maintenance in multiple tissues, partly by regulating oxidative stress. *Nat Cell Biol.* 12:999-1006.
- Connor, A.A., and S. Gallinger. 2022. Pancreatic cancer evolution and heterogeneity: integrating omics and clinical data. *Nat Rev Cancer.* 22:131-142.
- Dardare, J., A. Witz, J.L. Merlin, P. Gilson, and A. Harle. 2020. SMAD4 and the TGFbeta Pathway in Patients with Pancreatic Ductal Adenocarcinoma. *Int J Mol Sci.* 21.
- David, C.J., Y.H. Huang, M. Chen, J. Su, Y. Zou, N. Bardeesy, C.A. Iacobuzio-Donahue, and J. Massague. 2016. TGF-beta Tumor Suppression through a Lethal EMT. *Cell.* 164:1015-1030.
- David, C.J., and J. Massague. 2018. Contextual determinants of TGFbeta action in development, immunity and cancer. *Nat Rev Mol Cell Biol.* 19:419-435.
- Delpu, Y., N. Hanoun, H. Lulka, F. Sicard, J. Selves, L. Buscail, J. Torrisani, and P. Cordelier. 2011. Genetic and epigenetic alterations in pancreatic carcinogenesis. *Curr Genomics.* 12:15-24.

- di Magliano, M.P., and C.D. Logsdon. 2013. Roles for KRAS in pancreatic tumor development and progression. *Gastroenterology*. 144:1220-1229.
- Duda, D.G., M. Sunamura, L.P. Lefter, T. Furukawa, T. Yokoyama, T. Yatsuoka, T. Abe, H. Inoue, F. Motoi, S. Egawa, S. Matsuno, and A. Horii. 2003. Restoration of SMAD4 by gene therapy reverses the invasive phenotype in pancreatic adenocarcinoma cells. *Oncogene*. 22:6857-6864.
- F. T. Bosman, W.H.O., International Agency for Research on Cancer. 2010. WHO classification of tumours of the digestive system. International Agency for Research on Cancer, Lyon, 2010.
- Fei, L.R., W.J. Huang, Y. Wang, L. Lei, Z.H. Li, Y.W. Zheng, Z. Wang, M.Q. Yang, C.C. Liu, and H.T. Xu. 2019. PRDM16 functions as a suppressor of lung adenocarcinoma metastasis. *J Exp Clin Cancer Res*. 38:35.
- Feng, X.H., and R. Derynck. 2005. Specificity and versatility in tgf-beta signaling through Smads. *Annu Rev Cell Dev Biol*. 21:659-693.
- Ferde, P.E., and M.A. Jakubowska. 2017. Biology of pancreatic stellate cells-more than just pancreatic cancer. *Pflugers Arch*. 469:1039-1050.
- Ferrari, G., B.D. Cook, V. Terushkin, G. Pintucci, and P. Mignatti. 2009. Transforming growth factor-beta 1 (TGF-beta1) induces angiogenesis through vascular endothelial growth factor (VEGF)-mediated apoptosis. *J Cell Physiol*. 219:449-458.
- Fiorini, C., M. Cordani, C. Padroni, G. Blandino, S. Di Agostino, and M. Donadelli. 2015. Mutant p53 stimulates chemoresistance of pancreatic adenocarcinoma cells to gemcitabine. *Biochim Biophys Acta*. 1853:89-100.



- Freeman, J.W., C.A. Mattingly, and W.E. Strodel. 1995. Increased tumorigenicity in the human pancreatic cell line MIA PaCa-2 is associated with an aberrant regulation of an IGF-1 autocrine loop and lack of expression of the TGF-beta type RII receptor. *J Cell Physiol.* 165:155-163.
- Friess, H., Y. Yamanaka, M. Buchler, M. Ebert, H.G. Beger, L.I. Gold, and M. Korc. 1993. Enhanced expression of transforming growth factor beta isoforms in pancreatic cancer correlates with decreased survival. *Gastroenterology.* 105:1846-1856.
- Furukawa, T., M. Sunamura, and A. Horii. 2006. Molecular mechanisms of pancreatic carcinogenesis. *Cancer Sci.* 97:1-7.
- Gaglio, D., C.M. Metallo, P.A. Gameiro, K. Hiller, L.S. Danna, C. Balestrieri, L. Alberghina, G. Stephanopoulos, and F. Chiaradonna. 2011. Oncogenic K-Ras decouples glucose and glutamine metabolism to support cancer cell growth. *Mol Syst Biol.* 7:523.
- Goggins, M., M. Shekher, K. Turnacioglu, C.J. Yeo, R.H. Hruban, and S.E. Kern. 1998. Genetic alterations of the transforming growth factor beta receptor genes in pancreatic and biliary adenocarcinomas. *Cancer Res.* 58:5329-5332.
- Gomis, R.R., C. Alarcon, C. Nadal, C. Van Poznak, and J. Massague. 2006. C/EBPbeta at the core of the TGFbeta cytostatic response and its evasion in metastatic breast cancer cells. *Cancer Cell.* 10:203-214.
- Grapin-Botton, A. 2005. Ductal cells of the pancreas. *Int J Biochem Cell Biol.* 37:504-510.

- Grossberg, A.J., L.C. Chu, C.R. Deig, E.K. Fishman, W.L. Hwang, A. Maitra, D.L. Marks, A. Mehta, N. Nabavizadeh, D.M. Simeone, C.D. Weekes, and C.R. Thomas, Jr. 2020. Multidisciplinary standards of care and recent progress in pancreatic ductal adenocarcinoma. *CA Cancer J Clin.* 70:375-403.
- Gu, G., J.R. Brown, and D.A. Melton. 2003. Direct lineage tracing reveals the ontogeny of pancreatic cell fates during mouse embryogenesis. *Mech Dev.* 120:35-43.
- Hahn, S.A., M. Schutte, A.T. Hoque, C.A. Moskaluk, L.T. da Costa, E. Rozenblum, C.L. Weinstein, A. Fischer, C.J. Yeo, R.H. Hruban, and S.E. Kern. 1996. DPC4, a candidate tumor suppressor gene at human chromosome 18q21.1. *Science.* 271:350-353.
- Haigis, K.M. 2017. KRAS Alleles: The Devil Is in the Detail. *Trends Cancer.* 3:686-697.
- Hanahan, D. 2022. Hallmarks of Cancer: New Dimensions. *Cancer Discov.* 12:31-46.
- Harms, M.J., J. Ishibashi, W. Wang, H.W. Lim, S. Goyama, T. Sato, M. Kurokawa, K.J. Won, and P. Seale. 2014. Prdm16 is required for the maintenance of brown adipocyte identity and function in adult mice. *Cell Metab.* 19:593-604.
- Harms, M.J., H.W. Lim, Y. Ho, S.N. Shapira, J. Ishibashi, S. Rajakumari, D.J. Steger, M.A. Lazar, K.J. Won, and P. Seale. 2015. PRDM16 binds MED1 and controls chromatin architecture to determine a brown fat transcriptional program. *Genes Dev.* 29:298-307.

- Hayashi, A., J. Hong, and C.A. Iacobuzio-Donahue. 2021. The pancreatic cancer genome revisited. *Nat Rev Gastroenterol Hepatol*. 18:469-481.
- Hezel, A.F., A.C. Kimmelman, B.Z. Stanger, N. Bardeesy, and R.A. Depinho. 2006. Genetics and biology of pancreatic ductal adenocarcinoma. *Genes Dev*. 20:1218-1249.
- Hidalgo, M. 2010. Pancreatic cancer. *N Engl J Med*. 362:1605-1617.
- Hingorani, S.R., E.F. Petricoin, A. Maitra, V. Rajapakse, C. King, M.A. Jacobetz, S. Ross, T.P. Conrads, T.D. Veenstra, B.A. Hitt, Y. Kawaguchi, D. Johann, L.A. Liotta, H.C. Crawford, M.E. Putt, T. Jacks, C.V. Wright, R.H. Hruban, A.M. Lowy, and D.A. Tuveson. 2003. Preinvasive and invasive ductal pancreatic cancer and its early detection in the mouse. *Cancer Cell*. 4:437-450.
- Hingorani, S.R., L. Wang, A.S. Multani, C. Combs, T.B. Deramaudt, R.H. Hruban, A.K. Rustgi, S. Chang, and D.A. Tuveson. 2005. Trp53R172H and KrasG12D cooperate to promote chromosomal instability and widely metastatic pancreatic ductal adenocarcinoma in mice. *Cancer Cell*. 7:469-483.
- Hinz, B., and G. Gabbiani. 2003. Mechanisms of force generation and transmission by myofibroblasts. *Curr Opin Biotechnol*. 14:538-546.
- Hiraike, Y., H. Waki, J. Yu, M. Nakamura, K. Miyake, G. Nagano, R. Nakaki, K. Suzuki, H. Kobayashi, S. Yamamoto, W. Sun, T. Aoyama, Y. Hirota, H. Ohno, K. Oki, M. Yoneda, A.P. White, Y.H. Tseng, A.M. Cypess, T.J. Larsen, N.Z. Jespersen, C. Scheele, S. Tsutsumi, H. Aburatani, T. Yamauchi, and T.

- Kadowaki. 2017. NFIA co-localizes with PPARgamma and transcriptionally controls the brown fat gene program. *Nat Cell Biol.* 19:1081-1092.
- Iacobuzio-Donahue, C.A. 2012. Genetic evolution of pancreatic cancer: lessons learnt from the pancreatic cancer genome sequencing project. *Gut.* 61:1085-1094.
- Ijichi, H., A. Chytil, A.E. Gorska, M.E. Aakre, B. Bieri, M. Tada, D. Mohri, K. Miyabayashi, Y. Asaoka, S. Maeda, T. Ikenoue, K. Tateishi, C.V. Wright, K. Koike, M. Omata, and H.L. Moses. 2011. Inhibiting Cxcr2 disrupts tumor-stromal interactions and improves survival in a mouse model of pancreatic ductal adenocarcinoma. *J Clin Invest.* 121:4106-4117.
- Ijichi, H., A. Chytil, A.E. Gorska, M.E. Aakre, Y. Fujitani, S. Fujitani, C.V. Wright, and H.L. Moses. 2006. Aggressive pancreatic ductal adenocarcinoma in mice caused by pancreas-specific blockade of transforming growth factor-beta signaling in cooperation with active Kras expression. *Genes Dev.* 20:3147-3160.
- Innes, J.T., and L.C. Carey. 1994. Normal pancreatic dimensions in the adult human. *Am J Surg.* 167:261-263.
- Institute, N.C. 2020. Pancreatic Cancer Treatment (Adult) (PDQ®)–Patient Version.
- Izeradjene, K., C. Combs, M. Best, A. Gopinathan, A. Wagner, W.M. Grady, C.X. Deng, R.H. Hruban, N.V. Adsay, D.A. Tuveson, and S.R. Hingorani. 2007. Kras(G12D) and Smad4/Dpc4 haploinsufficiency cooperate to induce mucinous cystic neoplasms and invasive adenocarcinoma of the pancreas. *Cancer Cell.* 11:229-243.

- Jambhekar, A., A. Dhall, and Y. Shi. 2019. Roles and regulation of histone methylation in animal development. *Nat Rev Mol Cell Biol.* 20:625-641.
- Janda, E., K. Lehmann, I. Killisch, M. Jechlinger, M. Herzig, J. Downward, H. Beug, and S. Grunert. 2002. Ras and TGF[beta] cooperatively regulate epithelial cell plasticity and metastasis: dissection of Ras signaling pathways. *J Cell Biol.* 156:299-313.
- Jin, G., W. Hong, Y. Guo, Y. Bai, and B. Chen. 2020. Molecular Mechanism of Pancreatic Stellate Cells Activation in Chronic Pancreatitis and Pancreatic Cancer. *J Cancer.* 11:1505-1515.
- Joerger, A.C., and A.R. Fersht. 2007. Structural biology of the tumor suppressor p53 and cancer-associated mutants. *Adv Cancer Res.* 97:1-23.
- Jonckheere, N., R. Vasseur, and I. Van Seuningen. 2017. The cornerstone K-RAS mutation in pancreatic adenocarcinoma: From cell signaling network, target genes, biological processes to therapeutic targeting. *Crit Rev Oncol Hematol.* 111:7-19.
- Ju, H.Q., H. Ying, T. Tian, J. Ling, J. Fu, Y. Lu, M. Wu, L. Yang, A. Achreja, G. Chen, Z. Zhuang, H. Wang, D. Nagrath, J. Yao, M.C. Hung, R.A. DePinho, P. Huang, R.H. Xu, and P.J. Chiao. 2017. Mutant Kras- and p16-regulated NOX4 activation overcomes metabolic checkpoints in development of pancreatic ductal adenocarcinoma. *Nat Commun.* 8:14437.
- Kajimura, S., P. Seale, K. Kubota, E. Lunsford, J.V. Frangioni, S.P. Gygi, and B.M. Spiegelman. 2009. Initiation of myoblast to brown fat switch by a PRDM16-C/EBP-beta transcriptional complex. *Nature.* 460:1154-1158.



- Kajimura, S., P. Seale, T. Tomaru, H. Erdjument-Bromage, M.P. Cooper, J.L. Ruas, S. Chin, P. Tempst, M.A. Lazar, and B.M. Spiegelman. 2008. Regulation of the brown and white fat gene programs through a PRDM16/CtBP transcriptional complex. *Genes Dev.* 22:1397-1409.
- Khoo, K.H., C.S. Verma, and D.P. Lane. 2014. Drugging the p53 pathway: understanding the route to clinical efficacy. *Nat Rev Drug Discov.* 13:217-236.
- Kim, H., M. Kim, S.K. Im, and S. Fang. 2018. Mouse Cre-LoxP system: general principles to determine tissue-specific roles of target genes. *Lab Anim Res.* 34:147-159.
- Kreel, L., M. Haertel, and D. Katz. 1977. Computed tomography of the normal pancreas. *J Comput Assist Tomogr.* 1:290-299.
- Lin, J.C., T.P. Liu, and P.M. Yang. 2020. CDKN2A-Inactivated Pancreatic Ductal Adenocarcinoma Exhibits Therapeutic Sensitivity to Paclitaxel: A Bioinformatics Study. *J Clin Med.* 9.
- Maddalena, M., G. Mallel, N.B. Nataraj, M. Shreberk-Shaked, O. Hassin, S. Mukherjee, S. Arandkar, R. Rotkopf, A. Kapsack, G. Lambiase, B. Pellegrino, E. Ben-Isaac, O. Golani, Y. Addadi, E. Hajaj, R. Eilam, R. Straussman, Y. Yarden, M. Lotem, and M. Oren. 2021. TP53 missense mutations in PDAC are associated with enhanced fibrosis and an immunosuppressive microenvironment. *Proc Natl Acad Sci U S A.* 118.
- Magnuson, M.A., and A.B. Osipovich. 2013. Pancreas-specific Cre driver lines and considerations for their prudent use. *Cell Metab.* 18:9-20.

- Maitra, A., N.V. Adsay, P. Argani, C. Iacobuzio-Donahue, A. De Marzo, J.L. Cameron, C.J. Yeo, and R.H. Hruban. 2003. Multicomponent analysis of the pancreatic adenocarcinoma progression model using a pancreatic intraepithelial neoplasia tissue microarray. *Mod Pathol*. 16:902-912.
- Masciarelli, S., G. Fontemaggi, S. Di Agostino, S. Donzelli, E. Carcarino, S. Strano, and G. Blandino. 2014. Gain-of-function mutant p53 downregulates miR-223 contributing to chemoresistance of cultured tumor cells. *Oncogene*. 33:1601-1608.
- Massague, J. 2008. TGFbeta in Cancer. *Cell*. 134:215-230.
- Massague, J., J. Seoane, and D. Wotton. 2005. Smad transcription factors. *Genes Dev*. 19:2783-2810.
- Mizrahi, J.D., R. Surana, J.W. Valle, and R.T. Shroff. 2020. Pancreatic cancer. *Lancet*. 395:2008-2020.
- Mohammad, A.A. 2018. Advanced pancreatic cancer: The standard of care and new opportunities. *Oncol Rev*. 12:370.
- Morton, J.P., P. Timpson, S.A. Karim, R.A. Ridgway, D. Athineos, B. Doyle, N.B. Jamieson, K.A. Oien, A.M. Lowy, V.G. Brunton, M.C. Frame, T.R. Evans, and O.J. Sansom. 2010. Mutant p53 drives metastasis and overcomes growth arrest/senescence in pancreatic cancer. *Proc Natl Acad Sci U S A*. 107:246-251.
- Nagy, A. 2000. Cre recombinase: the universal reagent for genome tailoring. *Genesis*. 26:99-109.

- Nishikata, I., H. Sasaki, M. Iga, Y. Tateno, S. Imayoshi, N. Asou, T. Nakamura, and K. Morishita. 2003. A novel EVI1 gene family, MEL1, lacking a PR domain (MEL1S) is expressed mainly in t(1;3)(p36;q21)-positive AML and blocks G-CSF-induced myeloid differentiation. *Blood*. 102:3323-3332.
- Ohno, H., K. Shinoda, B.M. Spiegelman, and S. Kajimura. 2012. PPARgamma agonists induce a white-to-brown fat conversion through stabilization of PRDM16 protein. *Cell Metab*. 15:395-404.
- Ozaki, T., and A. Nakagawara. 2011. Role of p53 in Cell Death and Human Cancers. *Cancers (Basel)*. 3:994-1013.
- Parajuli, P., S. Kumar, A. Loumaye, P. Singh, S. Eragamreddy, T.L. Nguyen, S. Ozkan, M.S. Razzaque, C. Prunier, J.P. Thissen, and A. Atfi. 2018. Twist1 Activation in Muscle Progenitor Cells Causes Muscle Loss Akin to Cancer Cachexia. *Dev Cell*. 45:712-725 e716.
- Parajuli, P., T.L. Nguyen, C. Prunier, M.S. Razzaque, K. Xu, and A. Atfi. 2020. Pancreatic cancer triggers diabetes through TGF-beta-mediated selective depletion of islet beta-cells. *Life Sci Alliance*. 3.
- Parajuli, P., P. Singh, Z. Wang, L. Li, S. Eragamreddi, S. Ozkan, O. Ferrigno, C. Prunier, M.S. Razzaque, K. Xu, and A. Atfi. 2019. TGIF1 functions as a tumor suppressor in pancreatic ductal adenocarcinoma. *EMBO J*. 38:e101067.
- Park, H., J.H. Bang, A.R. Nam, J.E. Park, M.H. Jin, Y.J. Bang, and D.Y. Oh. 2020. The prognostic role of soluble TGF-beta and its dynamics in unresectable pancreatic cancer treated with chemotherapy. *Cancer Med*. 9:43-51.

- Park, S.W., J.M. Davison, J. Rhee, R.H. Hruban, A. Maitra, and S.D. Leach. 2008. Oncogenic KRAS induces progenitor cell expansion and malignant transformation in zebrafish exocrine pancreas. *Gastroenterology*. 134:2080-2090.
- Pei, D., X. Shu, A. Gassama-Diagne, and J.P. Thiery. 2019. Mesenchymal-epithelial transition in development and reprogramming. *Nat Cell Biol*. 21:44-53.
- Peng, J., B.F. Sun, C.Y. Chen, J.Y. Zhou, Y.S. Chen, H. Chen, L. Liu, D. Huang, J. Jiang, G.S. Cui, Y. Yang, W. Wang, D. Guo, M. Dai, J. Guo, T. Zhang, Q. Liao, Y. Liu, Y.L. Zhao, D.L. Han, Y. Zhao, Y.G. Yang, and W. Wu. 2019. Single-cell RNA-seq highlights intra-tumoral heterogeneity and malignant progression in pancreatic ductal adenocarcinoma. *Cell Res*. 29:725-738.
- Pickup, M.W., P. Owens, and H.L. Moses. 2017. TGF-beta, Bone Morphogenetic Protein, and Activin Signaling and the Tumor Microenvironment. *Cold Spring Harb Perspect Biol*. 9.
- Pierreux, C.E., F.J. Nicolas, and C.S. Hill. 2000. Transforming growth factor beta-independent shuttling of Smad4 between the cytoplasm and nucleus. *Mol Cell Biol*. 20:9041-9054.
- Pinheiro, I., R. Margueron, N. Shukeir, M. Eisold, C. Fritzsche, F.M. Richter, G. Mittler, C. Genoud, S. Goyama, M. Kurokawa, J. Son, D. Reinberg, M. Lachner, and T. Jenuwein. 2012. Prdm3 and Prdm16 are H3K9me1 methyltransferases required for mammalian heterochromatin integrity. *Cell*. 150:948-960.

- Ponnusamy, M.P., P. Seshacharyulu, I. Lakshmanan, A.P. Vaz, S. Chugh, and S.K. Batra. 2013. Emerging role of mucins in epithelial to mesenchymal transition. *Curr Cancer Drug Targets*. 13:945-956.
- Qi, Y., M.A. Gregory, Z. Li, J.P. Brousal, K. West, and S.R. Hann. 2004. p19ARF directly and differentially controls the functions of c-Myc independently of p53. *Nature*. 431:712-717.
- Reichert, M., and A.K. Rustgi. 2011. Pancreatic ductal cells in development, regeneration, and neoplasia. *J Clin Invest*. 121:4572-4578.
- Rocha, S., K.J. Campbell, and N.D. Perkins. 2003. p53- and Mdm2-independent repression of NF-kappa B transactivation by the ARF tumor suppressor. *Mol Cell*. 12:15-25.
- Roder, P.V., B. Wu, Y. Liu, and W. Han. 2016. Pancreatic regulation of glucose homeostasis. *Exp Mol Med*. 48:e219.
- Rozenblum, E., M. Schutte, M. Goggins, S.A. Hahn, S. Panzer, M. Zahurak, S.N. Goodman, T.A. Sohn, R.H. Hruban, C.J. Yeo, and S.E. Kern. 1997. Tumor-suppressive pathways in pancreatic carcinoma. *Cancer Res*. 57:1731-1734.
- Saiki, Y., C. Jiang, M. Ohmuraya, and T. Furukawa. 2021. Genetic Mutations of Pancreatic Cancer and Genetically Engineered Mouse Models. *Cancers (Basel)*. 14.
- Schutte, M., R.H. Hruban, J. Geradts, R. Maynard, W. Hilgers, S.K. Rabindran, C.A. Moskaluk, S.A. Hahn, I. Schwarte-Waldhoff, W. Schmiegel, S.B. Baylin, S.E. Kern, and J.G. Herman. 1997. Abrogation of the Rb/p16 tumor-suppressive pathway in virtually all pancreatic carcinomas. *Cancer Res*. 57:3126-3130.



- Seale, P., B. Bjork, W. Yang, S. Kajimura, S. Chin, S. Kuang, A. Scime, S. Devarakonda, H.M. Conroe, H. Erdjument-Bromage, P. Tempst, M.A. Rudnicki, D.R. Beier, and B.M. Spiegelman. 2008. PRDM16 controls a brown fat/skeletal muscle switch. *Nature*. 454:961-967.
- Seale, P., H.M. Conroe, J. Estall, S. Kajimura, A. Frontini, J. Ishibashi, P. Cohen, S. Cinti, and B.M. Spiegelman. 2011. Prdm16 determines the thermogenic program of subcutaneous white adipose tissue in mice. *J Clin Invest*. 121:96-105.
- Seale, P., S. Kajimura, W. Yang, S. Chin, L.M. Rohas, M. Uldry, G. Tavernier, D. Langin, and B.M. Spiegelman. 2007. Transcriptional control of brown fat determination by PRDM16. *Cell Metab*. 6:38-54.
- Seghers, P., A. Wiersma, S. Festen, M.E. Stegmann, P. Soubeyran, S. Rostoft, S. O'Hanlon, J.E.A. Portielje, and M.E. Hamaker. 2022. Patient Preferences for Treatment Outcomes in Oncology with a Focus on the Older Patient-A Systematic Review. *Cancers (Basel)*. 14.
- Seo, S.R., N. Ferrand, N. Faresse, C. Prunier, L. Abecassis, M. Pessah, M.F. Bourgeade, and A. Atfi. 2006. Nuclear retention of the tumor suppressor cPML by the homeodomain protein TGIF restricts TGF-beta signaling. *Mol Cell*. 23:547-559.
- Seoane, J., H.V. Le, L. Shen, S.A. Anderson, and J. Massague. 2004. Integration of Smad and forkhead pathways in the control of neuroepithelial and glioblastoma cell proliferation. *Cell*. 117:211-223.

Sharpless, N.E., N. Bardeesy, K.H. Lee, D. Carrasco, D.H. Castrillon, A.J. Aguirre, E.A. Wu, J.W. Horner, and R.A. DePinho. 2001. Loss of p16Ink4a with retention of p19Arf predisposes mice to tumorigenesis. *Nature*. 413:86-91.

Shimada, I.S., M. Acar, R.J. Burgess, Z. Zhao, and S.J. Morrison. 2017. Prdm16 is required for the maintenance of neural stem cells in the postnatal forebrain and their differentiation into ependymal cells. *Genes Dev*. 31:1134-1146.

Singh, B., R.F. Murphy, X.Z. Ding, A.B. Roginsky, R.H. Bell, Jr., and T.E. Adrian. 2007. On the role of transforming growth factor-beta in the growth inhibitory effects of retinoic acid in human pancreatic cancer cells. *Mol Cancer*. 6:82.

Slack, J.M. 1995. Developmental biology of the pancreas. *Development*. 121:1569-1580.

Society, A.C. 2023. Cancer facts and figures 2023.

Stathis, A., and M.J. Moore. 2010. Advanced pancreatic carcinoma: current treatment and future challenges. *Nat Rev Clin Oncol*. 7:163-172.

Stine, R.R., A.P. Sakers, T. TeSlaa, M. Kissig, Z.E. Stine, C.W. Kwon, L. Cheng, H.W. Lim, K.H. Kaestner, J.D. Rabinowitz, and P. Seale. 2019. PRDM16 Maintains Homeostasis of the Intestinal Epithelium by Controlling Region-Specific Metabolism. *Cell Stem Cell*. 25:830-845 e838.

Subramanian, A., P. Tamayo, V.K. Mootha, S. Mukherjee, B.L. Ebert, M.A. Gillette, A. Paulovich, S.L. Pomeroy, T.R. Golub, E.S. Lander, and J.P. Mesirov. 2005. Gene set enrichment analysis: a knowledge-based approach for interpreting genome-wide expression profiles. *Proc Natl Acad Sci U S A*. 102:15545-15550.

- Sugimoto, M., M.L. Kuo, M.F. Roussel, and C.J. Sherr. 2003. Nucleolar Arf tumor suppressor inhibits ribosomal RNA processing. *Mol Cell*. 11:415-424.
- Sundqvist, A., M. Morikawa, J. Ren, E. Vasilaki, N. Kawasaki, M. Kobayashi, D. Koinuma, H. Aburatani, K. Miyazono, C.H. Heldin, H. van Dam, and P. Ten Dijke. 2018. JUNB governs a feed-forward network of TGFbeta signaling that aggravates breast cancer invasion. *Nucleic Acids Res*. 46:1180-1195.
- Takahata, M., Y. Inoue, H. Tsuda, I. Imoto, D. Koinuma, M. Hayashi, T. Ichikura, T. Yamori, K. Nagasaki, M. Yoshida, M. Matsuoka, K. Morishita, K. Yuki, A. Hanyu, K. Miyazawa, J. Inazawa, K. Miyazono, and T. Imamura. 2009. SKI and MEL1 cooperate to inhibit transforming growth factor-beta signal in gastric cancer cells. *J Biol Chem*. 284:3334-3344.
- Tanay, A., and A. Regev. 2017. Scaling single-cell genomics from phenomenology to mechanism. *Nature*. 541:331-338.
- Tao, S., S. Wang, S.J. Moghaddam, A. Ooi, E. Chapman, P.K. Wong, and D.D. Zhang. 2014. Oncogenic KRAS confers chemoresistance by upregulating NRF2. *Cancer Res*. 74:7430-7441.
- Tuveson, D.A., A.T. Shaw, N.A. Willis, D.P. Silver, E.L. Jackson, S. Chang, K.L. Mercer, R. Grochow, H. Hock, D. Crowley, S.R. Hingorani, T. Zaks, C. King, M.A. Jacobetz, L. Wang, R.T. Bronson, S.H. Orkin, R.A. DePinho, and T. Jacks. 2004. Endogenous oncogenic K-ras(G12D) stimulates proliferation and widespread neoplastic and developmental defects. *Cancer Cell*. 5:375-387.

- Vander Heiden, M.G., L.C. Cantley, and C.B. Thompson. 2009. Understanding the Warburg effect: the metabolic requirements of cell proliferation. *Science*. 324:1029-1033.
- Vizan, P., L.G. Boros, A. Figueras, G. Capella, R. Mangués, S. Bassilian, S. Lim, W.N. Lee, and M. Cascante. 2005. K-ras codon-specific mutations produce distinctive metabolic phenotypes in NIH3T3 mice [corrected] fibroblasts. *Cancer Res*. 65:5512-5515.
- Warner, D.R., K.H. Horn, L. Mudd, C.L. Webb, R.M. Greene, and M.M. Pisano. 2007. PRDM16/MEL1: a novel Smad binding protein expressed in murine embryonic orofacial tissue. *Biochim Biophys Acta*. 1773:814-820.
- Waters, A.M., and C.J. Der. 2018. KRAS: The Critical Driver and Therapeutic Target for Pancreatic Cancer. *Cold Spring Harb Perspect Med*. 8.
- Weissmueller, S., E. Manchado, M. Saborowski, J.P.t. Morris, E. Wagenblast, C.A. Davis, S.H. Moon, N.T. Pfister, D.F. Tschaharganeh, T. Kitzing, D. Aust, E.K. Markert, J. Wu, S.M. Grimmond, C. Pilarsky, C. Prives, A.V. Biankin, and S.W. Lowe. 2014. Mutant p53 drives pancreatic cancer metastasis through cell-autonomous PDGF receptor beta signaling. *Cell*. 157:382-394.
- Westphalen, C.B., and K.P. Olive. 2012. Genetically engineered mouse models of pancreatic cancer. *Cancer J*. 18:502-510.
- Whittle, M.C., K. Izeradjene, P.G. Rani, L. Feng, M.A. Carlson, K.E. DelGiorno, L.D. Wood, M. Goggins, R.H. Hruban, A.E. Chang, P. Calses, S.M. Thorsen, and S.R. Hingorani. 2015. RUNX3 Controls a Metastatic Switch in Pancreatic Ductal Adenocarcinoma. *Cell*. 161:1345-1360.

- Wilentz, R.E., J. Geradts, R. Maynard, G.J. Offerhaus, M. Kang, M. Goggins, C.J. Yeo, S.E. Kern, and R.H. Hruban. 1998. Inactivation of the p16 (INK4A) tumor-suppressor gene in pancreatic duct lesions: loss of intranuclear expression. *Cancer Res.* 58:4740-4744.
- Williams, J.A. 2010. Regulation of acinar cell function in the pancreas. *Curr Opin Gastroenterol.* 26:478-483.
- Wu, A.A., E. Jaffee, and V. Lee. 2019. Current Status of Immunotherapies for Treating Pancreatic Cancer. *Curr Oncol Rep.* 21:60.
- Xia, X., W. Wu, C. Huang, G. Cen, T. Jiang, J. Cao, K. Huang, and Z. Qiu. 2015. SMAD4 and its role in pancreatic cancer. *Tumour Biol.* 36:111-119.
- Xue, H., T. Yao, M. Cao, G. Zhu, Y. Li, G. Yuan, Y. Chen, M. Lei, and J. Huang. 2019. Structural basis of nucleosome recognition and modification by MLL methyltransferases. *Nature.* 573:445-449.
- Yang, S., X. Wang, G. Contino, M. Liesa, E. Sahin, H. Ying, A. Bause, Y. Li, J.M. Stommel, G. Dell'antonio, J. Mautner, G. Tonon, M. Haigis, O.S. Shirihai, C. Doglioni, N. Bardeesy, and A.C. Kimmelman. 2011. Pancreatic cancers require autophagy for tumor growth. *Genes Dev.* 25:717-729.
- Ying, H., A.C. Kimmelman, C.A. Lyssiotis, S. Hua, G.C. Chu, E. Fletcher-Sananikone, J.W. Locasale, J. Son, H. Zhang, J.L. Coloff, H. Yan, W. Wang, S. Chen, A. Viale, H. Zheng, J.H. Paik, C. Lim, A.R. Guimaraes, E.S. Martin, J. Chang, A.F. Hezel, S.R. Perry, J. Hu, B. Gan, Y. Xiao, J.M. Asara, R. Weissleder, Y.A. Wang, L. Chin, L.C. Cantley, and R.A. DePinho. 2012.

- Oncogenic Kras maintains pancreatic tumors through regulation of anabolic glucose metabolism. *Cell*. 149:656-670.
- Yonezawa, S., M. Higashi, N. Yamada, and M. Goto. 2008. Precursor lesions of pancreatic cancer. *Gut Liver*. 2:137-154.
- Yun, J., C. Rago, I. Cheong, R. Pagliarini, P. Angenendt, H. Rajagopalan, K. Schmidt, J.K. Willson, S. Markowitz, S. Zhou, L.A. Diaz, Jr., V.E. Velculescu, C. Lengauer, K.W. Kinzler, B. Vogelstein, and N. Papadopoulos. 2009. Glucose deprivation contributes to the development of KRAS pathway mutations in tumor cells. *Science*. 325:1555-1559.
- Zeisberg, E.M., S. Potenta, L. Xie, M. Zeisberg, and R. Kalluri. 2007. Discovery of endothelial to mesenchymal transition as a source for carcinoma-associated fibroblasts. *Cancer Res*. 67:10123-10128.
- Zhang, M.Z., O. Ferrigno, Z. Wang, M. Ohnishi, C. Prunier, L. Levy, M. Razzaque, W.C. Horne, D. Romero, G. Tzivion, F. Colland, R. Baron, and A. Atfi. 2015. TGIF governs a feed-forward network that empowers Wnt signaling to drive mammary tumorigenesis. *Cancer Cell*. 27:547-560.
- Zhao, M., L. Mishra, and C.X. Deng. 2018. The role of TGF-beta/SMAD4 signaling in cancer. *Int J Biol Sci*. 14:111-123.
- Zhao, R., B.Y. Choi, M.H. Lee, A.M. Bode, and Z. Dong. 2016. Implications of Genetic and Epigenetic Alterations of CDKN2A (p16(INK4a)) in Cancer. *EBioMedicine*. 8:30-39.
- Zhao, S., Y. Wang, L. Cao, M.M. Ouellette, and J.W. Freeman. 2010. Expression of oncogenic K-ras and loss of Smad4 cooperate to induce the expression of



EGFR and to promote invasion of immortalized human pancreas ductal cells.  
*Int J Cancer*. 127:2076-2087.

Zhou, B., J. Wang, S.Y. Lee, J. Xiong, N. Bhanu, Q. Guo, P. Ma, Y. Sun, R.C. Rao, B.A. Garcia, J.L. Hess, and Y. Dou. 2016. PRDM16 Suppresses MLL1r Leukemia via Intrinsic Histone Methyltransferase Activity. *Mol Cell*. 62:222-236.